STIFFNESS OVER THE MID-SUPPORT FOR A MODIFIED SINGLE OVERLAP JOINT OF A SINGLE BAY TRAPEZOIDAL STEEL SHEET PROFILE USED IN LONG SPANS

Master Thesis – February 2017

Abraham Cardenas
SUSCOS Master Programme | Steel Structures

Abstract

Trapezoidal steel sheets are very popular in the construction industry, they are part of a structure as walls and roofing systems. It is because its low weight, easy assembly and durability that they are widely used in all kinds of building types, ranging from small residential buildings to big industrial warehouses.

In roofing systems, single overlap joints in the supports are one of the most common ways to make connections between two profiles, and the location of the fasteners that connect this profiles vary from different designers and engineers.

By using different positions for the fasteners in the overlap section, the structural behavior of the system will be different from one to another. For this thesis, a single bay trapezoidal steel sheet profile (LHP200) is used, which is made by the International Group Lindab.

The goal of this research is to test and analyze the current single overlap connection in order to get the spring stiffness acting there and see if improvements can be made. Theoretical analysis, Finite Element Modelling and an Experimental Test were implemented to do the investigation. Any differences between the two approaches were avoided to have the most accurate comparison between the results.

Preface

The work done in this Master Thesis was in collaboration with members of the Steel Structures group at the Department of Civil Environmental and Natural Resources Engineering, Luleå University of Technology (LTU), and with the company Lindab, an international group that develops construction products and systems worldwide.

The research done, was directly supervised by Assistant Supervisor PhD Naveed Iqbal from the department of Steel Structures at LTU. The experimental test was supervised by Erik Andersson, Ulf Stenman and Thomas Forsberg of the LTU laboratory. All the materials for the test, advice for test configuration and technical background was given by Jan-Christer Mäki and Erik Andersson from Lindab Group.

Final review of this work was made by my Supervisor and Senior Lecturer from the department of Steel Structures at LTU Efthymios Koltsakis.

Acknowledgements

I want to thank my Thesis Supervisor Professor Efthymios Koltsakis for giving me the opportunity of working on this project, for his supervision, and for accommodating me as part of his research team at LTU. I also want to extend my gratitude to Assistant Thesis Supervisor PhD Naveed Iqbal, for his counsel, guidance and for overseeing my work along the whole project.

I want give credit to Professor Ove Lagerqvist for contacting the Lindab engineering team and made this research possible for me. I want to show my appreciation to Jan-Christer Mäki and Erik Andersson from Lindab Group, for assisting me, and for sharing their knowledge and expertise on this subject. In the same way, I want to thank Erik Andersson, Ulf Stenman and Thomas Forsberg of the LTU Laboratory for their assistance in the test set up, sharing their experience and for their disposition on helping me get everything I needed for the test.

I also want to thank all my professors and colleagues that have taught me, helped me and supported me through my whole career.

Finally, I want to thank my family and friends for being there for me in this chapter of my life, in particularly my parents for their love, support and encouragement throughout my whole studies.

Table of Contents

Symbols and Abbreviations

δ	Deflection of the Whole System
δg	Total Gap Between the Profiles
δo	Deflection of the Overlap
δt	Theoretical Deflection Without Overlap
E	Modulus of Elasticity
e	Overlap Length
f	Factor that Depends on the Span Configuration
FEM	Finite Element Model
Fs	Overlap Reaction Force that Depends on the Overlap Connection Screws
Fu	Overlap Reaction Force that Depends on the Profiles
g	Total Gap of the Overlap
g_1	Gap on the Bottom of the Overlap
g_2	Gap on the Top of the Overlap
I	Moment of Inertia
k	Spring Stiffness of the Overlap
L	Span Length
M	Bending Moment
P	Point Load
t	Nominal Thickness of the Profile
t_d	Design Thickness of the Profile

1 Introduction

1.1 Background

1.1.1 Cold-Formed Steel Sections

Cold-formed members are steel based products that are made by putting flat strip of steel coils into a cold-roll forming machine to get the desired shape, that can have a constant or a variable cross-section. There are a lot of different type of cold-formed structural members, but they are usually divided into two major types:

- Individual structural framing members
- Panel decks

The individual structural framing members, which are also called bar members, are the sections that include open sections like “C” and “Z” shape channels, open built-up sections, like joining two “C” shape members back to back, and closed built-up sections, which could be two “C” shape sections front to front.

In this master thesis, the aim is to study the behavior of a modified overlap joint between two single bay trapezoidal steel profiles. For this reason, we will be focusing on panel decks, or more specifically roof decks.

Panel and decks are made from profiled sheets and liner trays, usually with trapezoidal cross section like shown in figure 1.1. They are widely used in the construction industry as roof systems and wall cladding thanks to their many advantages that will be mentioned later in this chapter. The depth of the panels usually ranges from 20 to 200mm, and they have thicknesses between 0.6 and 1.5mm [1].

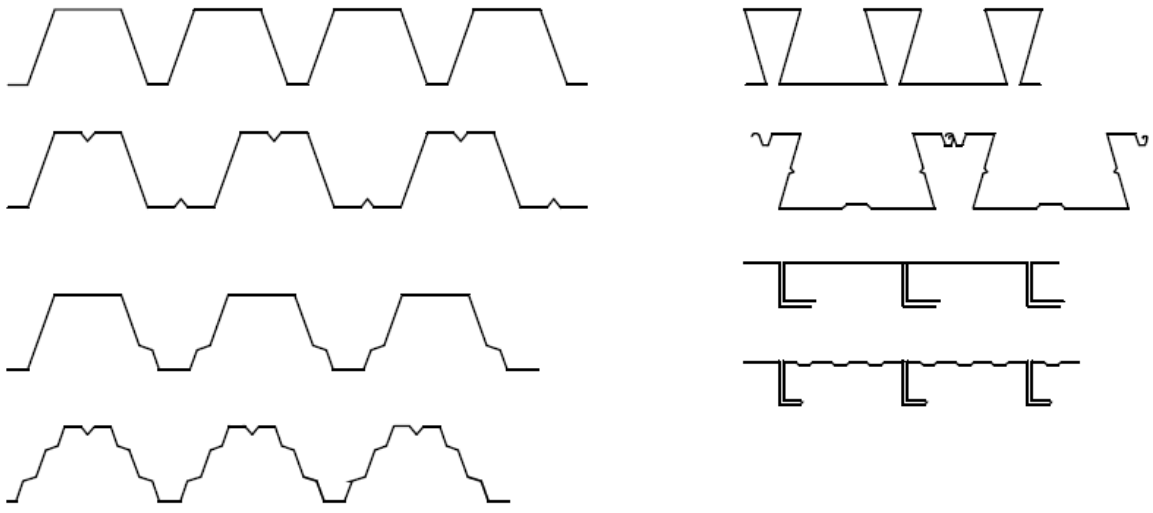

Figure 1.1. Typical Trapezoidal Steel Sheet Cross-Sections

Figures 1.2a, b and c, show examples of Rannila corrugated sheets for roofing, wall cladding systems and load-bearing deck panels.

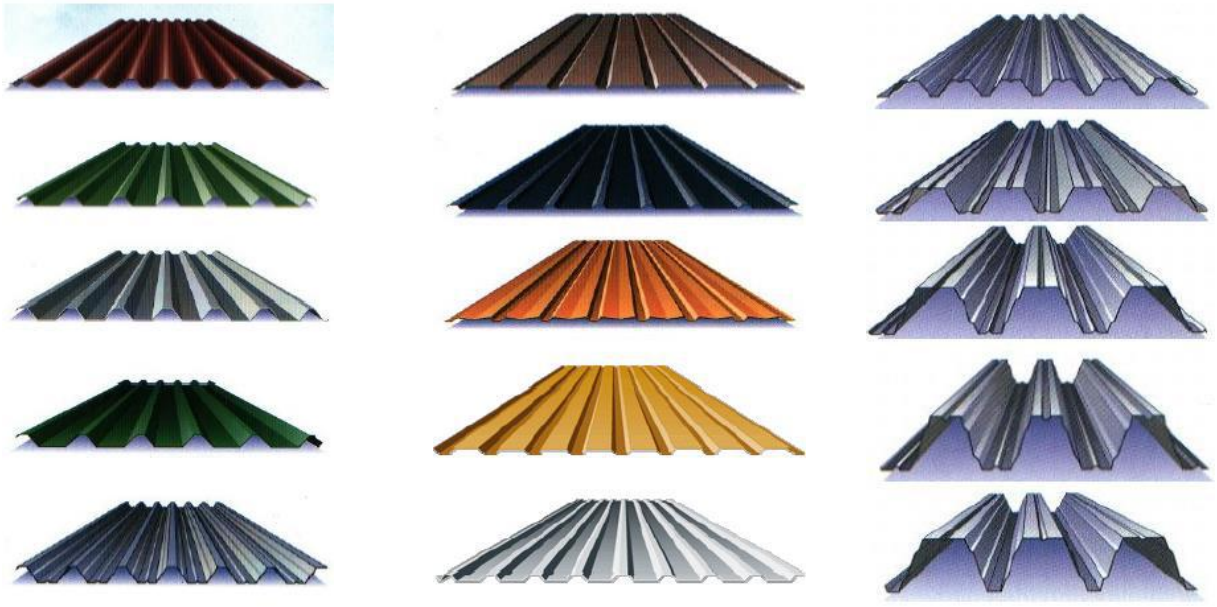

a) b) c)

Figure 1.2. Corrugated Sheets for Roofing and Wall Cladding

Cold-formed steel sections have many advantages in the building construction industry, which make them very popular all over the world. In general, the main advantages are the following:

- Can be manufactured for relatively light loafs and short spans, compared to hot-rolled sections, which are thicker and heavier.
- The way that they can be packed, offer a more efficient way of shipping compared to other type of section.
- Because the sections are produced with cold-forming process, unusual configurations can be economically made, and favorable strength to weight ratio can be obtained.
- Load carrying panels and decks provide useful surfaces for floors, roofs and walls.
- Beside of withstanding loads normal to their surfaces, load carrying panels and decks can act as a diaphragm for the structure if connected properly between the supporting members.

Cold-formed steel structural members can also be compared with other materials such as timber and concrete, and they have plenty of advantages as well:

- Lightness of the elements
- High strength and stiffness of the material
- Ability to provide long spans, up to 12m
- Ease of prefabrication and mass production

- Fast and easy erection and installation
- Substantial elimination of delays due to weather
- More accurate detailing
- Non-shrinking and non-creeping at ambient temperatures
- Formwork unnecessary
- Termite proof and rot proof
- Uniform quality
- Non-combustibility
- Recyclable material

Taking into account all the previous advantages, the use of cold-formed elements in the construction industry, can lead into a big cost savings [1].

1.1.2 Metal cladding

Metal cladding can be used as a building envelope system, in an efficient, appealing and safe way. For a long time, they have been used as part of the agricultural constructions as a single skin cladding, but over the years they have evolved into a more sophisticated and developed systems that are used in industrial buildings. Nevertheless, the functionality of the building envelope, depend on the correct installation and interaction between all the components of a building.

Metal cladding can be used in a variety of types for different buildings, which are mainly divided into two categories:

Single skin trapezoidal sheeting:

In buildings where no insulation is needed, single skin trapezoidal sheeting is used, this commonly tend to be industrial and agricultural buildings. the sheeting is installed by fixing it directly to the purlins or side rails like shown in figure 1.3.

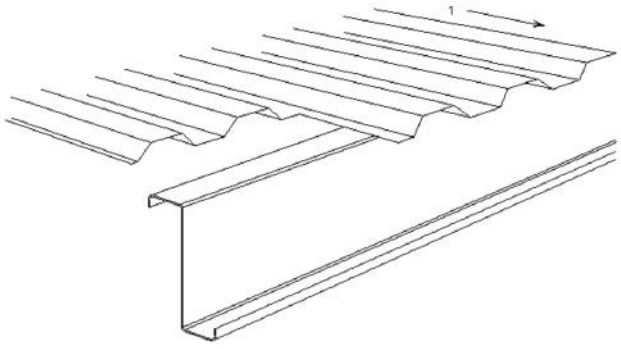

Figure 1.3. Single Skin Trapezoidal Steel Sheet

Built-up double skin cladding:

Built-up double skin cladding systems are usually used when a middle layer is needed in the envelope, most commonly for insulation. It is made of a metal liner, a layer of insulation, a spacer system and an outer metal sheet. Figure 1.4 shows an example of this system [2].

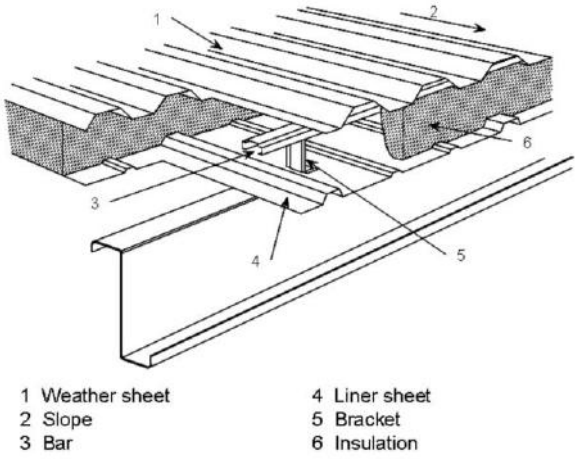

Figure 1.4. Built-Up Double Skin Cladding

1.2 LHP 200 Profile

The primary structural function of roof decks is to carry gravity loads, wind loads, and sometimes, based on the location of the structure, snow loads normal to its plane. Depending on the cross section and thickness of the sheet, the load capacity of the roofing will be different. For this reason, there is a wide range of profiles available in the market [3].

LHP200 profile is a single bay trapezoidal steel sheet used for roof decking produced by the company Lindab, which develops construction products and systems worldwide. Due to its geometry, this profile is made for large spans, often present in stadiums and other type of large buildings. It is is mounted with special supports, or support cleats, which increase the load capacity of the profile. Figures 1.5, and 1.6 show the geometric properties of the LHP200 profile and its support cleat respectively [4].

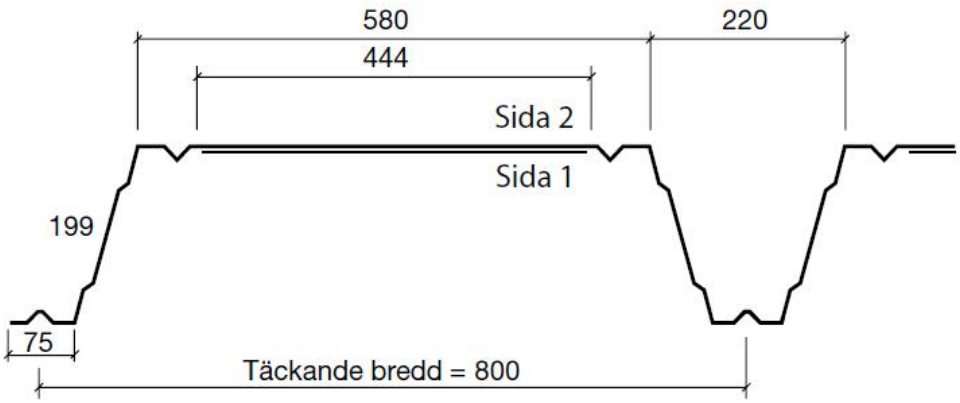

Figure 1.5. LHP200 Profile Cross-Section

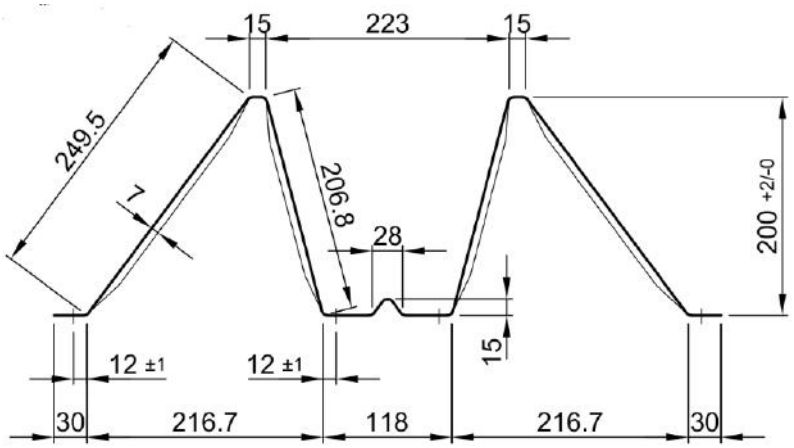

Figure 1.6. Support Cleats Cross-Section

1.3 Aim, scope and limitations

The work done in this thesis, is a research proposal from the Lindab Group located in Luleå, Sweden. They are interested in studying the behavior of a single overlap connection over a mid-support from the LHP200 profile that it is used for large spans.

The main objective is to find the spring stiffness of this overlap joint, by testing, making a theoretical analysis based on the test results, and finally to simulate the experimental test in order to do a parametric study.

The reason of finding the spring stiffness of the overlap joint is because the company needs this parameter to implement it into a software that they use for design. Nevertheless, the interest of doing this study is also to understand the behavior of the connection and give room for a possible optimization of this connection.

2 State of the Art

2.1 Theoretical Background

2.1.1 Structural Analysis

Structural analysis describes or predicts how a structure will perform under specific loading and/or external effects, like support movements and temperature changes. Its role is a fundamental piece in the development of structural engineering projects, assuring a safety performance in the structure designed.

In structural analysis, the determination of stresses or stress resultants, such as axial forces, shear forces, bending moments, deflections and support reactions, are the quantities of most interest to assure a good design, which are caused by a given loading condition [5].

2.1.2 Slope-Deflection Equations

A continuous beam that is under the influence of an external load, it will usually develop internal moments at the ends of its individual members. This moments located at the ends, can be related to the rotations and displacements of its ends, and the external loads acting on the beam by using the slope-deflection equations.

In order to understand the derivation of slope-deflection equations, we need to define first the behavior of a structural element, and its response under a given load. Imagining an arbitrary member *AB* of a continuous beam (figure 2.1(a)) subjected under external loads and supported settlements, the member will deform, and it will consequently generate internal moments at its ends. Figure 2.1(b) shows the free-body diagram and the elastic curve of member *AB*, where we can appreciate the end moments M_{AB} and M_{BA}, which correspond to the end moments of end *A* and *B*, respectively. The end moments have double-subscript notations, where the first indicate the member end at which the moment is acting and the second subscript indicate the other end of the member.

The rotations of the member ends *A* and *B* are indicated as θ_A and θ_B, respectively, and they are with respect to the horizontal undeformed position of the member. In this same figure, it is also shown a relative translation between the two ends *A* and *B* of the member, which are denoted with Δ, and it's in the direction perpendicular to the undeformed axis of the member [5].

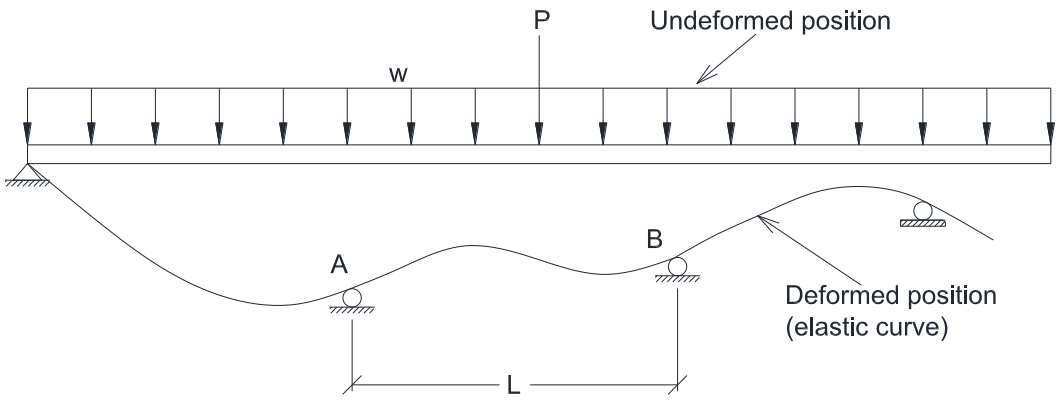

(a)

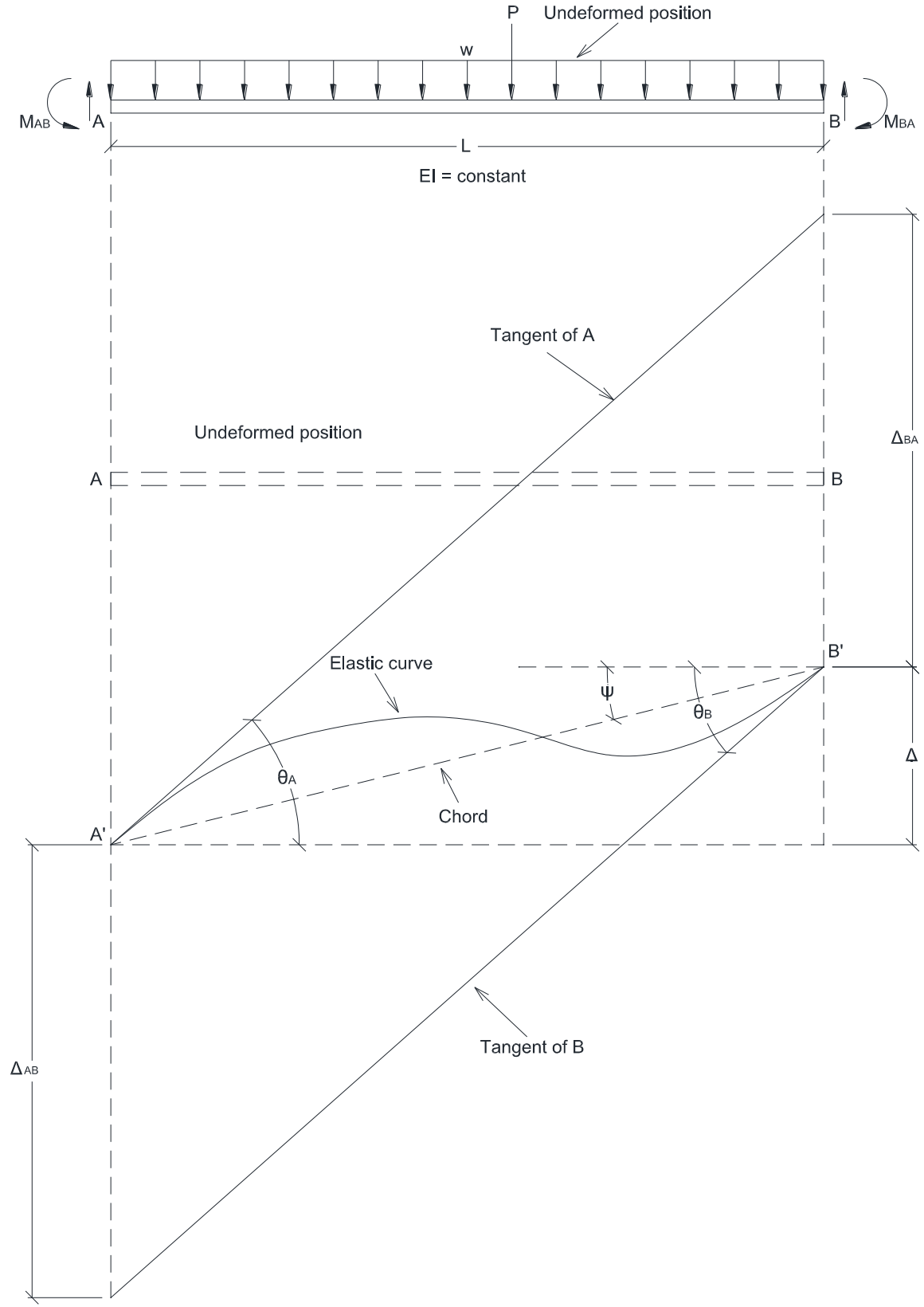
P
Undeformed position
w
MAB
A
B
MBA
L
EI = constant
Tangent of A
Undeformed position
ΔBA
A
B
B'
Elastic curve
ψ
θB
θA
Chord
A'
Δ
ΔAB
Tangent of B

(b)

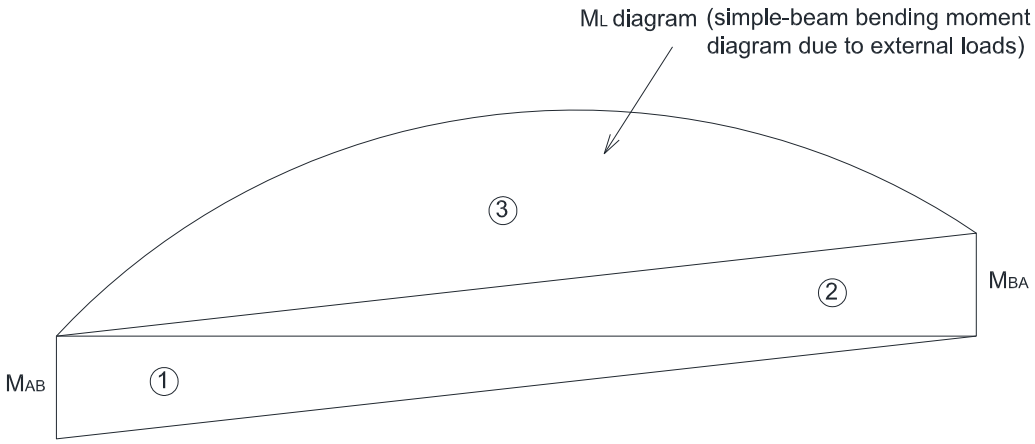

Bending moment diagram

(c)

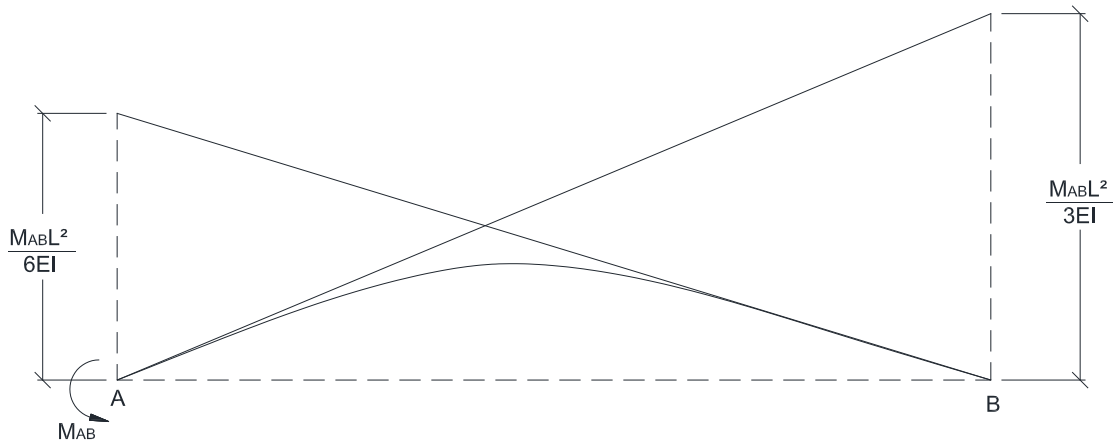

Tangential deviations due to M_{AB}

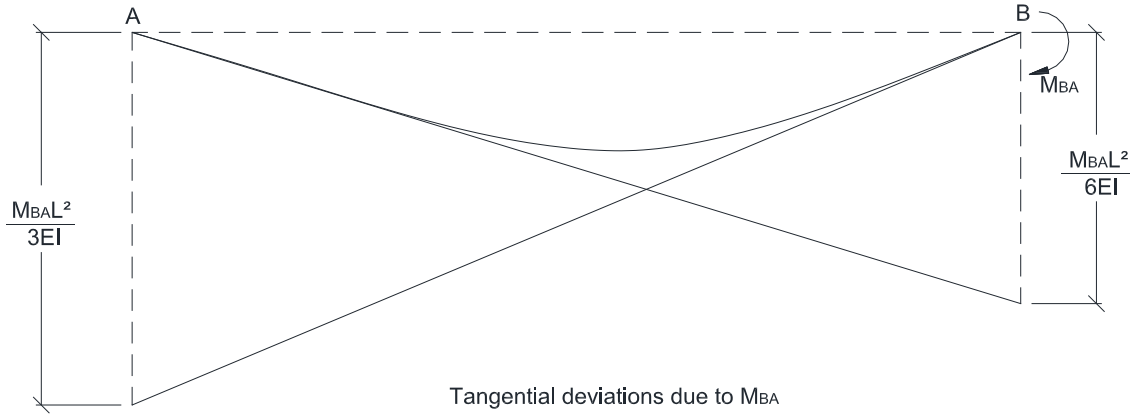

Tangential deviations due to M_{BA}

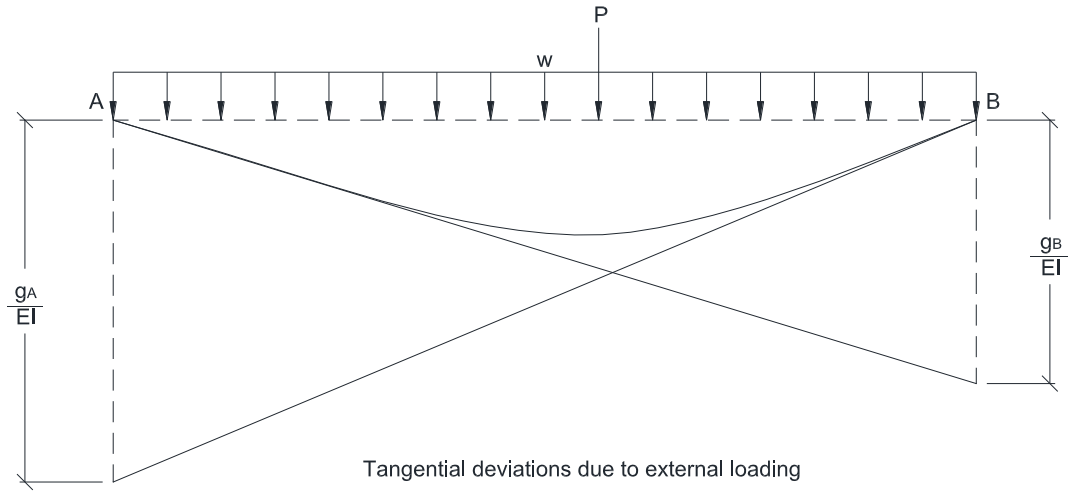

(d)

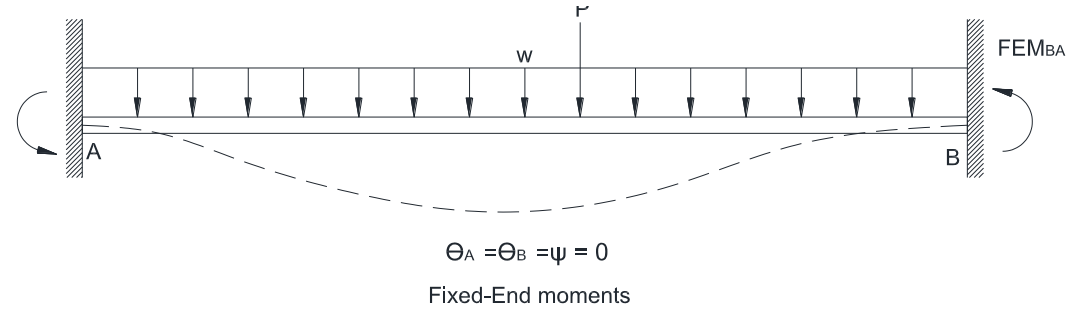

Figure 2.1

A rotation on the member's chord is also present, denoted with ψ, which is caused by the relative translation Δ. This deformation is assumed to be small, hence the chord rotation can be expressed as:

$$\psi = \frac{\Delta}{L} \tag{2.1}$$

In figure 2.1(b), the moments and rotations are shown in the positive sense (counterclockwise direction). By applying the second moment area theorem, the slope-deflection equations can be derived by doing a relation between the moments and rotations of the member ends. Moreover, from figure 2.1(b) we can recognize the following:

$$\theta_A = \frac{\Delta_{BA}+\Delta}{L} \tag{2.2a}$$

$$\theta_B = \frac{\Delta_{AB}+\Delta}{L} \tag{2.2b}$$

By substituting $\Delta/L = \psi$; we write:

$$\theta_A - \psi = \frac{\Delta_{BA}}{L} \tag{2.3a}$$

$$\theta_B - \psi = \frac{\Delta_{AB}}{L} \tag{2.3b}$$

From the previous equations, and, also illustrated in figure 2.1(b), Δ_{BA} represent the tangential deviations of the end *B* from the tangent to the elastic curve at end *A*, and Δ_{AB} is the tangential deviation of the end *A* from the tangent to the elastic curve at end *B*. These tangential deviations can be obtained by applying the second moment-area theorem, where Δ_{BA} and Δ_{AB}, can be obtained by summing the moments about the ends *A* and *B*, respectively, of the area under the *M/EI* diagram between the two ends.

To build the bending moment diagram of the member, M_{AB}, M_{BA}, and the external loading are applied separately on the member with simply supported ends. The three resultant bending moment diagrams under the *M*/EI are then summed about the ends *B* and *A*, respectively to determine the tangential deviations. It is important to point out that the member is assumed to be prismatic, which means that *EI* is constant along the member's length. Figure 2.1(c) shows the diagrams obtained.

$$\Delta_{BA} = \frac{M_{AB}L^2}{3EI} - \frac{M_{BA}L^2}{6EI} - \frac{g_B}{EI} \tag{2.4a}$$

$$\Delta_{AB} = -\frac{M_{AB}L^2}{6EI} + \frac{M_{BA}L^2}{3EI} + \frac{g_A}{EI} \tag{2.4b}$$

From equations (2.4a) and (2.4b), the three terms shown, are the representations of the tangential deviations caused by M_{AB}, M_{BA}, and the external loading, acting separately on the member as illustrated in figure 2.1(d). The negative term represents the tangential deviation that is opposite to the elastic curve of the member shown in figure 2.1(b). And g_B and g_A are the moments about the ends *B* and *A*, respectively, of the area under the simple-beam bending moment diagram due to external loading (M_L diagram in figure 2.1(c)).

Making a substitution of the expressions of Δ_{BA} and Δ_{AB} (equations (2.4)), into equations (2.3), result in the following:

$$\theta_A - \psi = \frac{M_{AB}L}{3EI} - \frac{M_{BA}L}{6EI} - \frac{g_B}{EIL} \quad (2.5a)$$

$$\theta_B - \psi = -\frac{M_{AB}L}{6EI} + \frac{M_{BA}L}{3EI} + \frac{g_A}{EIL} \quad (2.5b)$$

To be able to express the member end moments in terms of the rotations and external loading, equations (2.5a) and (2.5b) must be solved simultaneously for M_{AB} and M_{BA}, and equation (2.5a) can now be written as:

$$\frac{M_{BA}L}{3EI} = \frac{2M_{AB}L}{3EI} - \frac{2g_B}{EIL} - 2(\theta_A - \psi)$$

Now this equation can be substituted into equation (2.5b) and solving the resulting equation for M_{AB}, we get:

$$M_{AB} = \frac{2EI}{L}(2\theta_A + \theta_B - 3\psi) + \frac{2}{L^2}(2g_B - g_A) \quad (2.6a)$$

And by substituting equation (2.6a) into either equation (2.5a) or (2.5b), we obtain the expression for M_{BA}:

$$M_{BA} = \frac{2EI}{L}(\theta_A + 2\theta_B - 3\psi) + \frac{2}{L^2}(g_B - 2g_A) \quad (2.6b)$$

Equations (2.6) show the end moments of the member are dependent of the rotations and translations on its ends, and of the external loading applied.

So far, the member has been considered as a part of a bigger structure, but if this is changed by considering it now as an isolated member with its ends completely fixed against rotations and translations (figure 2.1(e)), moments would develop at the end the fixed ends of the beam. This moments are known as fixed-end moments, and their expressions can be obtained from equations (2.6) by setting $\theta_A = \theta_B = \psi = 0$:

$$FEM_{AB} = \frac{2}{L^2}(2g_B - g_A) \quad (2.7a)$$

$$FEM_{BA} = \frac{2}{L^2}(2g_B - g_A) \quad (2.7b)$$

Where FEM_{AB} and FEM_{BA} are the fixed-end moments caused by the external loading at the fixed ends *A* and *B*. respectively, of the beam *AB* (figure 2.1(e)).

Checking equations (2.6), we can see that the second terms on the right side are equal to the fixed-end moments that would develop if the member had fixed ends, restricting rotations and translations (equations (2.7)). Moreover, of equations (2.7) are substituted into equations (2.6) we will obtain the following:

$$M_{AB} = \frac{2EI}{L}(2\theta_A + \theta_B - 3\psi) + FEM_{AB} \tag{2.8a}$$

$$M_{BA} = \frac{2EI}{L}(\theta_A + 2\theta_B - 3\psi) + FEM_{BA} \tag{2.8b}$$

Equations (2.8), are called the slope-deflection equations, and they express the end moments of a member in terms of its rotations and translations originated for a defined external loading. It is important to mention that the slope-deflection equations are valid only for prismatic members with linear elastic material properties, and that are subjected to small deformations. These equations take into account the bending deformations of members, for this reason, the deformations due to axial forces and shears are neglected.

Since equations (2.8) have the same form, both can be obtained one from the other just by switching the *A* and *B* subscripts. For this reason, it is favorable to express them as a single slope-deflection equation:

$$M_{nf} = \frac{2EI}{L}\left(\theta_n + 2\theta_f - 3\psi\right) + FEM_{nf} \tag{2.9}$$

Where the subscript *n* and *f* define the near end of the member where the moment M_{nf} acts, and the far (other) end of the member, respectively [5].

Equations (2.8) and (2.9), are the slope-deflection equations considering both ends of the member rigidly connected to the joints, this means that the member end rotations θ_A and θ_B are equal to the rotations of the adjacent joints.

On the other hand, in the situation of having one of the member's ends with a hinged connection, the moment at the hinged end will be equal to zero, and the slope-deflection equations can be modified to reflect this condition:

$$M_{rh} = \frac{3EI}{L}(\theta_r - \psi) + \left(FEM_{rh} - \frac{FEM_{hr}}{2}\right) \tag{2.10a}$$

$$M_{hr} = 0 \tag{2.10b}$$

2.1.3 Member Stiffness

A beam *AB*, which is considered to be prismatic with one end hinged and the other end fixed, *A* and *B*, respectively, is illustrated in figure 2.2(a). In this figure, a moment *M* is applied at the end hinged *A*. The moment applied makes the beam rotate by an angle θ at the hinged end *A* and it develops a moment M_{BA} at the fixed end *B*. By using the slope-deflection derived in Section 2.1.2, a relationship between the applied moment *M* and the rotation θ can be established. In this manner, substituting $M_{nf} = M$; $\theta_n = \theta$; $\theta_f = \psi = FEM_{nf} = 0$ into the slope-deflection equation, leads to:

$$M = \left(\frac{4EI}{L}\right)\theta \tag{2.11}$$

The moment that must be applied at an end of the member to cause a unit rotation of that end is called the bending stiffness $\overline{K}$. Therefore, giving a value of $\theta = 1rad$ in the equation (2.11), the bending stiffness of the beam illustrated in figure 2.2(a) will be obtained:

$$\overline{K} = \frac{4EI}{L} \tag{2.12}$$

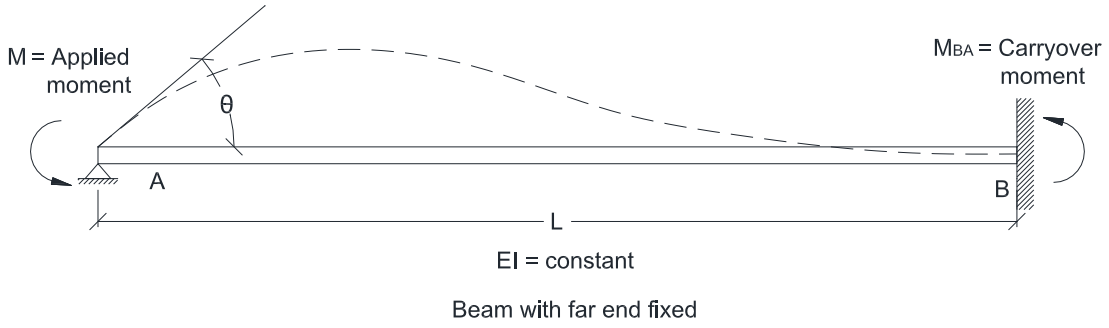

(a)

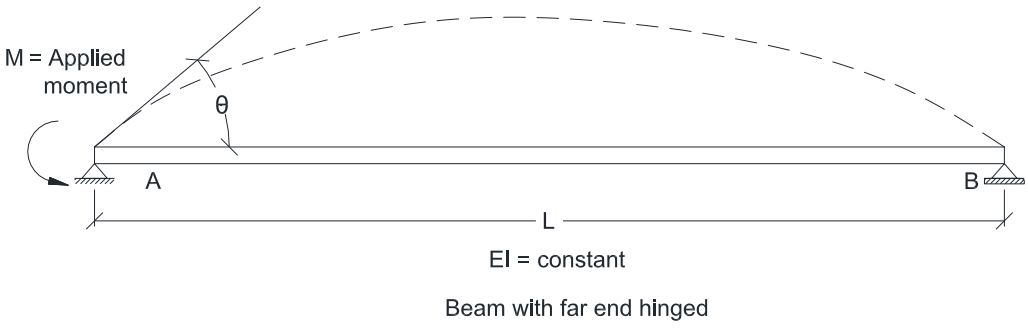

(b)

Figure 2.2

If the modulus of elasticity *E* of all the members of a structure is constant, it is favorable to use the relative bending stiffness *K* of the members when doing the analysis. This is obtained by dividing the bending stiffness $\overline{K}$ of the member by *4E*. Therefore, the relative bending stiffness of the beam of figure 2.2(a) will be the following:

$$K = \frac{\bar{K}}{4E} = \frac{I}{L} \tag{2.13}$$

Equations 2.11 to 2.13 were obtained from the hinged-fixed beam of figure 2.2(a). Now, considering a beam with both ends hinged like the one shown in figure 2.2(b), the applied moment *M* and the rotation θ of the end *A* of the beam, can be obtained by applying equations 2.10 (modified slope-deflection equations), defined in section 2.1.2. When substituting $M_{rh} = M$; $\theta_r = \theta$; and $\psi = FEM_{rh} = FEM_{hr} = 0$ into equation (2.10a), equation (2.14) is acquired:

$$M = \left(\frac{3EI}{L}\right)\theta \tag{2.14}$$

As done in equation (2.11), giving a value of $\theta = 1rad$, will lead to the expression for the bending stiffness of the beam of figure 2.2(b):

$$\bar{K} = \frac{3EI}{L} \tag{2.15}$$

Looking closely to equations (2.11) and (2.15), it is shown that when the fixed support at the end *B* is replaced by a hinged support, the bending stiffness is reduced by 25 percent. Similarly as in equation (2.13), the relative bending stiffness is acquired by dividing the bending stiffness by *4E*:

$$K = \frac{3}{4}\left(\frac{I}{L}\right) \tag{2.16}$$

The relationship between the applied end moment *M* and the corresponding rotation θ of equations (2.12) and (2.15), can be summarized as shown in equation (2.17).

$$M = \begin{cases} \left(\frac{4EI}{L}\right)\theta & Far\ end\ of\ the\ member\ fixed \\ \left(\frac{3EI}{L}\right)\theta & Far\ of\ the\ member\ hinged \end{cases} \tag{2.17}$$

And in the same way, based on equations (2.11) and (2.15), the bending stiffness of a member is given by:

$$\overline{K} = \begin{cases} \left(\frac{4EI}{L}\right) & Far\ end\ of\ the\ member\ fixed \\ \left(\frac{3EI}{L}\right) & Far\ end\ of\ the\ member\ hinged \end{cases} \tag{2.18}$$

Finally, the relative bending stiffness of a member can be expressed as:

$$K = \begin{cases} \frac{I}{L} & Far\ end\ of\ the\ member\ fixed \\ \frac{3}{4}\left(\frac{I}{L}\right) & Far\ end\ of\ the\ member\ hinged \end{cases} \tag{2.19}$$

2.1.4 Carryover Moment

When a moment *M* is applied to a hinged end *A* of a hinged-fixed beam like the one shown in figure 2.2(a), the beam generates a moment M_{BA} at the fixed end *B*. This moment M_{BA}, is defined as the carryover moment of that member. If we write the slope-deflection equation for M_{BA}, the relationship between the applied moment *M* and the carryover moment M_{BA} can be done, and by substituting $M_{nf} = M_{BA}$; $\theta_f = \theta$; and $\theta_n = \psi = FEM_{nf} = 0$ into equation (2.9) we have:

$$M_{BA} = \left(\frac{2EI}{L}\right)\theta \tag{2.20}$$

And substituting $\theta = ML/(4EI)$ from equation (2.1) into equation (2.20), we have:

$$M_{BA} = \frac{M}{2} \tag{2.21}$$

Equation (2.21) shows that when a moment *M* is applied to a hinged end of a beam, half of the magnitude of the applied moment is carried over to the far end, with the assumption that the far end is fixed. It is important to notice that the direction of the carryover moment M_{BA} and the applied moment *M* are the same.

As seen previously, figure 2.2(b) is a hinged-hinged beam. In this situation, the carryover moment will be equal to zero. Hence, the carryover moment can be expressed as:

$$M_{BA} = \begin{cases} \frac{M}{2} & Far\ end\ of\ the\ member\ fixed \\ 0 & Far\ end\ of\ the\ member\ hinged \end{cases} \tag{2.22}$$

The carryover factor (COF) is the ratio of the carryover moment to the applied moment (M_{BA}/M), and it represents the fraction of the applied moment M that is carried over to the far end of the member. Thus, the carryover factor of equations (2.22) will be [5]:

$$COF = \begin{cases} \frac{1}{2} & Far\ end\ of\ the\ member\ fixed \\ 0 & Far\ end\ of\ the\ member\ hinged \end{cases} \tag{2.23}$$

2.1.5 Distribution Factors

To explain how to distribute a moment applied (by moment-distributed method) on a joint where several members are connected, a joint with three members belonging to a frame can be considered. When applying a moment M to the joint B, a rotation with the angle θ is caused, like shown in figure 2.3(a). Each member resists a fraction of that moment M applied, and in order to determine the corresponding value of each member the drawing of the free-body diagrams of joint B and for the three members AB, BC and BD must be done (figure 2.3(b)). By considering the moment equilibrium of the free body of joint B (i.e., $\Sigma M_B = 0$), we write:

$$\begin{gathered} M + M_{BA} + M_{BC} + M_{BD} = 0 \\ or \\ M = -(M_{BA} + M_{BC} + M_{BD}) \end{gathered} \tag{2.24}$$

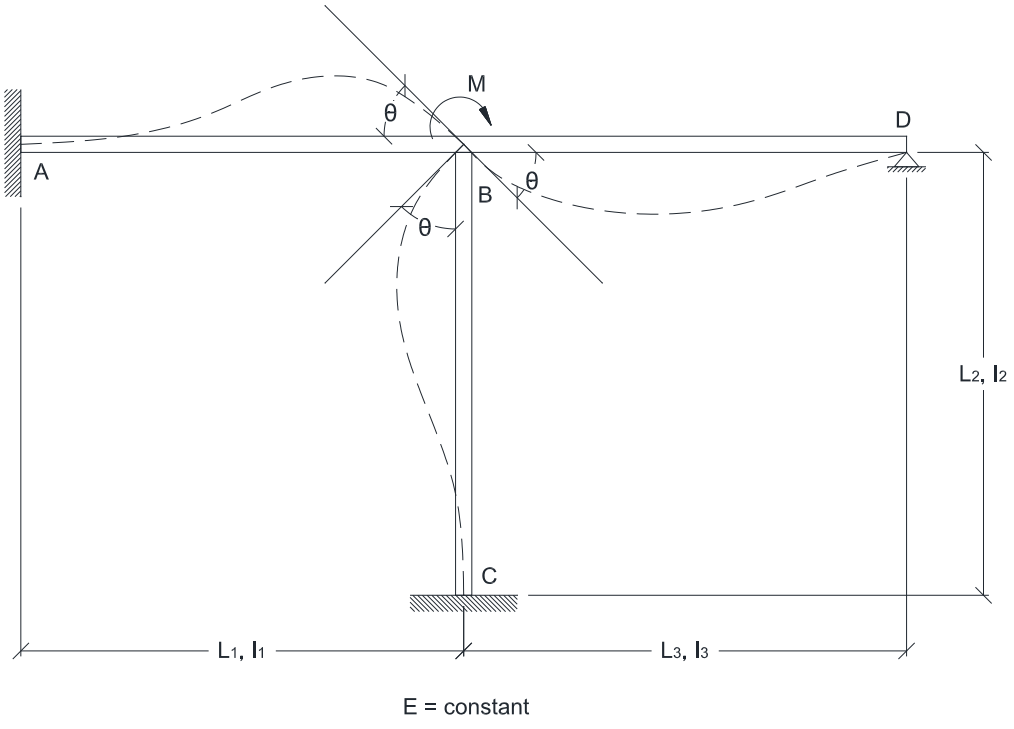

(a)

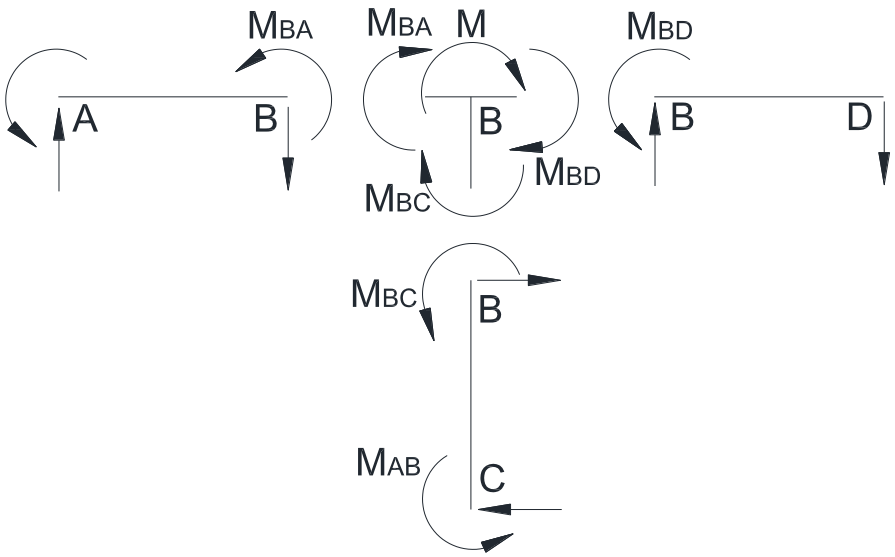

Figure 2.3

Member *AB*, *BC* and *BD* are rigidly connected to joint *B*, this means that the rotations at the end *B* of these members is the same as in the joint. Moreover, by applying equations (2.17) through (2.19), the moments at the end *B* of the members can expressed in terms of the joint rotation θ to each member.

$$M_{BA} = \left(\frac{4EI_1}{L_1}\right)\theta = \overline{K}_{BA}\theta = 4EK_{BA}\theta \tag{2.25}$$

$$M_{BC} = \left(\frac{4EI_2}{L_2}\right)\theta = \overline{K}_{BC}\theta = 4EK_{BC}\theta \tag{2.26}$$

$$M_{BD} = \left(\frac{4EI_3}{L_3}\right)\theta = \overline{K}_{BD}\theta = 4EK_{BD}\theta \tag{2.27}$$

And substituting the equations (2.25) through (2.27) into the equilibrium equation (eq. (2.24)):

$$M = -\left(\frac{4EI_1}{L_1} + \frac{4EI_2}{L_2} + \frac{3EI_3}{L_3}\right)\theta = -(\overline{K}_{BA} + \overline{K}_{BC} + \overline{K}_{BD})\theta = -(\Sigma\overline{K}_B)\theta \tag{2.28}$$

Where $\Sigma\,\overline{K}_B$ is the sum of the bending stiffnesses of the members connected to joint *B*.

The moment needed to cause a unit rotation of a joint is defined as the rotational stiffness. Equation (2.28) shows that the sum of the bending stiffnesses of the member rigidly connected

to the joint is equal to the rotational stiffness acting there. The adopted sing convention considers the member end moments as positive when are in the counterclockwise direction, and the moments acting on joints are considered positive when they act in the clock wise direction.

The member end moments can be expressed in terms of the applied moment *M*, to accomplish this, the first thing is to rewrite equation (2.28) in terms of the relative bending stiffness of the members:

$$M = -4E(K_{BA} + K_{BC} + K_{BD})\theta = -4E(\Sigma K_B)\theta$$

Where:

$$\theta = -\frac{M}{4E\Sigma K_B} \tag{2.29}$$

Substituting equation (2.29) into equations (2.25) through (2.27) into the equilibrium equation (eq. (2.24)), getting:

$$M_{BA} = -\left(\frac{K_{BA}}{\Sigma K_B}\right) M \tag{2.30}$$

$$M_{BC} = -\left(\frac{K_{BC}}{\Sigma K_B}\right) M \tag{2.31}$$

$$M_{BD} = -\left(\frac{K_{BD}}{\Sigma K_B}\right) M \tag{2.32}$$

As shown in equations (2.30), (2.31), and (2.32), the distribution of the applied moment *M* is proportional to the relative bending stiffness of the three members. Where the distribution factor of that member for end *B*, is the ratio $K/\Sigma K_B$, and symbolizes the portion of the applied moment *M* that is distributed to the end *B* of the member. Consequently, equations (2.30), (2.31), and (2.32), can be expressed as:

$$M_{BA} = -DF_{BA}M \tag{2.33}$$

$$M_{BC} = -DF_{BC}M \tag{2.34}$$

$$M_{BD} = -DF_{BD}M \tag{2.35}$$

Where $DF_{BA} = K_{BA}/\Sigma K_B$; $DF_{BC} = K_{BC}/\Sigma K_B$ and $DF_{BD} = K_{BD}/\Sigma K_B$ are the distribution factors for ends *B* of the members *AB*, *BC* and *BD*, respectively [5].

2.1.6 Fixed-End Moments

The moment distribution method also takes into account joint translations caused by support settlements and side-sway, through fixed-end moments. To explain this, a beam fixed at both ends is taken into consideration (figure 2.4(a)), the beam's chord is rotating counterclockwise by the angle $\psi = \Delta/L$, which is caused by a small settlement Δ of the left end *A* of the beam with respect to the right end *B*.

The slope-deflection equation (equation (2.9)), can be written for two end moments with $\psi = \Delta/L$ and by setting θ_A, θ_B, and fixed-end moments FEM_{AB}, and FEM_{BA} due to external loading equal to zero, we have:

$$FEM_{AB} = FEM_{BA} = -\frac{6EI\Delta}{L^2}$$

FEM_{AB} and FEM_{BA} define the fixed-end moments caused by the relative translation Δ between the two ends of the beam. In order to keep the beam's ends to rotate, the two fixed-end moments must act in the clockwise (negative) direction (figure 2.4(a)), when a relative displacement causes a chord rotation in the counterclockwise direction. In the same way, if the relative displacement creates a clockwise rotation (figure 2.4(b)), then fixed-end moments act in the counterclockwise (positive) direction [5].

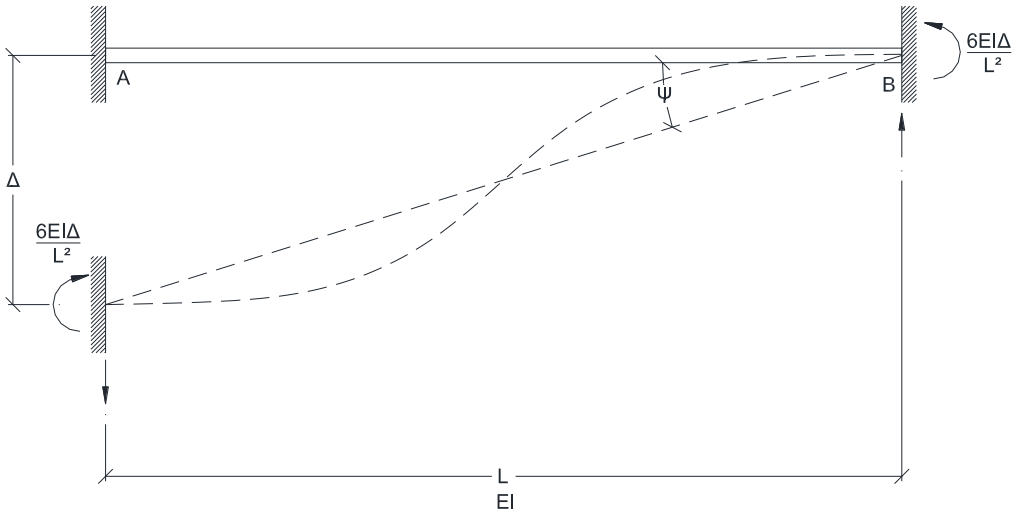

(a)

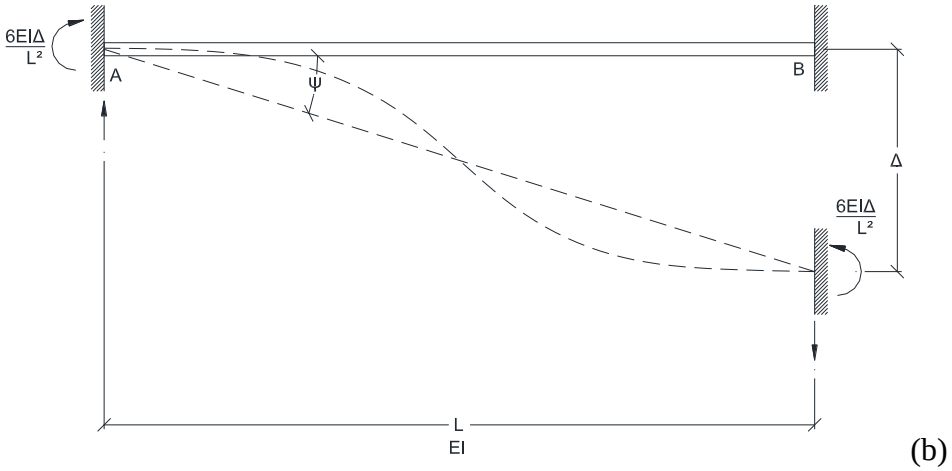

Figure 2.4

2.2 Matrix Structural Analysis

2.2.1 Analytical Model

The matrix stiffness analysis, considers the structure to be assembled by straight members connected all together at its ends to joints. A member, which is also called element, can be defined as a part of a structure where the force-displacement relations can be used. This means that when applying displacements on a member ends, the forces and moments at its ends should be able to be determined by using the force-displacement relations. A joint, also referred as node, is the structural part of infinitesimal size to which the member ends are connected.

In the analytical model, the joints and members of the structure are identified with numbers, in which the member's numbers are enclosed by a rectangle, and the joint's numbers by a circle. Figure 2.5(a) illustrates a frame, the analytical model of the frame is represented in figure 2.5(b), where members and joints can be distinguished from each other. Also in this figure, it is shown that the frame is composed by four members and five joints. As mentioned before, the member force-displacement relations can only be used in for prismatic members only, for this reason, the vertical column of the frame has been subdivided into two members, each with constant cross-sectional properties (*I* and *A*) along its length [5].

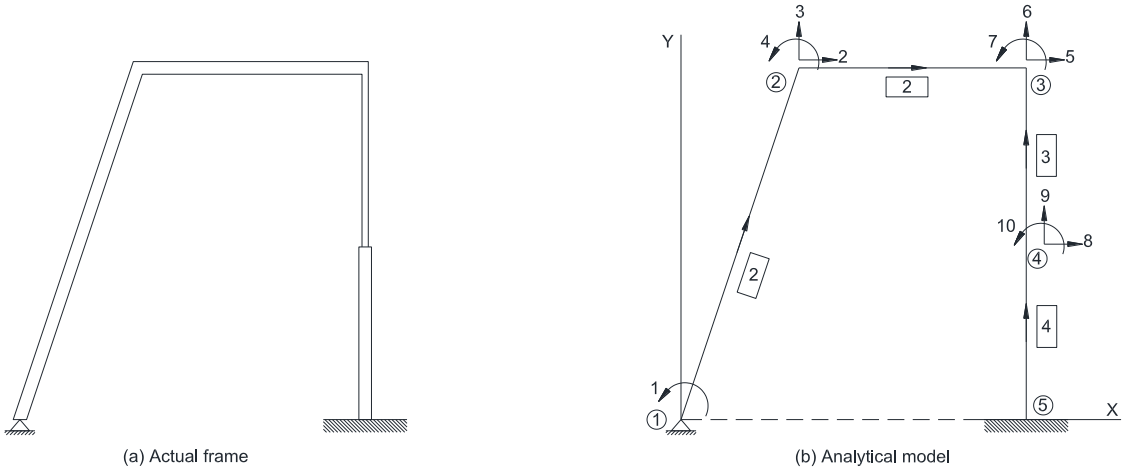

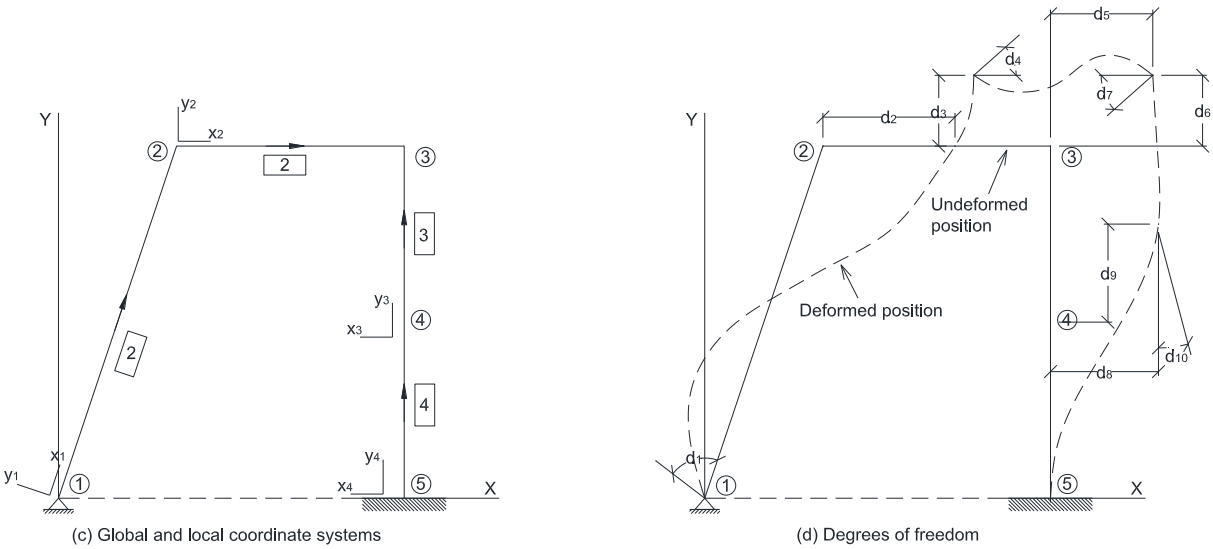

Figure 2.5

2.2.2 Global and Local Coordinate Systems

The stiffness method uses a Cartesian or rectangular global coordinate system to describe the overall geometry and behavior of the structure. A right-handed *XYZ*, with the plane structure on the *XY* plane is used for the global coordinate system. This can be seen in figure 2.5(b).

To get the basic force-displacement relations in reference of the forces and displacements in the directions along and perpendicular to members, it is favorable to define a local coordinate system for each member of the structure. The local *xyz* coordinate system's origin can be arbitrary positioned in one of the member's ends, with the *x* axis directed along its centroidal axis. To choose the direction of the *y* axis, its positive direction must be set so that the coordinate system is right-handed, with the local *z* axis pointing to the global *Z* axis positive direction.

Each member indicates the positive direction of the *x* axis with an arrow along the member line diagram of the structure, like shown in figure 2.4(b). In more detail, this figure displays that the origin of the member *1* is located at its end on joint *1*, and that the direction of the x_1 axis is from joint *1* to joint *2*. Also, each member has a beginning joint and an end joint. The beginning joint is defined as the joint in which the end member end with the origin of the local coordinate system is connected, while the end joint is the one adjacent to the opposite end of the member.

An example of this can also be seen in figure 2.5(b), where the member *1* begins at joint *1* and ends at joint *2*, and member *2* begins at joint *2* ending at joint *3*, and so on. After the local *x* axis for the members are determined, by applying the right-hand rule the local *y* axes are defined (figure 2.5(c)).

Finally, when applying the right-hand rule, the extended thumb (pointing out of the plane of the page) will indicate the local *z* axis, which is the same as the positive direction of the global Z axis [5].

2.2.3 Degrees of Freedom

The necessary displacements or translational rotations to define the deformed shape of a structure under loading are defined as the structure's degrees of freedom. The deformed shape of the frame used in the previous section (figure 2.5(a)) is displayed in figure 2.5(d). In this figure, the support conditions of the joints of the structure can be visualized, hence the degrees of freedom of the structure can be obtained. In the left column, joint *1* is located at a hinged support, which means that the member can freely rotate in the *X* and *Y* plane, but it won't translate in any direction, therefore joint *1* has one degree of freedom d_1. Joint *2* is not attached to any support, so it can freely translate in *X* and *Y* axes (d_2 and d_3), and rotate about the *Z* axis (d_4), so joint *2*, has three degrees of freedom. Joints *3* and *4* are in the same case as joint *2* (free joints), thus, they have three degrees of freedom each. Joint *5*, is fully fixed in the support of the right column, and it will not generate any translations and rotations, hence, it does not have any degrees of freedom. The frame has in total ten degrees of freedom, and the displacements are in accordance to the global coordinate system. The translations are defined as positive when in positive directions of the *X* and *Y* axes, the rotations are positive when they act on the counterclockwise direction. The matrix form of the joint displacements can be written as:

$$d = \begin{bmatrix} d_1 \\ d_2 \\ \vdots \\ d_9 \\ d_{10} \end{bmatrix}$$

Where d is the joint displacement vector of the structure.

In the stiffness method, it is unnecessary to sketch the deformed shape of the structure to distinguish the degrees of freedom. Usually, they are represented by numbered arrows on each joint of the line diagram of the structure like is displayed in figure 2.5(b). A suitable way of numbering the degrees of freedom of joints that have more than one degree of freedom, is to put first the translation on the *X* axis, followed by the translation on the *Y* axis, and finally the rotation.

In the case of continuous beams, lateral loads do not produce any axial deformations, consequently, the joint displacements along the centroidal axis of the member are omitted. Figure 2.6(a) represents a continuous beam with four degrees of freedom shown in figure 2.6(b), it can be noticed that each joint of the beam has up to two degrees of freedom and not three [5].

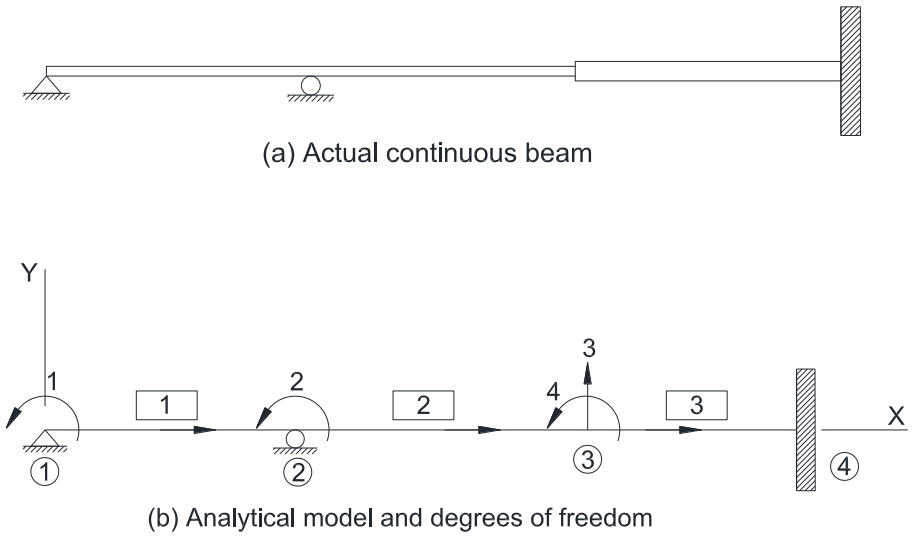

Figure 2.6. Degrees of Freedom in a Continuous Beam

2.3 Member Stiffness Relations in Local Coordinates

The structure's joint displacements are obtained by solving a simultaneous system of equations defined in equation (2.36).

$$\bar{P} = Sd \tag{2.36}$$

As mentioned in section 2.2.3, *d* represents the joint displacement vector, while the effects of external loads are at the joints are symbolized by $\overline{P}$, and *S* is the structure stiffness matrix. To acquire the structure's stiffness matrix, it is necessary to assemble the individual member's stiffness matrices of the structure. The stiffness matrix of a member expresses the forces at the ends of the member as a function of its end displacements [5].

2.3.1 Continuous Beam Members

As mentioned previously, continuous beam member's degrees of freedom in the direction of its centroidal axis are not considered. Consequently, the members of plane continuous beams have only four degrees of freedom to be considered. Figure 2.7(a) show the degrees of freedom acting in a continuous beam plane member.

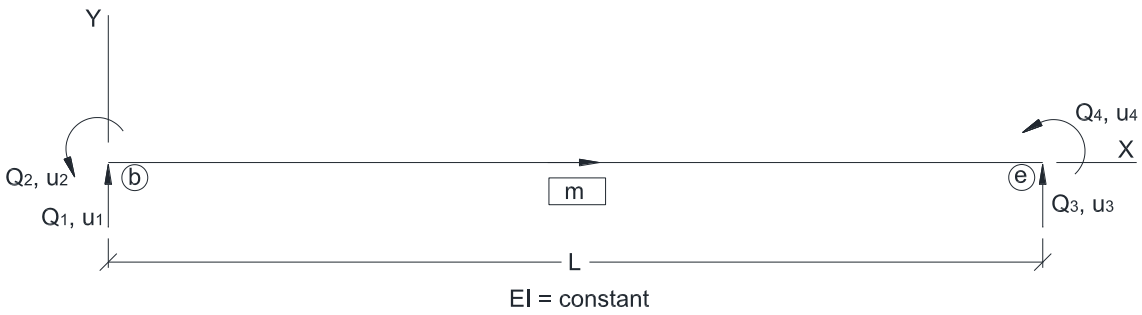
Y
Q4, u4
X
Q2, u2
b
m
e
Q1, u1
Q3, u3
L
EI = constant

(a)

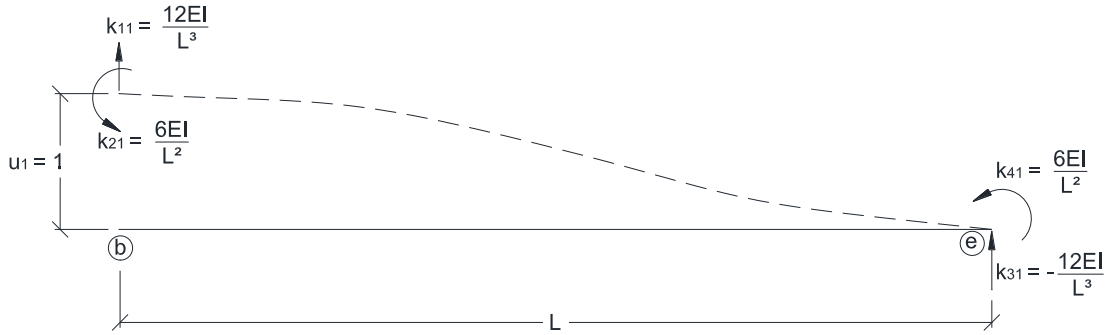
k11 = 12EI / L³
k21 = 6EI / L²
u1 = 1
k41 = 6EI / L²
b
e
k31 = -12EI / L³
L

(b)

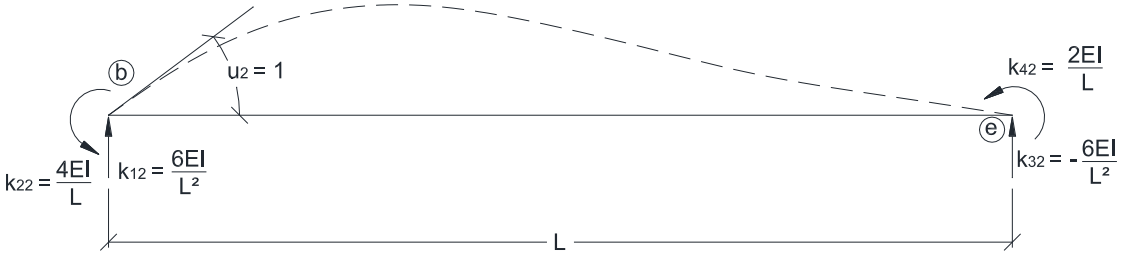
b
u2 = 1
k42 = 2EI / L
e
k22 = 4EI / L
k12 = 6EI / L²
k32 = -6EI / L²
L

(c)

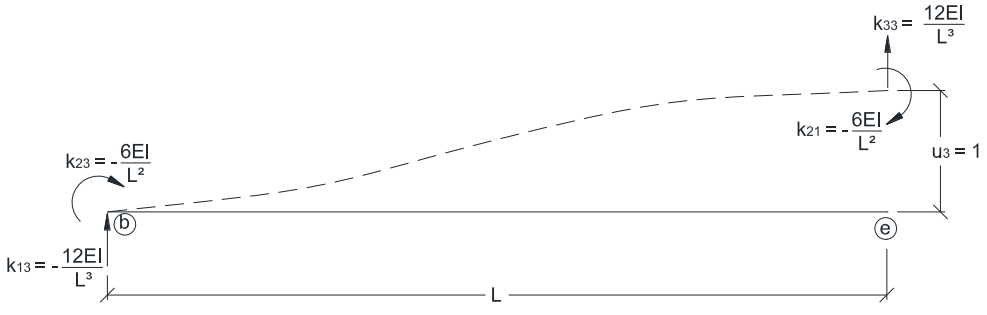
k33 = 12EI / L³
k21 = -6EI / L²
u3 = 1
k23 = -6EI / L²
b
e
k13 = -12EI / L³
L

(d)

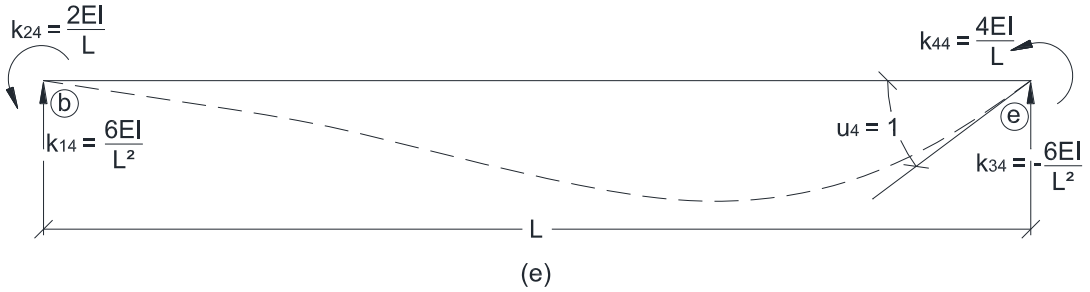

Figure 2.7

The member's end displacements with its corresponding end forces are represented by u_1 through u_4 and by Q_1 through Q_4, respectively.

The relationships between the member end forces and end displacements in terms of the external loads acting on the member, can be arranged by separately subjecting the member to each of the four end displacements and external loads, and by expressing the algebraic sum of the end forces required to cause the individual end displacements and the forces caused by the external loads, as the total member end forces. And according to figures 2.7(b) through (e), it can be expressed:

$$Q_1 = k_{11}u_1 + k_{12}u_2 + k_{13}u_3 + k_{14}u_4 + Q_{f1} \tag{2.37a}$$

$$Q_2 = k_{21}u_1 + k_{22}u_2 + k_{23}u_3 + k_{24}u_4 + Q_{f2} \tag{2.37b}$$

$$Q_3 = k_{31}u_1 + k_{32}u_2 + k_{33}u_3 + k_{34}u_4 + Q_{f3} \tag{2.37c}$$

$$Q_4 = k_{41}u_1 + k_{42}u_2 + k_{43}u_3 + k_{44}u_4 + Q_{f4} \tag{2.37f}$$

From the previous equations, the stiffness coefficients k_{ij} are the forces at a joint required to have a unit displacement u_j in the direction of Q_i, without having any other end displacements. Finally, the dixed-end forces caused by the external loads are represented as Q_{fi}.

Equations (2.37) can be represented in the matrix form by using the matrix multiplication definition:

$$\begin{bmatrix} Q_1 \\ Q_2 \\ Q_3 \\ Q_4 \end{bmatrix} = \begin{bmatrix} k_{11} & k_{12} & k_{13} & k_{14} \\ k_{21} & k_{22} & k_{23} & k_{24} \\ k_{31} & k_{32} & k_{33} & k_{34} \\ k_{41} & k_{42} & k_{43} & k_{44} \end{bmatrix} \begin{bmatrix} u_1 \\ u_2 \\ u_3 \\ u_4 \end{bmatrix} + \begin{bmatrix} Q_{f1} \\ Q_{f2} \\ Q_{f3} \\ Q_{f4} \end{bmatrix} \tag{2.38}$$

Or, symbolically as:

$$Q = ku + Q_f \tag{2.39}$$

Where the member end force is represented as *Q*, *u* is the member end displacement vectors, *k* represents the member stiffness matrix, and Q_f is the member fixed-end force vector, all in the local coordinate system.

To acquire the stiffness coefficients k_{ij}, the four end displacements of the member are subjected independently to unit values. Then, by applying the principals of mechanic of materials, the slope-deflection equations and the equations of equilibrium, the member end forces required to cause the individual unit displacement can be determined, and they represent the stiffness coefficients for the member.

Figure 2.7(b), displays a beam with its deformed shape caused by a unit displacement u_1, while all the other end displacements are equal to zero. The deflected shape is caused by the end moments of the member, and they can be determined by using the slope-deflection equations. Substituting $M_{AB} = k_{21}$; $M_{BA} = k_{61}$; $\theta_A = \theta_B = 0$; $\psi = -1/L$; and $FEM_{AB} = FEM_{BA} = 0$ into equations (2.8) we will have:

$$k_{21} = k_{61} = \frac{6EI}{L^2}$$

And by applying the equilibrium equations the end forces in the *y* direction can be obtained:

$$+\circlearrowleft \Sigma M_e = 0; \qquad 2\left(\frac{12EI}{L^2}\right) - k_{11}(L) = 0$$

$$k_{11} = \frac{12EI}{L^3}$$

$$+\uparrow \Sigma F_y = 0; \qquad \frac{12EI}{L^2} - k_{31} = 0$$

$$k_{31} = -\frac{12EI}{L^3}$$

The member end forces required to cause a displacement $u_3 = 1$ (figure 2.7(d)) can be determined in a similar manner:

$$k_{13} = -\frac{12EI}{L^3}\ ; \quad k_{23} = k_{43} = -\frac{6EI}{L^2}\ ; \quad k_{33} = \frac{12EI}{L^3}$$

Figure 2.7(c) shows the deformed shape of the member caused by the rotation $u_2 = 1$, with u_1, u_3, $u_4 = 0$. The member end moments can be obtained by substituting $M_{AB} = k_{22}$, $M_{BA} = k_{42}$, $\theta_A = 1$, and $\theta_B = \psi = FEM_{AB} = FEM_{BA} = 0$ into the slope-deflection equations:

$$k_{22} = \frac{4EI}{L} \; ; \qquad k_{42} = \frac{2EI}{L}$$

And with the equations of equilibrium, we determine:

$$k_{12} = \frac{6EI}{L^2} \qquad k_{32} = -\frac{6EI}{L^2}$$

Similarly, the stiffness coefficients corresponding to the unit displacement $u_4 = 1$ (figure (e)), will be:

$$k_{14} = -k_{34} = \frac{6EI}{L^2} \qquad k_{24} = \frac{2EI}{L} \qquad k_{44} = \frac{4EI}{L}$$

Substituting the values previously obtained into equation (2.38), will deliver the stiffness matrix for the members of continuous beams in local coordinates [5]:

$$k = \frac{EI}{L^3}\begin{bmatrix} 12 & 6L & -12 & 6L \\ 6L & 4L^2 & -6L & 2L^2 \\ -12 & -6L & 12 & -6L \\ 6L & 2L^2 & -6L & 4L^2 \end{bmatrix} \tag{2.40}$$

2.4 Member Stiffness Relations in Global Coordinates

2.4.1 Continuous Beam Members

In continuous beams, the local coordinates of the member are oriented in a way that the positive directions of *x* and *y* local axes, are in the same direction of the positive *X* and *Y* global axes. For this reason, there is no need to make a transformation of coordinates of the member, being the stiffness relations in the local and global coordinates the same [5].

2.5 Clapeyron's Theorem of Three Moments

A continuous beam with concentrated forces and under a partial uniform distributed load is shown in figure 2.8. Instead of the beam's reactions, the bending moments of the continuous beam are considered to be the unknowns. Next, the deformation equations are written in terms of these bending moments, that will finally deliver the three-moment theorem:

$$M_A L_1 + 2M_B(L_1 + L_2) + M_C L_2 = -\frac{6A_1 x_1}{L_1} - \frac{6A_2 x_2}{L_2} \tag{2.41}$$

Where M_A, M_B, and M_C are bending moments, at the supports *A*, *B* and *C* respectively, the span lengths are represented as L_1 and L_2, the areas of the moment diagrams are defined as A_1 and A_2 with the temporary assumption that each of the spans of the beam is simply supported, and the distances of the centroids of each of these moment diagrams from *A* and *C* will be x_1 and y_1 respectively. Whenever a continuous beam has the supports at the same level, the three-moment theorem is suitable [6].

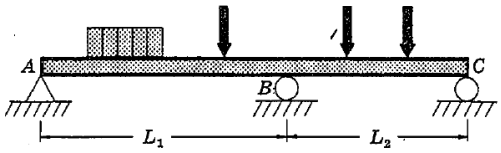

Figure 2.8. Continuous Beam Under Differen Load Conditions

For a roofing system acting as a continuous beam like shown in figure 2.9, the Clapeyron's equation applied to a support *n* would look like:

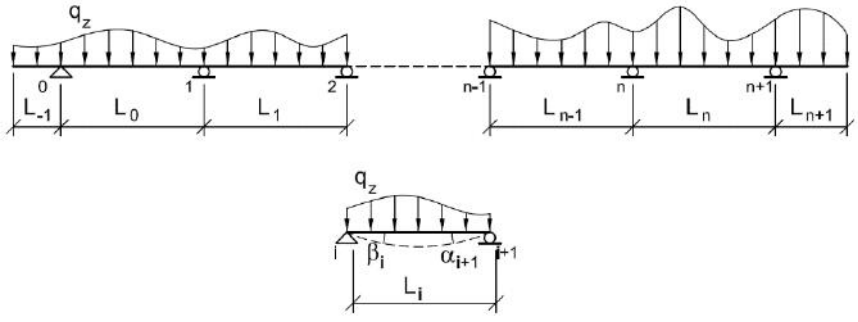

Figure 2.9. Roofing System-Continuous Beam Representation

$$M_{i-1}\frac{L_{i-1}}{6EI_{i-1}} + 2M_i\left(\frac{L_{i-1}}{6EI_{i-1}} + \frac{L_i}{6EI_i}\right) + M_{i+1}\frac{L_i}{6EI_i} = -(\alpha_i + \beta_i) \tag{2.42}$$

For a continuous beam with more than two supports, the equations can be written as a matrix $[A] \cdot [M_s] = [H]$:

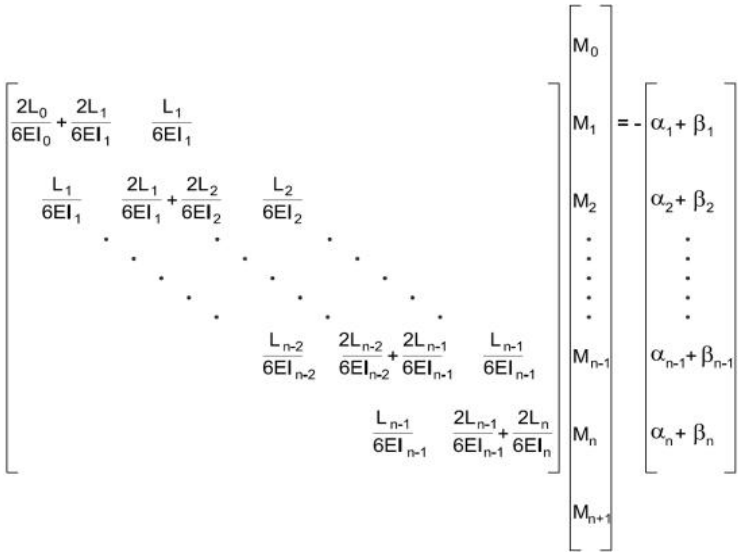

Stiffness matrix *[A]* is built up with terms that depend on the beam stiffness and spans for each bay. Also, the design of beam joints affects the stiffness.

Support moment matrix $[M_s]$ is the solution vector for the system of equations. Any cantilever bending moment at end support, M_0 and M_{n+1}. Note that if there are cantilever bending moment, it will affect the beam constants for adjacent support.

Matrix *[H]* is built up with so called beam constants that is the inclination angle at the support regardless of the beam continuity. The beam constants are dependent on the type of load that is acting on the beam.

3 Experimental Test

For the experimental test, since we are studying the behavior of the connection in the mid-support, testing procedures in accordance with the Annex A of EN 1993-1-3 are used. The company produces four thicknesses of the LHP200 profile: 0.85mm, 1.00mm, 1.25mm, and 1.50mm. In this experiment the lowest and the highest thicknesses are tested to cover the whole range of the product, and three tests are made for each one. The length of the real span considered is of 8m, with a single overlap of 720mm starting 80mm from the mid-support.

- **EN1993-1-3 A.2.1 (3):** in this section EN1993-1-3 says that to prevent the spreading of corrugations, transverse ties or appropriate test accessories such can be applied to the test specimen (figure 3.1). In this case "L" shape sections are used as ties and special supports are delivered from the company to place them at its ends (figure 3.2).

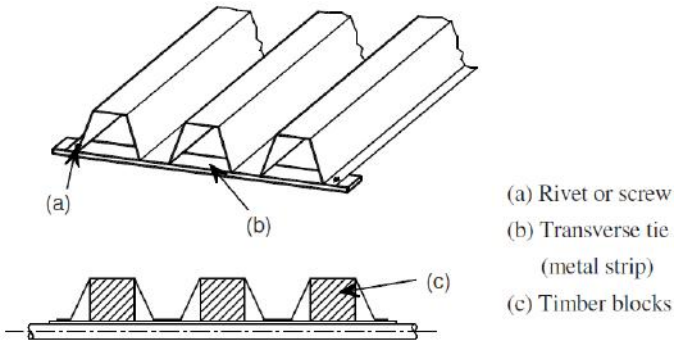

Figure 3.1 Appropriate test accessories

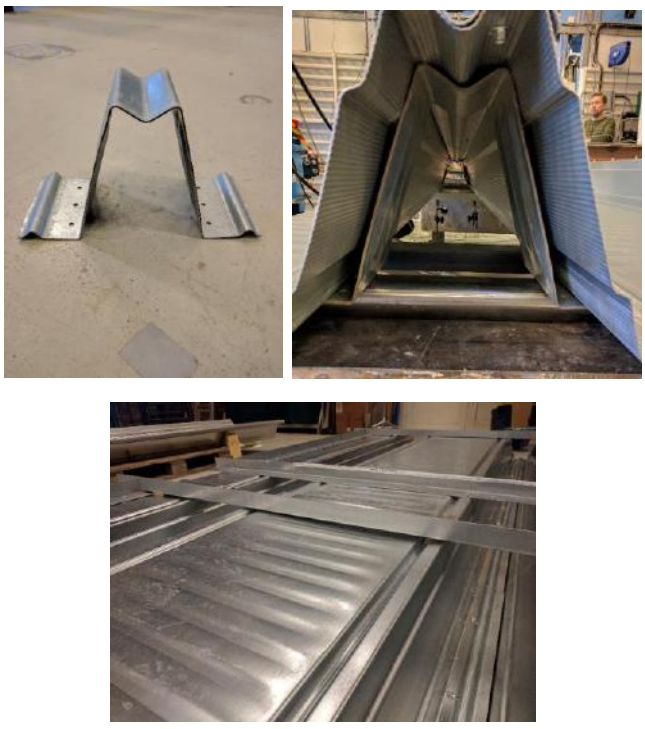

Figure 3.2 Accessories used in the Test

- **EN 1993-1-3 A.3.2 Double span test:** this point gives the appropriate set-up to make a continuous beam over two or more spans. But since modelling the real span lengths of the test is a lot of time consuming and occupies a lot of space in the test, an alternative also from EN-1993-1-3 was used to measure test the internal support.

- **A.3.4 Internal support test:** EN1993-1-3 gives the alternative test set-up for an internal support test of a continuous beam with two or more spans. This set-up consists in using the distance of the points of contra-flexure of the bending moment diagram for a continuous beam at the support that is going to be studied. The load applied will simulate the up-lifting force acting in the support generated by the bending moment.

  The advantages of this procedure are that it is a lot simpler to analyze, it occupies much less space in the laboratory and it is easier to assembly, resulting in a good and efficient way analysis. Figure 3.3 shows this procedure.

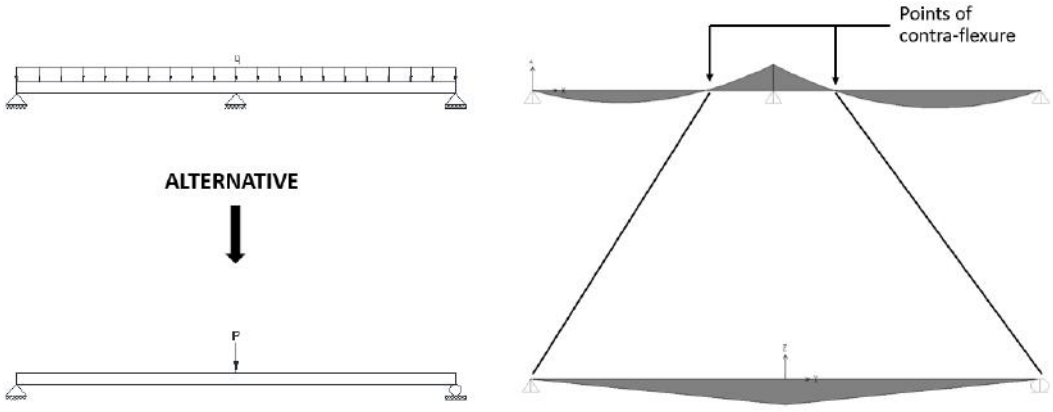

Figure 3.3

3.1 Experimental Test Configuration

As mentioned before, since we are looking the behavior of the single overlap joint over the mid-support, the negative bending moment in that area is the critical action of the system. In this sense, the segments where the bending moment is equal to zero are considered as simply supported boundary conditions in the experiment, and instead of a mid-support, a displacement is applied to study the deformation. Figures 3.4 and 3.5 show the distributed load and the bending moment diagram over the real spans.

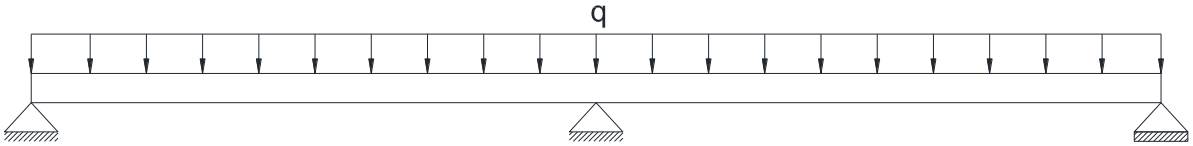

Figure 3.4

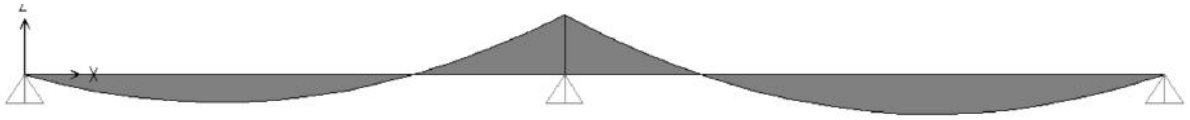

Figure 3.5

In the real structure, both profiles have the same length, but it is because of the overlap connection that the spans of this system are different. In this case the first span (the one on the left), has 7.20m in and the second span is 8m (figure 3.6).

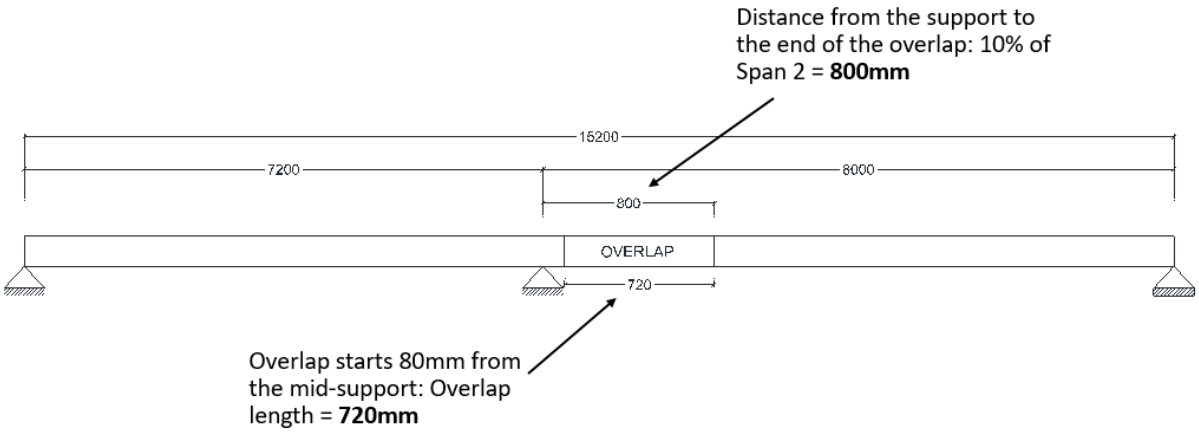

Figure 3.6

The distances from the mid-support to where the bending moment is equal to zero are 2m and 1.82m for span 1 and span 2 respectively as shown in figure 3.7. The profile is also set upside down to avoid any complications and simulate the behavior of the system under a distributed load.

By applying the testing procedures from EN1993-1-3 to the lengths used for the test, will lead to the following configuration:

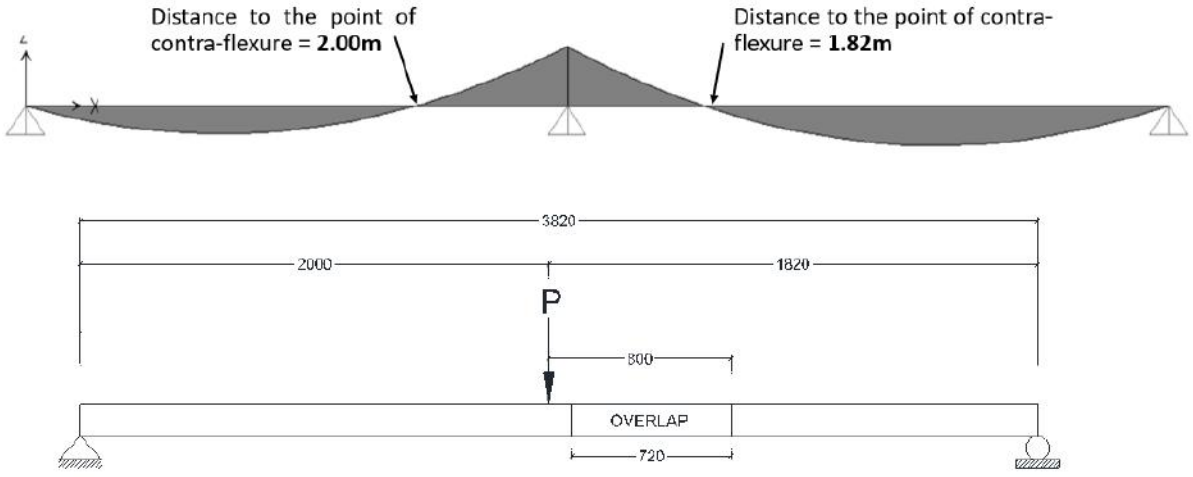

Figure 3.7

As shown in figure 3.8, the profile is turned upside-down to simulate a lifting load that a negative bending moment will produce in a mid-support. In this figure, we can also see de connection details of the overlap. It is important to mention that for the thicker profile, three screws are used in the web of the profile to give more resistance (figure 3.9).

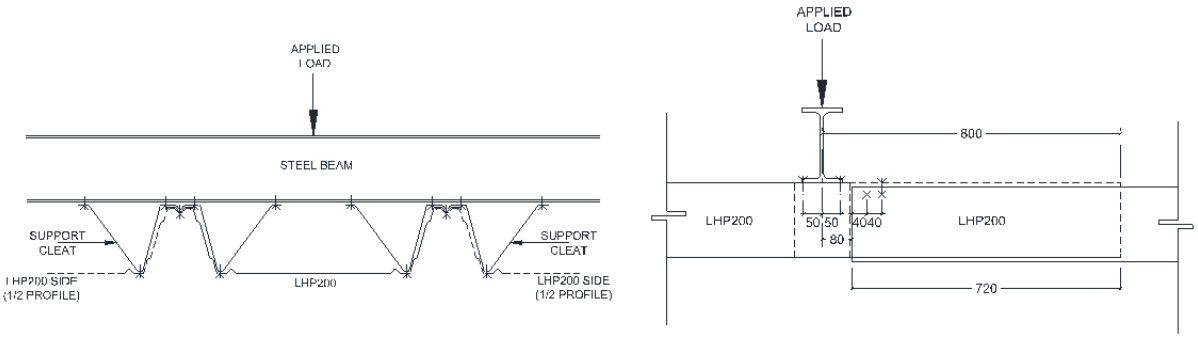

Figure 3.8 Overlap Connection Details

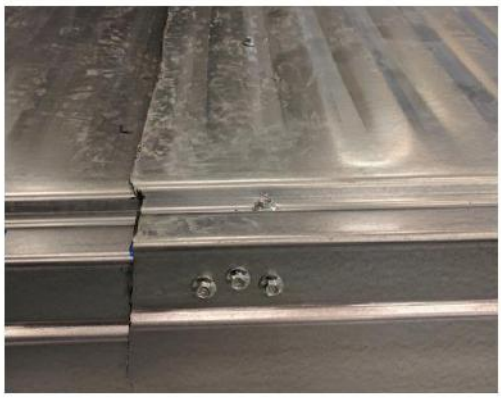

Figure 3.9 LHP200 profile, t=1.50mm

Note in figure 3.8 that one half of the LHP200 profile on each side is also set in the configuration, the idea of this is to simulate the continuity of that the roof system will have in the real situation.

The displacement will be applied with a hydraulic actuator to the steel beam at a rate of 2mm/min, and 12 points of interest will be chosen to measure the force-displacement relation. With this relations, stiffness and rotations of the new modified joint, and to find the residual bending moment in the support after failure will be found.

The points of interest were chosen with the purpose of being able to measure the displacement of the beam, the displacement of the top flanges and the gap between the profiles in the overlap (figure 3.10).

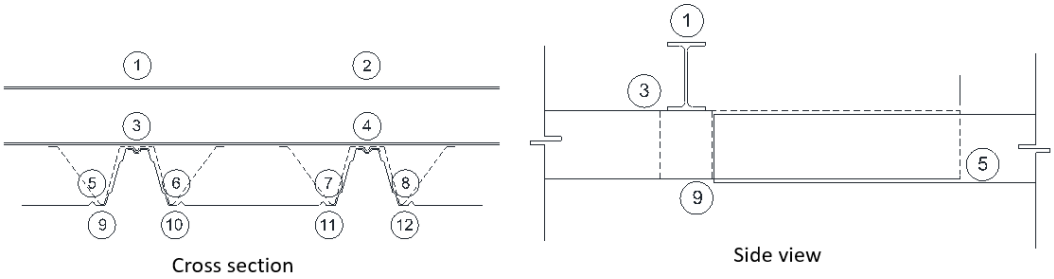

Figure 3.10

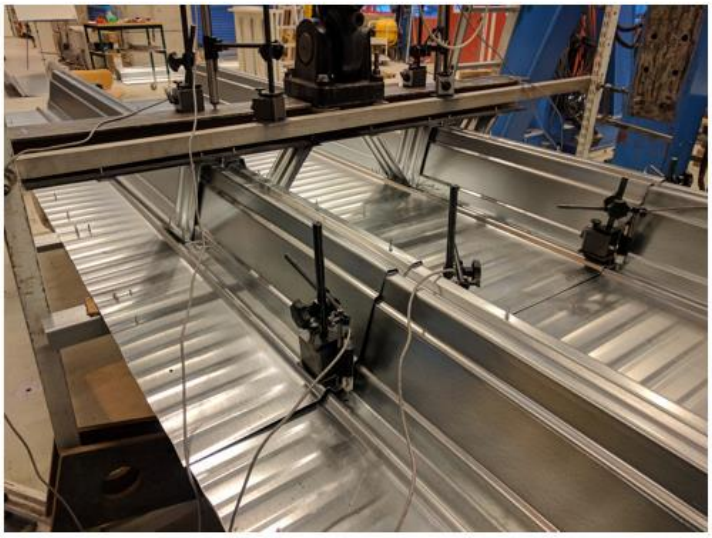

Figure 3.11 LVDT's placed in position

It is important to mention that the behavior of some points should have big similarities to follow the continuity of the system. For example, point 5 should be really similar to point 7, and point 10 to point 12, and so on.

The sing convention of the LVDT's is shown in figure 3.12:

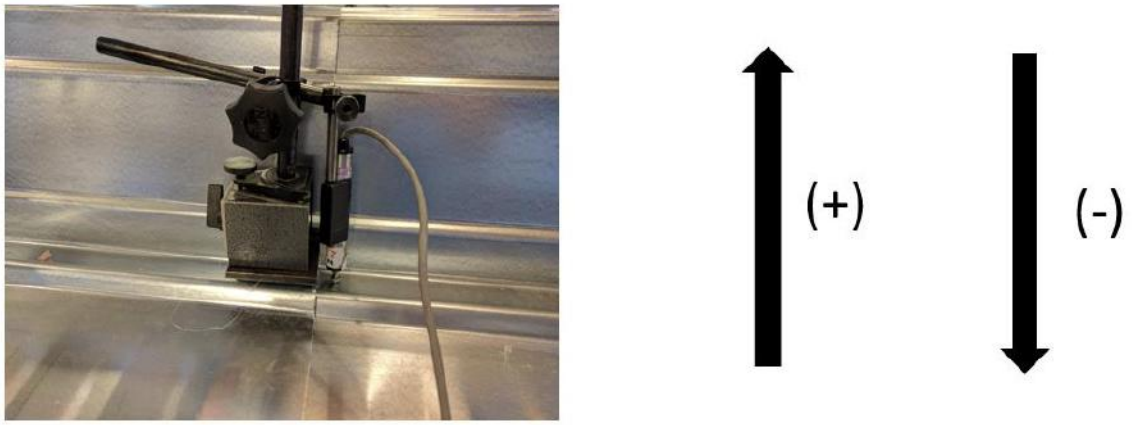

Figure 3.12 LVDT's Sing Convention

This means that when the LVDT closes it will register a positive displacement, and a negative displacement when it opens.

3.2 Experimental Test Results

In this section, we will check the similarities between the points that were mentioned before. There will be shown only some points of some tests, but all the graphs will be included in the Annex.

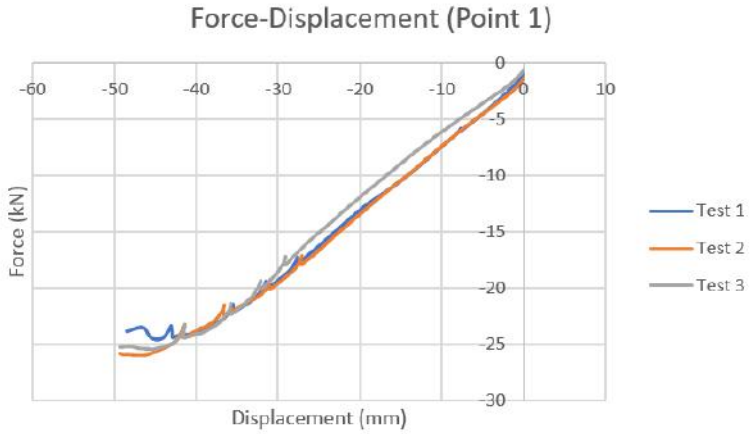

Graph 3.1 Force-Displacement of the Three Tests at Point 1

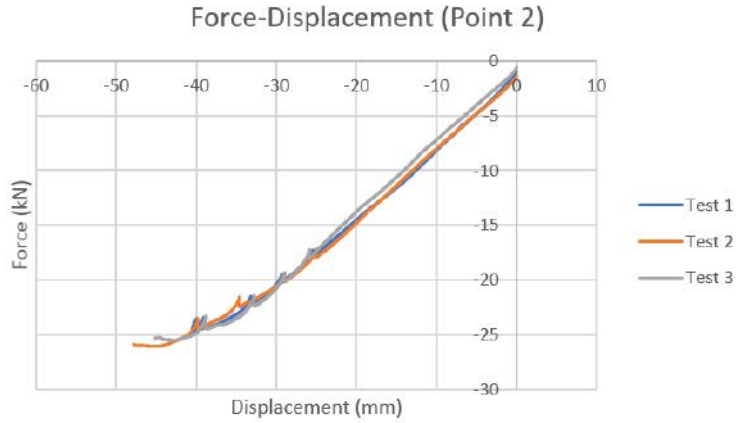

Graph 3.2 Force-Displacement of the Three Tests at Point 2

Test	Max. Force (kN)	Disp. Point 1 (mm)	Disp. Point 2 (mm)
1	-24.648	-44.607	-40.292
2	-26.028	-47.737	-46.021
3	-25.488	-45.066	-42.504

Table 3.1 Displacements of Points 1 and 2 at the Max. Load

As shown in the previous graphs, all the points have almost the same behavior, which means that the tests were consistent. We can also appreciate this in table 3.1 which shows the displacements at the maximum load.

The same case is for points 5 and 7, which correspond to the top gap measurement:

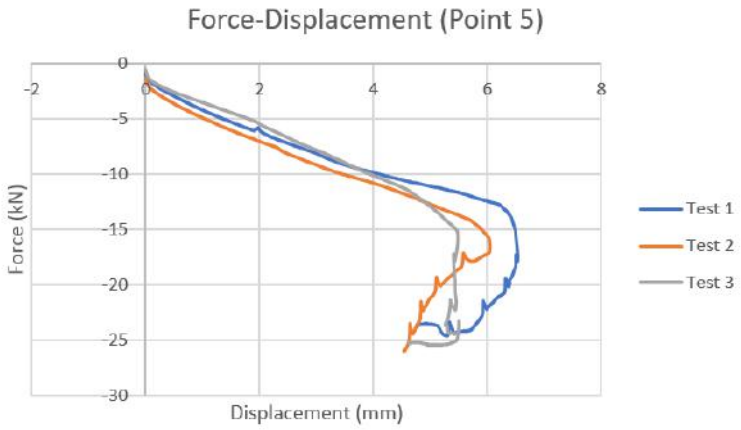

Graph 3.3 Force-Displacement of the Three Tests at Point 5 for a Thickness of 0.85mm

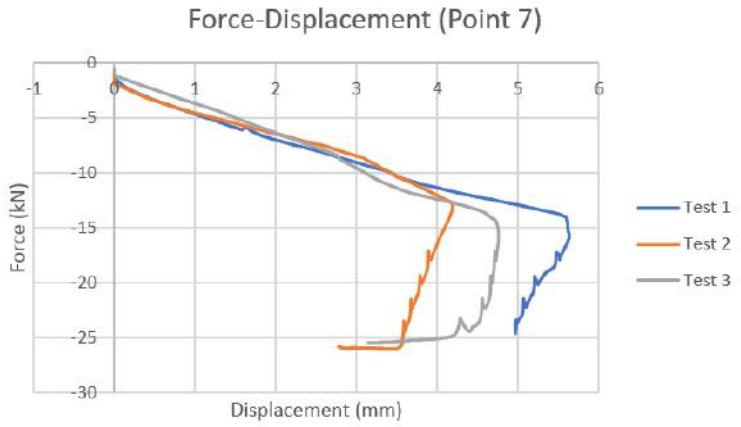

Graph 3.4 Force-Displacement of the Three Tests at Point 7 for a Thickness of 0.85mm

Test	Max. Force (kN)	Disp. Point 5 (mm)	Disp. Point 7 (mm)
1	-24.648	5.292	4.965
2	-26.028	4.540	3.309
3	-25.488	5.186	3.280

Table 3.2 Table 3.3 Displacements of Points 5 and 7 at the Max. Load for a Thickness of 0.85mm

Next, the comparison between points 1 and 2 are seen in graph 3.5, and between points 5 and 7 in graph 3.6:

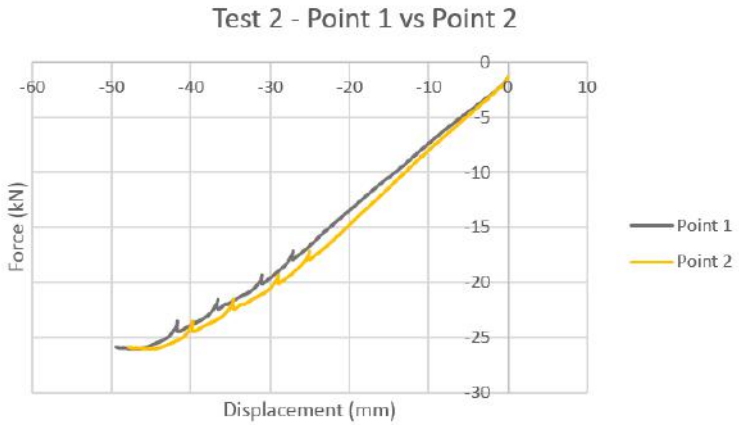

Graph 3.5 Force-Displacement Point 1 vs Point 2; Test 2 for a Thickness of 0.85mm

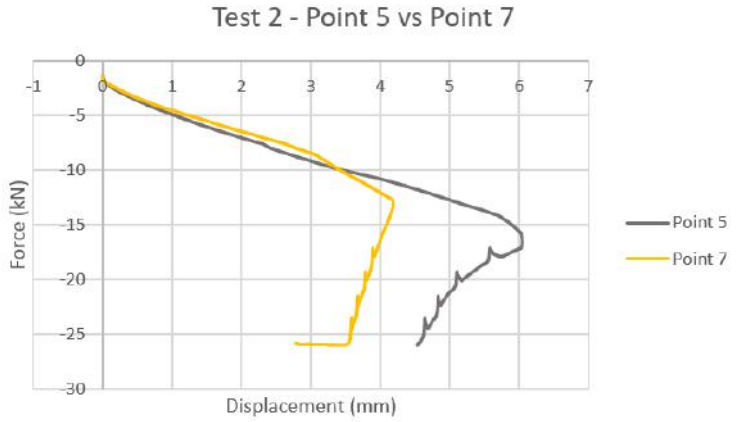

Graph 3.6 Force-Displacement Point 5 vs Point 7; Test 2 for a Thickness of 0.85mm

To be able to calculate the stiffness by a theoretical analysis, an average was calculated for the points that correspond to displacements that will influence the stiffness of the overlap. For example, the average of points 1 and 2 will correspond to the displacement of the whole system, the average of points 5 to 8 will be the displacement of the top gap and the average from points 9 to 12 is the bottom gap. The following graphs show the displacement and average displacement of some of the points.

Since we are mainly interested in the behavior of the overlap connection before the failure of the system, we limit to work with the values that are in the elastic range at around 95% of the maximum load.

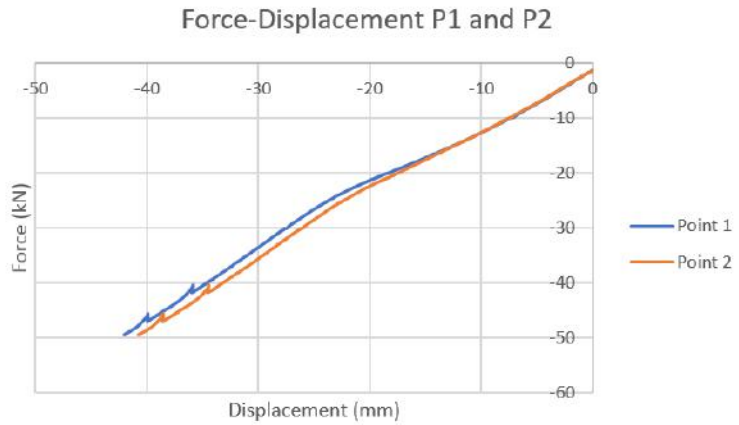

Graph 3.7 Displacement of Point 1 and 2 in Test 3 for a Thickness of 1.50mm

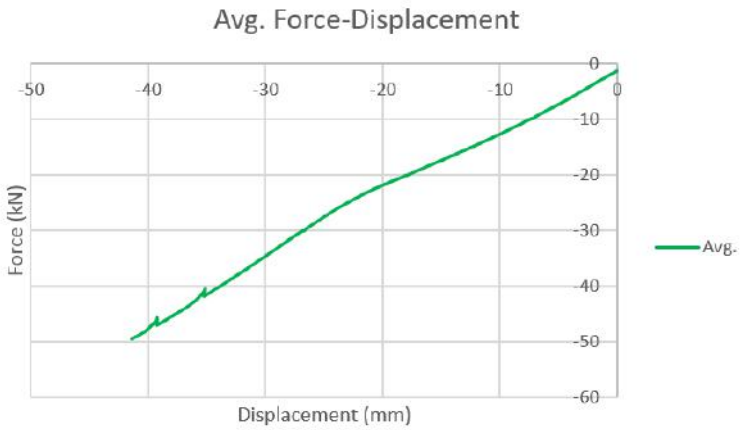

Graph 3.8 Average Displacement of Point 1 and 2 in Test 3 for a Thickness of 1.50mm

Graph 3.9 Displacement of Point 5 to 8 in Test 3 for a Thickness of 1.50mm

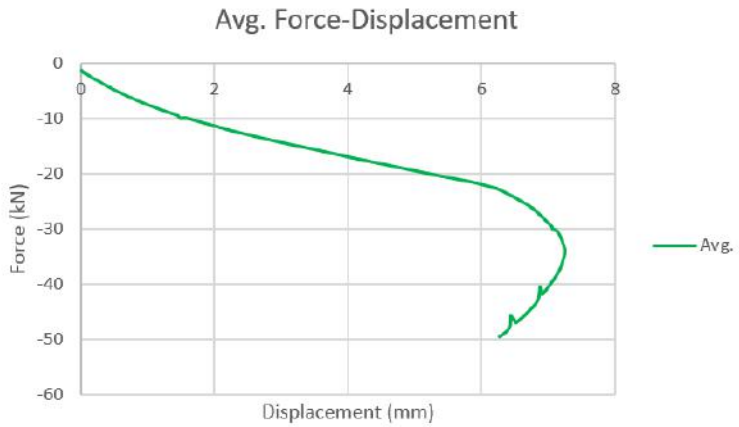

Graph 3.10 Average Displacement of Point 5 to 8 in Test 3 for a Thickness of 1.50mm

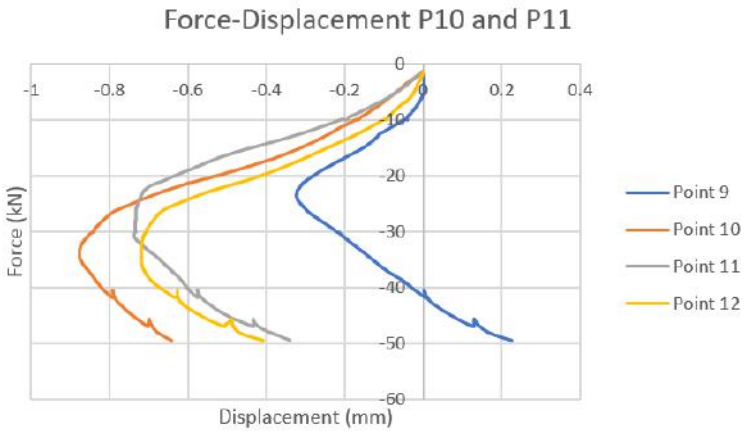

Graph 3.11 Displacement of Point 9 to 12 in Test 3 for a Thickness of 1.50mm

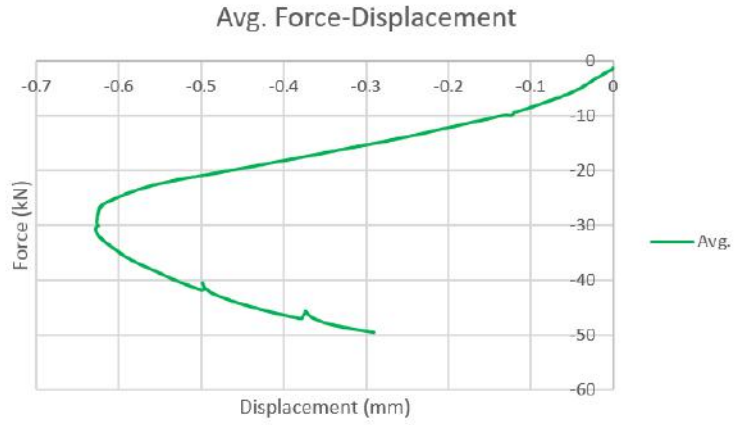

Graph 3.12 Average Displacement of Point 9 to 12 in Test 3 for a Thickness of 1.50mm

Graphs 3.8, 3.10 and 3.12 represent the total displacement of the system, the top gap and the bottom gap respectively at 95% of the maximum load. Remembering the sign convention of the LVDT's mentioned before, we can wee that the top gap tends to close and the bottom gap to open in relation with the systems deflection.

Before continuing with the theoretical analysis for obtaining the spring stiffness in the overlap, it is important to understand what happens to the profiles during the tests, and to see the points of failure and local buckling and deformations.

3.2.1 Buckling and deformations

The following figures are the most significant deformed shapes and buckling, or any significant behavior that can help to understand what happens in this type of connection.

- t=0.85mm

Figure 3.13 Local Web Buckling of LHP200, t=0.85mm

We can see in figure 3.13 that there are compression forces acting in the web of the profiles which produce local buckling. First, the buckling starts in the bottom profile and then it propagates to the top profile until the whole system fails. In this part of the connection, the upper profile wants to lift the lower one, but the connection screws have reaction forces that want to keep them apart, therefore we have this behavior.

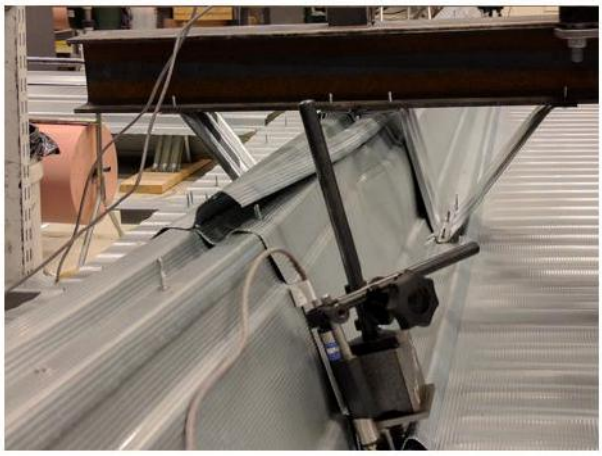

Figure 3.14 Pull-Out of the Side-Overlap Connection Screws

After the failure of the system, the load was still applied, and we can see here that the overlap connection has a pull-out failure, but it is important to be clear that this is not the reason of the system failure.

- t=1.50mm

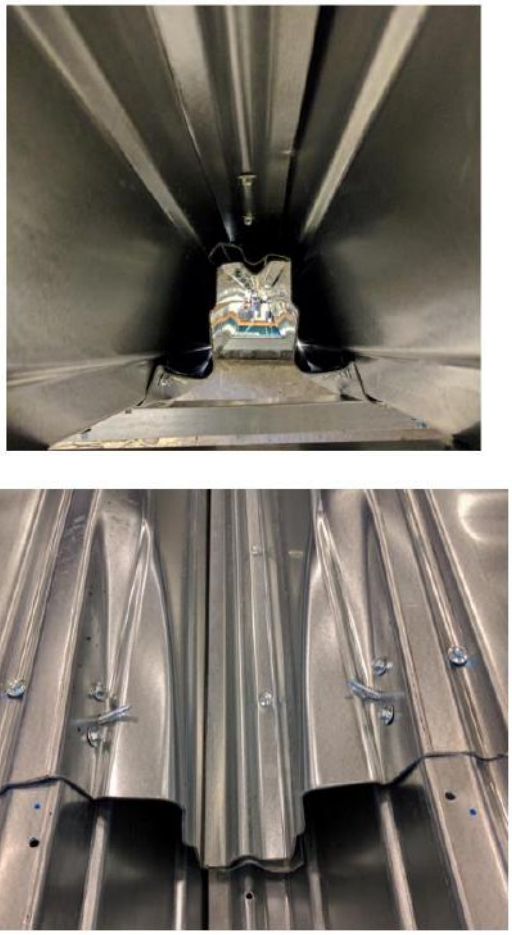

Figure 3.15 Local Web Buckling of LHP200, t=1.50mm

For this thickness, we can see that we have the same buckling behavior in the bottom profile, however in this case, the buckling does not propagate to the top profile and instead the side overlap connection screws have a tensile failure which make the whole system fail (figure 3.16).

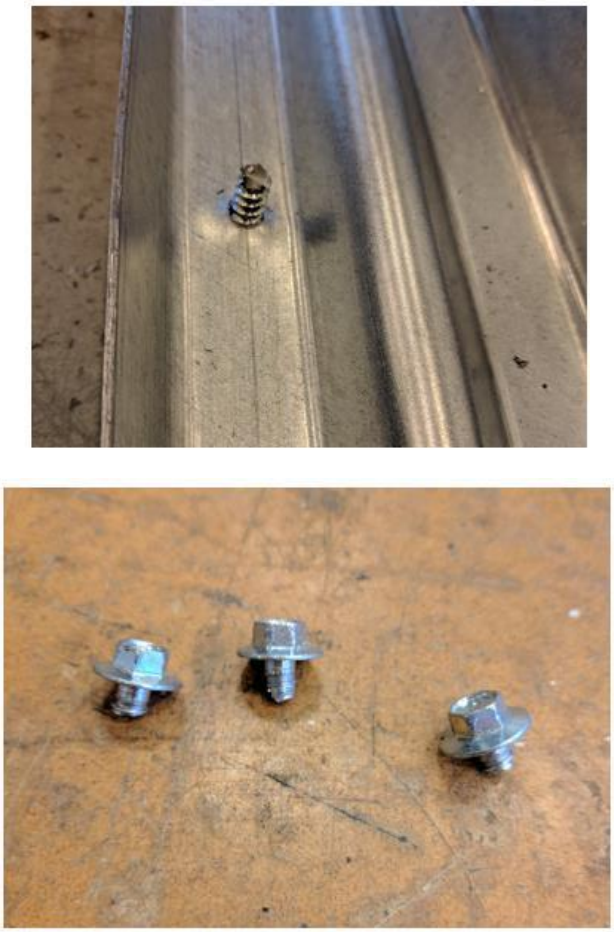

Figure 3.16 Tensile Failure of the Side-Overlap Connection Screws, LHP200, t=1.50mm

It is important to point out that all the tests have exactly the same type of failure in the same position, and that failure always occurs in the side where the half side profile is on the top using the test configuration as reference.

4 Computation of the overlap stiffness

4.1 Contribution of the overlap to the structure's deflection

Graph 4.1 show the experimental force-displacement of the system and the theoretically calculated displacement without considering the overlap.

We can notice that there is a difference in the displacement that is due to the contribution of the overlap, so to be able to calculate this contribution, first we need to understand what happens in this part of the profiles.

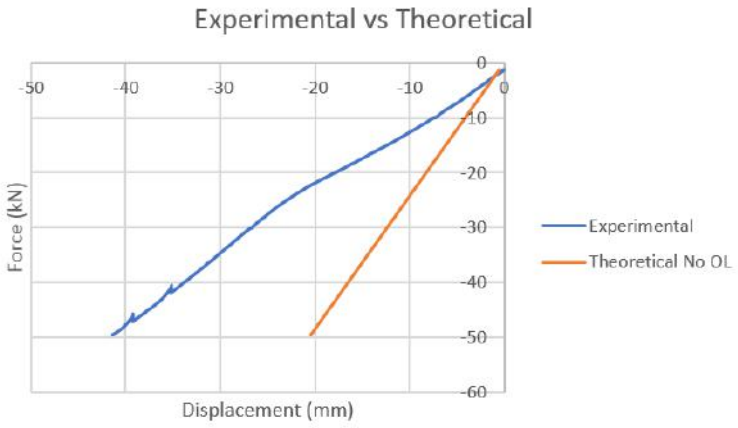

Graph 4.1 Experimental vs Theoretical Force-Displacement

As we mentioned in the previous chapter, the top gap tens to close and the bottom gap tends to open when the whole structure has a deflection. To understand the behavior of the overlap under these conditions, we can separate the profiles and evaluate the forces acting in the overlap due to a global load "P" (figure 4.1).

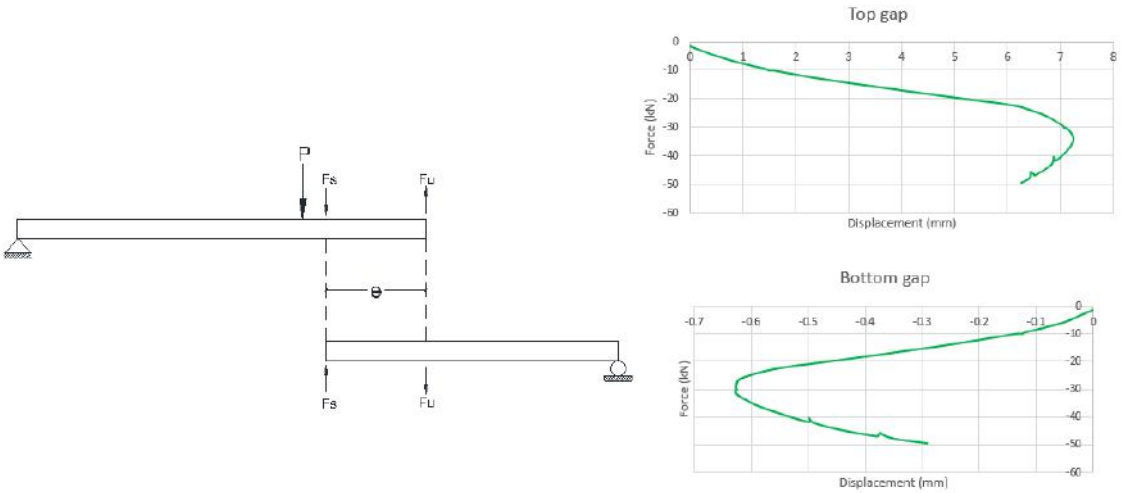

Figure 4.1 Internal Forces in the Overlap

"Fs" is the force that depend on the overlap connection screws that keep the profiles from separating, and "Fu" is the force that depend on the profiles that prevent the sheets from closing, while a global force "P" is acting in the system.

The following figure represents the behavior of the overlap, and it's a simplification of figure 4.1. In here we can see the same forces "Fs" and "Fu" represented as a moment "M" divided by the overlap length "e". We can also see that there is a spring stiffness acting in the connection.

To get these value of the M/e, we would have to compute for the value of the bending moment acting where the force "Fs" is located, and divide it by the overlap length. Instead, since we already have the values of the forces of the load "P" applied, and because they are very close to each other, we compute for the bending moment at the load point by using a formula for a simply supported beam shown in figure 4.3, and which will leave us in the safe side.

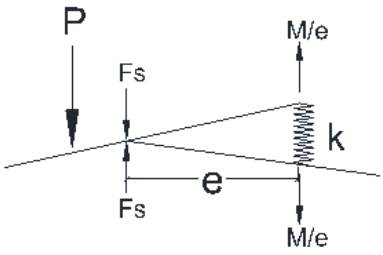

Figure 4.2 Overlap Connection Diagram

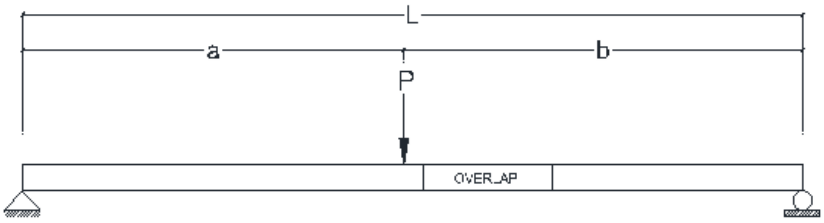

$$M = \frac{Pab}{L}$$

Figure 4.3 Simply Supported Beam Bending Moment

Once we have the bending moment at that point we can have the force acting in the overlap. Similarly, we could compute for the force "Fs" with the difference that we would need the bending moment acting where the "Fu" load is.

After this we need to compute for a factor "f" that will depend on the spans and overlap lengths, and it will be the relation between the total gap between the profiles and the overlap displacement.

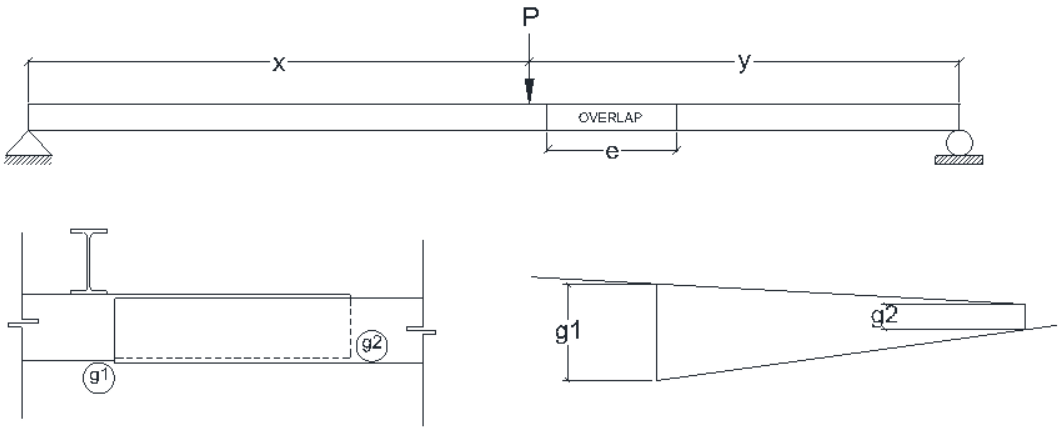

Figure 4.4 Gaps in the Overlap Connection

Figure 4.4 show the two gaps acting on the profile, which with the experimental test results, saw that one opens and one closes. These two gaps can be added together and take it into account as a single total gap to find the relation with the overlap deflection.

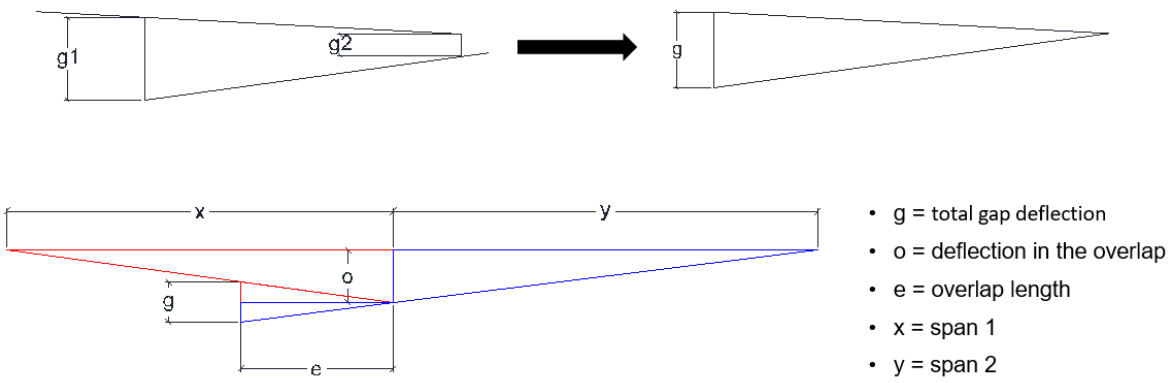

Figure 4.5 Relation of Triangles of the Overlap Deflections

Once we have the total gap, we can make the relation between the triangles. In figure 4.5, we can see that the big triangles represent the overlap displacement, and the small ones the gap between the profiles. We can also observe that the red triangles are similar and the same for the blue triangles.

If we want to know how much the overlap displacement will be when the gap has a value of 1mm, we can have the following expressions:

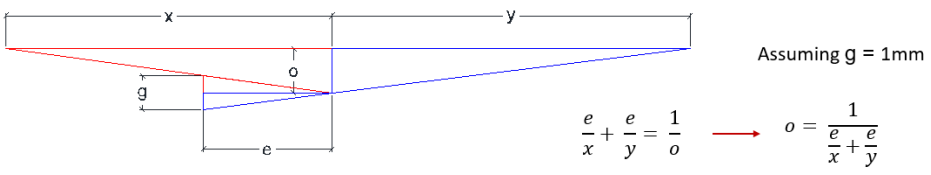

Figure 4.6 Computation of Factor "f"

And by substituting the values of our Test we have:

$$o=1.32mm$$

which means that each millimeter in the gap will produce 1.32mm in the overlap, hence:

$$f=1.32$$

By using the values from the test and the theoretical value at a certain load, we can check if the factor is correct:

δ = deflection of the whole system (experimental test) = -41.42mm

δt = deflection without considering the overlap (theoretical) = -20.44mm

δo = deflection of the overlap ($\delta - \delta t$) = -20.98mm

δg = total gap between the profiles (experimental test) = 6.55mm

Should satisfy:

$$\delta g \cdot f = \delta o$$

$$6.66\ (1.32) = 8.646$$

As we can see, by multiplying the gap with the factor, we don't have the deflection of the overlap. The possible reasons for this is that as the system bends, local buckling occurs in the web where the overlap connection in located (figure 4.7). This deformation could be missing from the deflection measured in the gap.

A better way to measure the gap between the profiles could be by somehow placing the LVDT's in a way to measure the gap between the webs instead of the flanges.

Another possibility is that as the system bends, the LVDT's on the top start to rotate, resulting in possible changes in measurements (figure 4.8). It will be interesting to place the LVDT's in a way that the deformation of the profiles does not affect in any way its position, and see if there are any significant differences.

Figure 4.7 Web Gap Between the Profiles

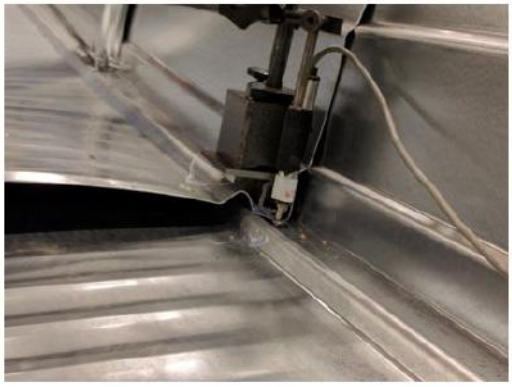

Figure 4.8 Rotation of LVDT

As we mentioned, the overlap has an influence in the deflection of the system, and the contribution of the overlap to this deflection must be represented:

$$\delta = \frac{Px^2y^2}{3EIL} + \frac{M}{e}fk \tag{4.1}$$

And by solving for a thickness of 0.85mm k:

$$k = \left[\delta - \frac{Px^2y^2}{3EIL}\right]\frac{e}{Mf} = 0.0004269\frac{mm}{N}$$

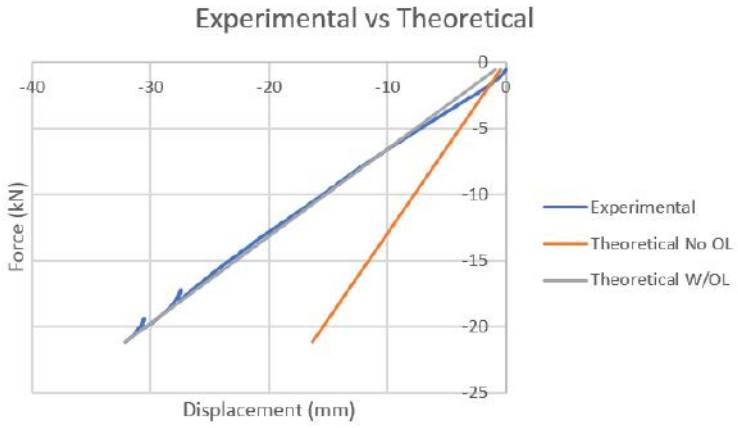

Graph 4.2 Experimental vs Theoretical vs Theoretical W/Overlap; t=0.85mm

And for the profile with t=1.50mm:

$$k = \left[\delta - \frac{Px^2y^2}{3EIL}\right]\frac{e}{Mf} = 0.0002419\frac{mm}{N}$$

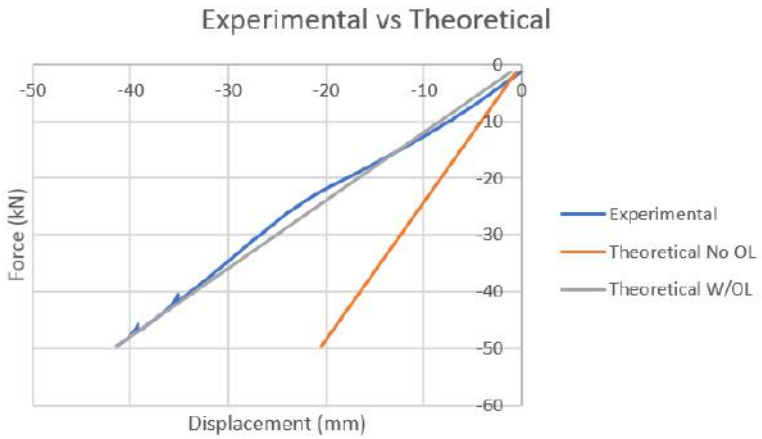

Graph 4.3 Experimental vs Theoretical vs Theoretical W/Overlap; t=150mm

We can see that for both profiles that when we add the overlap deflection to the theoretical deflection we have similar results for the Force-Displacement in the experimental test and the theoretical considering the overlap.

5 Finite Element Model

The finite element analysis was made using Abaqus/CAE 6.14 software. It is divided into modules, where each module defines a logical aspect of the modeling process. As you move from module to module, you build the model from which the software generates an input file that you submit to analysis. After the analysis is completed, you can visualize a deformed shape of the of the elements and read the output of the results [7].

5.1 Description

The aim of the Finite Element Model is to do an exact simulation of the experimental test so that a parametric study can be made later. Thus, the model is made as close as possible to the test, by using the same thicknesses, span lengths, boundary conditions, material properties and load application. As mentioned in the previous chapter, the experimental test will be made with the lowest and highest thicknesses of the LHP200 profiles, that being the case, there will be two different FE models as well, simulating these two tests.

Since Abaqus software is unitless, a unit configuration must be adopted since the beginning, and one must be careful to keep track of it to avoid further errors on the analysis. The following table shows the units used:

Length	Force	Stress	Time
mm	N	MPa	s

Table 5.1. Units Used in the FE Model

5.1.1 Part

Since the geometry of the LHP200 profile is a bit complex to create in Abaqus, the different parts used were first made in Autodesk AutoCAD software, and then imported to the model as ".sat" files. By doing this, we facilitate the creation of the whole model, and it will give us a first view of how are model will look.

Two different lengths of LHP200 profiles were used one of 1740mm (figure 4.1(a)) and another of 2800mm (figure 4.1(b)) which correspond to the spans of 1820mm and 2000mm respectively.

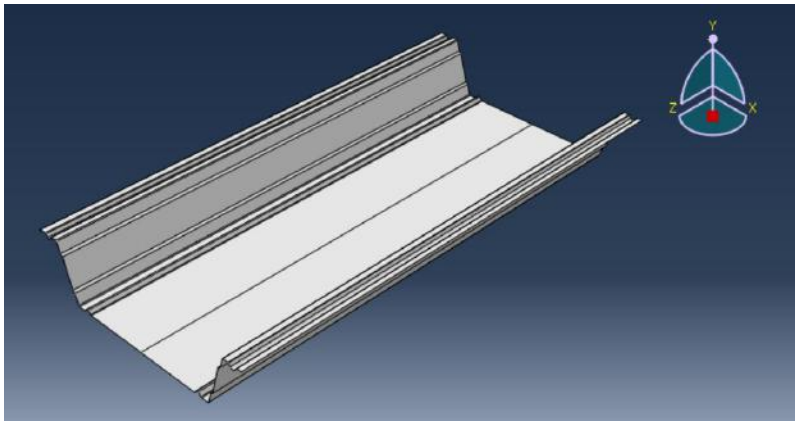

(a)

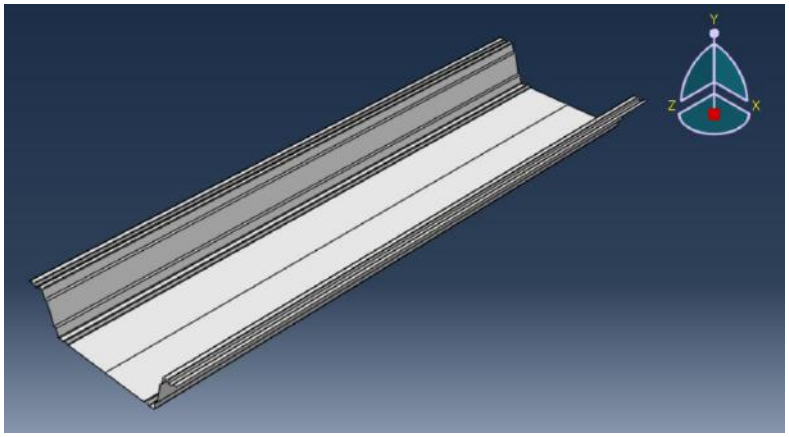

(b)

Figure 5.1 LHP200 Profiles

And used in the test, side profiles cut in half in the longitudinal direction for both 1740mm and 2800mm are created as shown in figure 4.2(a) and (b) respectively.

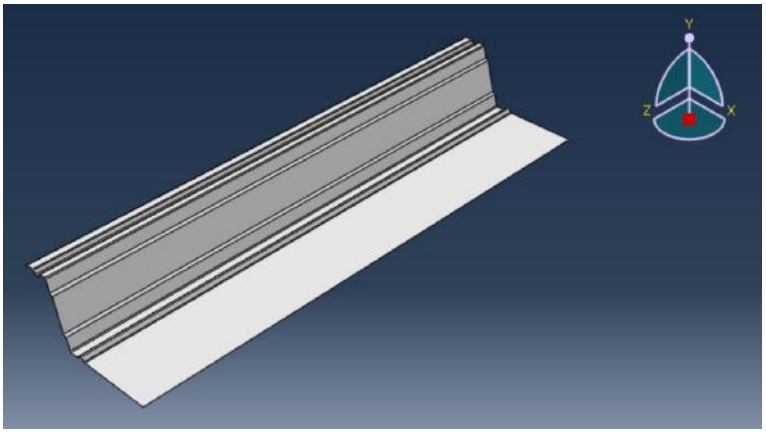

(a)

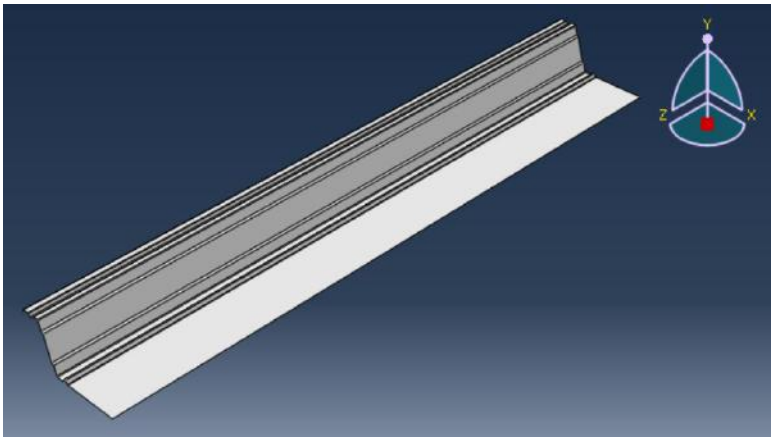

(b)

Figure 5.2

The support cleats are of 150mm (figure 4.3) and they are placed along the displacement application area, which is the overlap support. Note that the support cleat does not have the "ribs" that the real profile has. In order to simulate the rigidity of the real support cleat, a bigger thickness is used providing a bigger stiffnes.

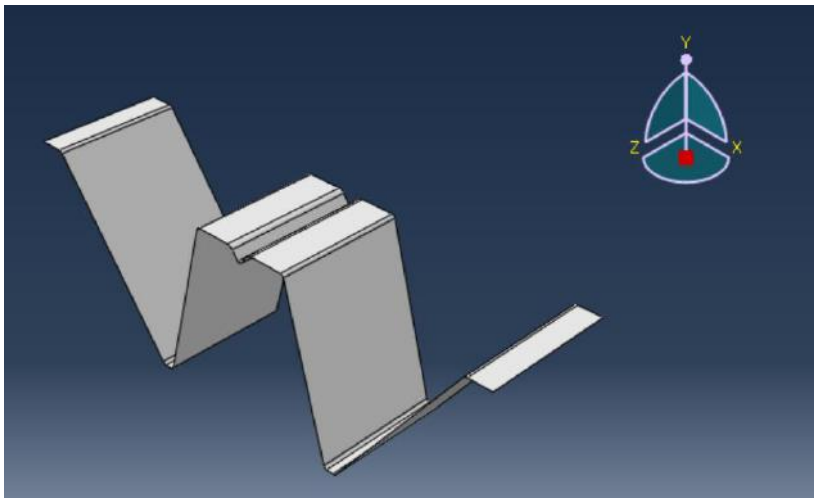

Figure 5.3 Support Cleat

And finally, a hollow section of 200x200mm (figure 4.4) which is used to transfer the displacement in all the support cleats.

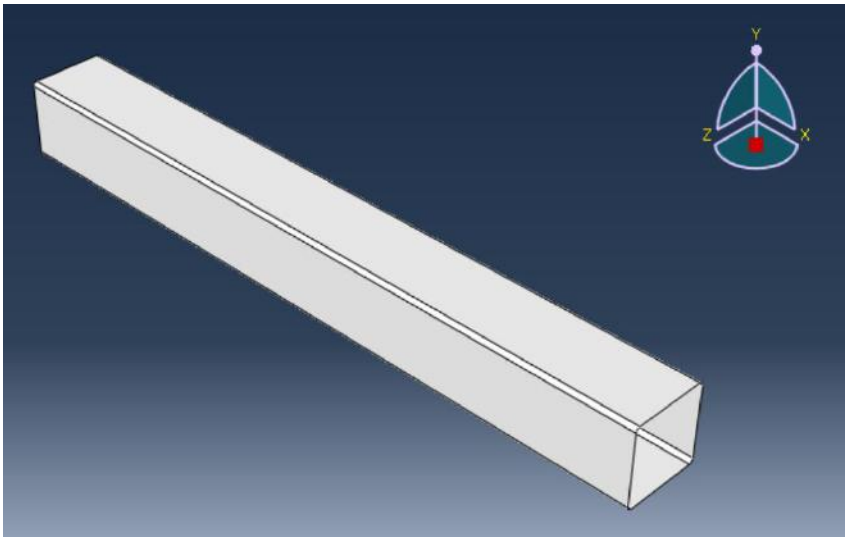

Figure 5.4 Hollow Section 200x200mm

5.1.2 Property

In this module, the properties of the parts made are defined. First, we start by creating the material that will be used in our sections. In this case, all the sections are made of steel with a yield strength of 420MPa, with the exception of the LHP200 profiles and support cleats with a thickness of 1.5mm, which have a yield strength of 350MPa. Table 4.2 shows the properties of the parts used.

Part	Length (mm)	Thickness (mm)	Modulus of Elasticity (MPa)	Poisson's Ratio
LHP200	1740	0.85	420	0.3
LHP200	2800	0.85	420	0.3
1/2 LHP200	1740	0.85	350	0.3
1/2 LHP200	2800	0.85	350	0.3
Support Cleat	150	3.00	420	0.3
Hollow Section	3500	6.30	420	0.3

Table 5.2. Part Properties

The values of stress-strain relationship are obtained from a tensile test with a specimen with the same material yield strength properties, and it shown in the next graph.

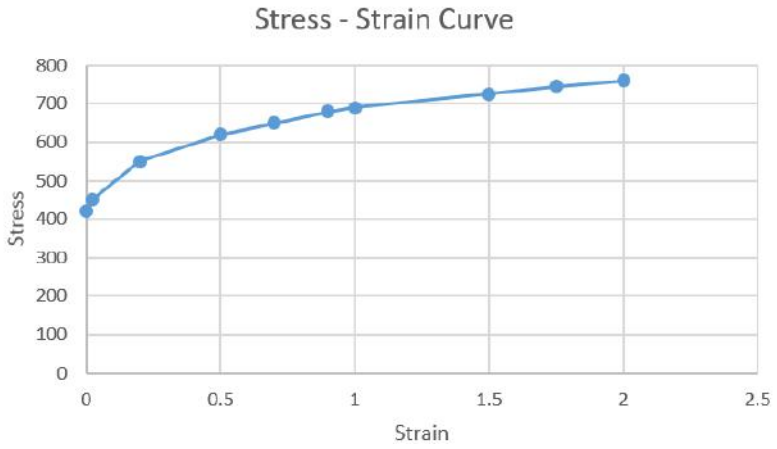

Graph 5.1. Stress-Strain Relationship

5.1.3 Assembly

The assembly module is where the part instances are created and arranged according to our specifications, which in this case is the experimental test. This instances come from the parts created before, and they include all the properties as well.

As mentioned in Chapter 3, only the segment between the points of contra-flexure on each is arranged, thus the model is assembled the same way (figure 5.5).

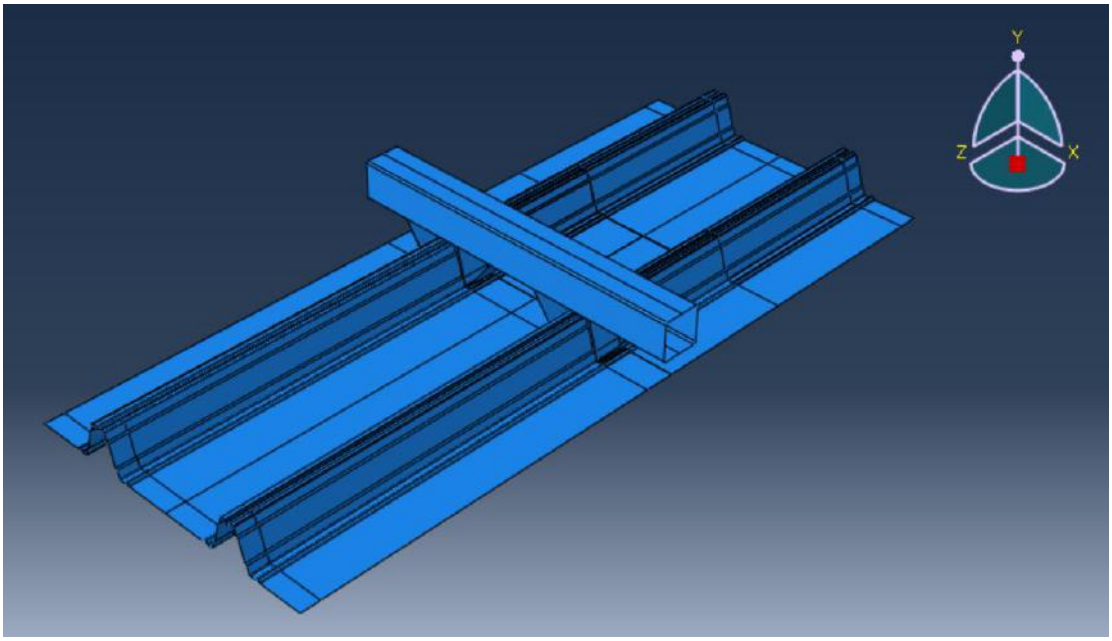

Figure 5.5. FE Model Assembly

5.1.4 Step

The step will define the type of analysis that the software will use. In this master thesis, a "Static, Riks" procedure was selected, which is a load-displacement analysis, that uses the "arc length" along the static equilibrium path in load-displacement space. This method provides solutions whether the response of the structure is stable or unstable.

In this model the following parameters for time incrementation and arc length are used:

Maximum Number of Increments	200
Initial Arc Length Increment	0.01
Minimum Arc Length Increment	1E-008

Maximum Arc Length Increment	0.1
Estimated Total Arc Length	1

Table 5.3. Parameters for Static, Riks Analysis.

Thin shell profiles, like the ones used in this model suffer large deformations when a load or a displacement is applied, and geometric non-linearity is recommended. In order to include a non-linear geometry in the "Static, Riks" analysis, the NLGEOM option is activated in the step definition. This means that the load-displacement curve will no longer be proportional, and that there is geometric non-linearity due to the changes in geometry during the analysis.

5.1.5 Interaction

Surface to Surface Interaction

In this module, the interaction properties of the different instances created previously are defined. Considering that an overlap joint between the shell profiles is studied, surface interactions between the elements are very important to take into consideration in the analysis.

In this case, we have different type of material surfaces, that means that the interaction between some elements will behave differently. The LHP200 profiles are galvanized shell elements, hence a Zinc coat is considered in the steel. In the case of the Support Cleats and the Hollow Section, no coating is present in the surface and only the steel is considered.

Due to the different surface materials, three different Interaction Properties are defined, *Zinc-Zinc* and *Zinc-Steel*, for the surface contact of the different materials. Each Interaction Property has a *Normal Behavior*, and a *Tangential Behavior*. The next diagram shows the properties of the different surface interactions.

$$\text{Zinc} - \text{Zinc} \begin{cases} \text{Normal} \{\text{Pressure Overclosure} \rightarrow \text{Hard Contact} \\ \text{Tangential} \begin{cases} \text{Friction Formulation} \rightarrow \text{Penalty} \\ \text{Friction Coefficient} \rightarrow 0.6 \end{cases} \end{cases}$$

$$\text{Zinc} - \text{Steel} \begin{cases} \text{Normal} \{\text{Pressure Overclosure} \rightarrow \text{Hard Contact} \\ \text{Tangential} \begin{cases} \text{Friction Formulation} \rightarrow \text{Penalty} \\ \text{Friction Coefficient} \rightarrow 0.5 \end{cases} \end{cases}$$

After creating the interaction properties, the surface interactions are defined, this is when the surfaces that will be in contact are selected in the model. In this case, four interactions are made, one for the overlap between the LHP200 over the joint, another for the side overlap between the LHP200 profiles, one for the contact between the support cleats and the LHP200 profiles and one between the hollow section and the support cleats.

Each interaction has its own master and slave surfaces, and the properties vary depending on the surface material of the instances.

Interaction	Interaction Property	Sliding Formulation	Discretization Method
LHP200 - LHP200 Joint Overlap	Zinc - Zinc	Finite Sliding	Surface to Surface
LHP200 - LHP200 Side Overlap	Zinc - Zinc	Finite Sliding	Surface to Surface
LHP200 - Suppor Cleats	Zinc - Steel	Finite Sliding	Surface to Surface
Support Cleats - Hollow Section	Steel - Steel	Finite Sliding	Surface to Surface

Table 5.4. Interaction Properties According to Each Interaction

Connector Sections and Fasteners

Besides the surface interaction between the instances, in this module, the connector sections and the fasteners to attach all the instances are defined. According to Lindab's specifications, the LHP200 profiles use 6.3D32F Self Drilling Screws to make the connection between the profiles and between the profile to the support cleats, and fire shot nails to attach the support cleats to the support.

The connector sections define the design values of the resistance of the screws, which are derived from EN-1993-1-3: Bearing, Pull Out, Pull Through, Shear and Tensile resistance. In this case, since the only relevant failure observed in the experimental test was the tensile failure, only this is used. These design values were taken from the specifications tables of the fastener supplier of the company which are shown next.

Screw material	Screw diameter ϕ mm			
	4.8	5.5	6.3	8.0
Carbon steel, case hardened	4.99	6.91	9.41	15.6
Stainless steel	4.42	6.24	8.16	13.7

Table 5.5. Tensile Design Values

For a screw with 6.3mm diameter we have a tensile design value of 9.41kN

Fasteners

The fasteners used in both models are point based fasteners, which were implemented with attachment points. There are fasteners for each connection between all the elements of the structure (LHP200 to LHP200, LHP200 to support cleat, etc.), and each fastener has its corresponding connector section.

The approach used for the fasteners is “fasten specified surfaces by proximity” which mean that one specify the surfaces to connect to each other. The they all have a physical radius of 3.15mm which correspond to the 6.3D32F Self Drilling Screws, and they all have *UR1*, *UR2*, and *UR3* constrained degrees of freedom.

Constraints

In order to truly model a simple supported element, a kinematic constraint is defined for each LHP200 profile in both ends. First the centroid of the profiles was found using Autodesk AutoCAD (figures 4.6 (a) and (b)), and 6 reference points were created in the centroid of each profile at both ends. This reference points are the kinematic constraints master nodes, while the edges of the profiles are the slave surfaces (figure 4.7).


```
Command: MASSPROP

Select objects: Specify opposite corner: 1 found

Select objects:

 ----------------   REGIONS   ----------------

Area:                     1038.9180
Perimeter:                2446.2130
Bounding box:           X: -444.7051  --  434.0000
                        Y: -0.4250  --  199.4250
Centroid:               X: -5.8038
                        Y: 65.4632
Moments of inertia:     X: 10868704.6808
                        Y: 79919767.9119
Product of inertia:    XY: -1176598.3063
Radii of gyration:      X: 102.2818
                        Y: 277.3553
Principal moments and X-Y directions about centroid:
                        I: 6408179.0525 along [0.9999 -0.0106]
                        J: 79893093.3240 along [0.0106 0.9999]
```

(a)

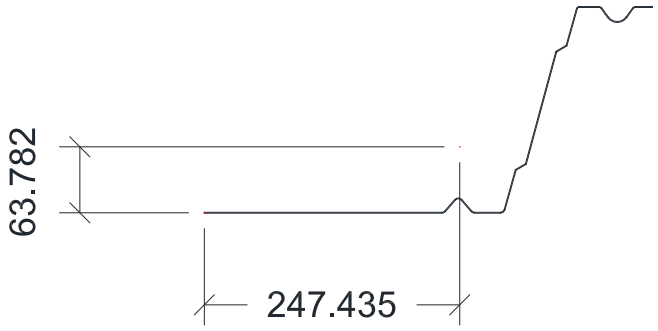


```
Command: MASSPROP

Select objects: 1 found

Select objects:

 ----------------   REGIONS   ----------------

Area:                      512.8328
Perimeter:                 1208.3654
Bounding box:           X: -12157.0857  --  -11723.0857
                        Y: -824.8588  --  -625.0088
Centroid:               X: -11909.5884
                        Y: -760.6520
Moments of inertia:     X: 299813315.1622
                        Y: 72746519088.4619
Product of inertia:    XY: 4649549115.5188
Radii of gyration:      X: 764.6058
                        Y: 11910.1770
Principal moments and X-Y directions about centroid:
                        I: 850488.3791 along [0.8595 0.5111]
                        J: 9432873.9427 along [-0.5111 0.8595]
```

(b)

Figure 5.6. LHP200 Centroid

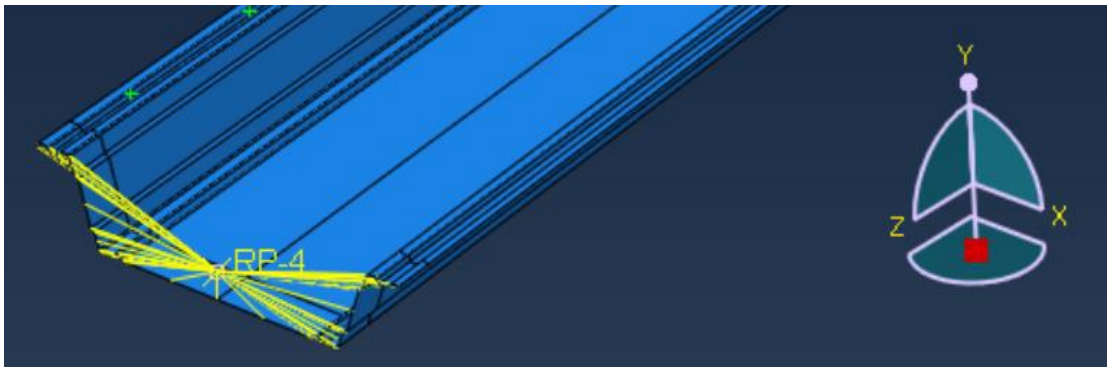

(a)

(b)

Figure 5.7. Kinematic Constraint on LHP200 Profiles

All the degrees of freedom of the kinematic constraints applied to the LHP200 profiles are fully constrained (*U1 = U2 = U3 = UR1= UR2 = UR3 = 0)*. This is because the reference points that are used as master nodes, will have the corresponding boundary conditions to simulate a simply supported element.

5.1.6 Load

In the load module, the boundary conditions for the reference points used for the kinematic constraints, as well as the displacement used to analyze the LHP200 profiles are defined. As mentioned in the previous point, the kinematic constraints degrees of freedom are fully fixed, so no rotations or translations are allowed. In order to make the profiles simply supported, boundary conditions are applied to the reference points, constraining the translational degrees (*U1 = U2= U3= 0*) of freedom, allowing only the rotations in the *X*, *Y* and *Z* axes. Also, boundary condition along the side edges are used to simulate the L sections used in the experimental test which prevent lateral displacements in the *X* axis (*U1=0)* (figure 4.8).

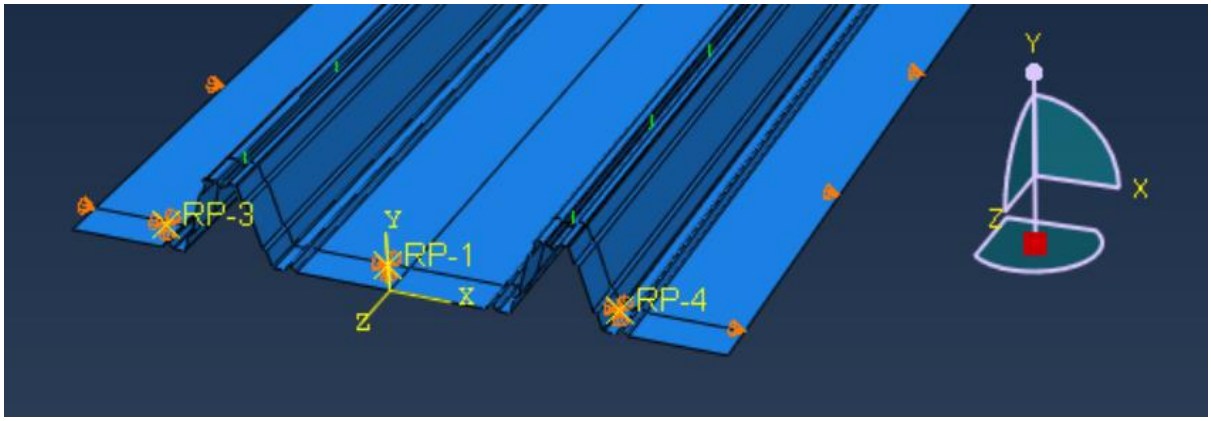

Figure 5.8. Boundary Conditions on Reference Points and Side Edges

As mentioned in Chapter 3, a displacement will be applied to the overlap joint to simulate the displacement caused by the negative bending moment in the mid-support. In order to have a similar approach as in the experimental test, instead of a load, a displacement is applied in the overlap joint by assigning a boundary condition in the *Y* axis of -1 (*U2 = -1*). This boundary condition is applied to the hollow section that will transfer uniformly the displacement to the support cleats and hence to the LHP200 profiles. Figure 5.9 shows this arrangement.

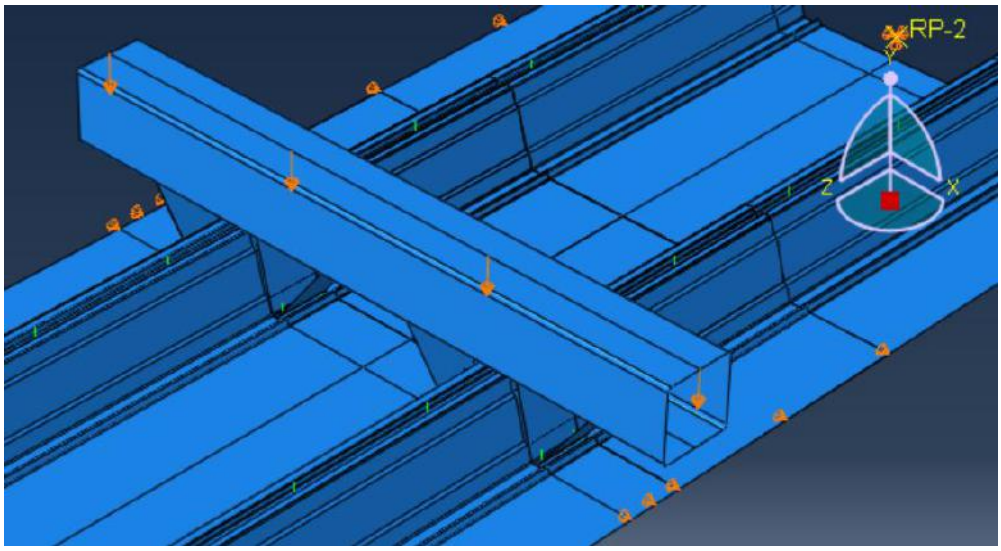

Figure 5.9. Displacement Applied

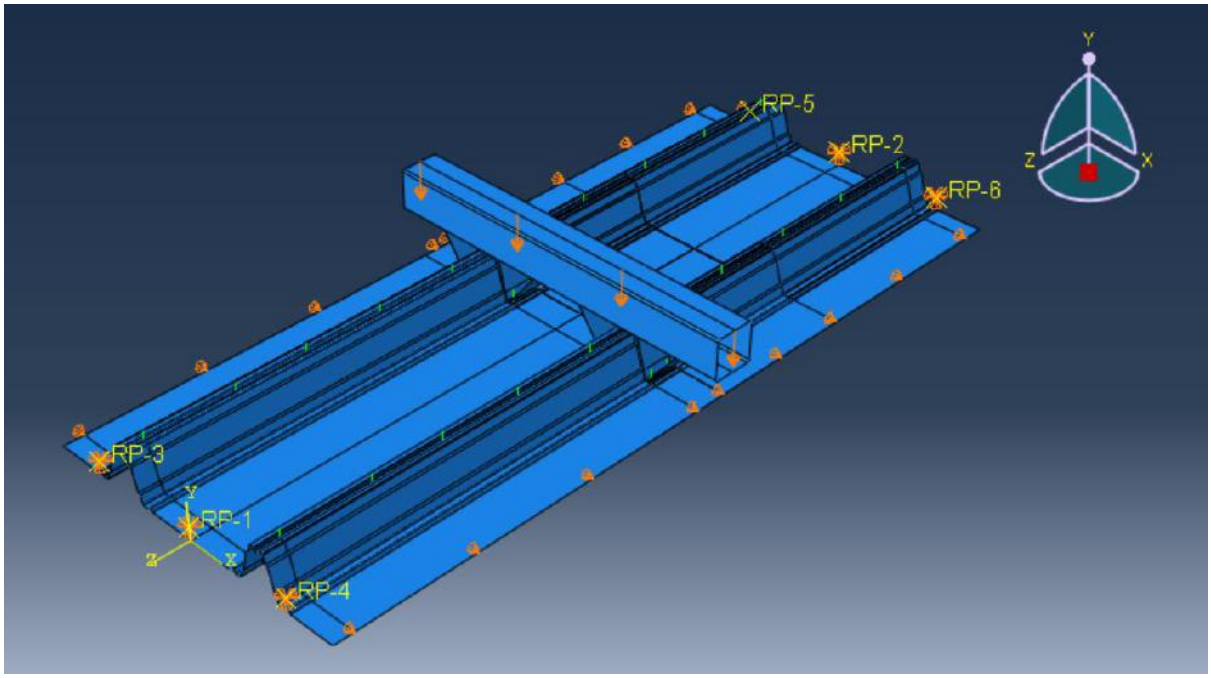

Figure 5.10. Boundary Conditions and Displacement Applied

5.1.7 Mesh

In the model, the mesh size used in the LHP200 profiles and the hollow section is the same, which is 40mm. For the support cleats, a smaller mesh of 4mm is used due to the difference on size between the other instances. The following figure shows the mesh used in the model.

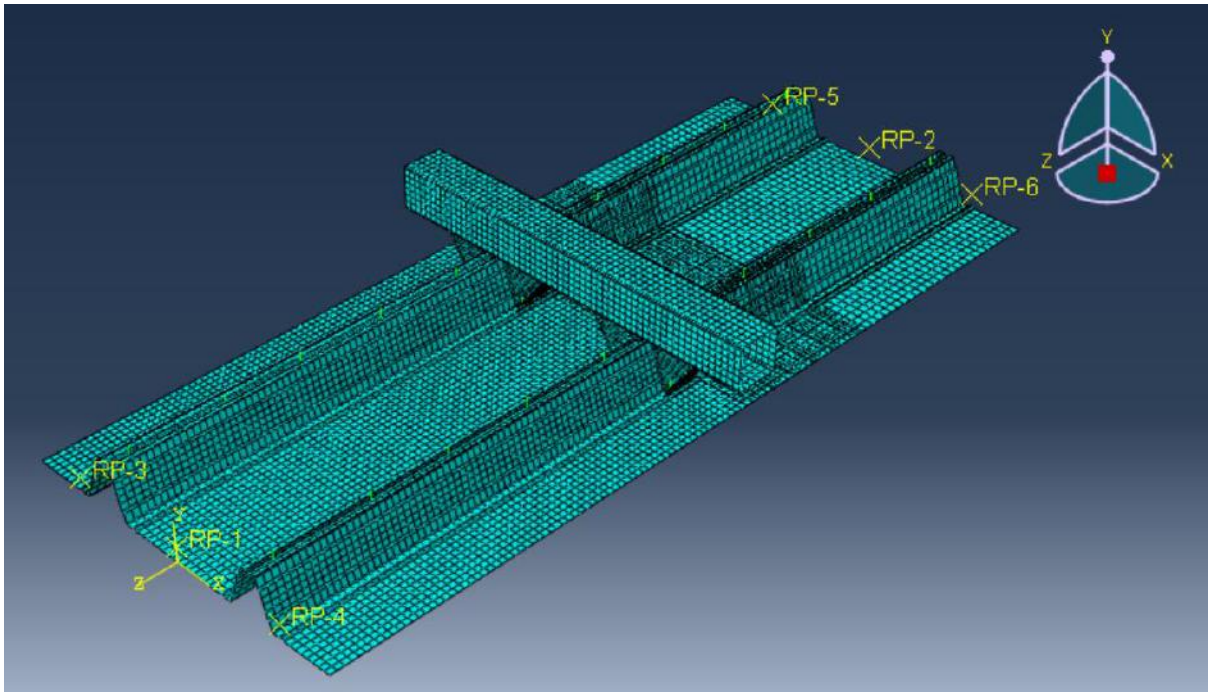

Figure 5.11. Mesh Used in the Model

5.1.8 Job

After completed all the previous modules, we can now run the analysis in the job module. In here, several jobs can be made with different definitions of (boundary conditions, step, interaction, etc.) and later compare the different results.

As mentioned in point 4.1.4, a "Static, Riks" method will be analyzed, but it is important to take into consideration the possible buckling that the profiles could have when the displacement is applied. So, in order to include the buckling shape in the analysis, a linear perturbation step was created for buckle, resulting in negative eigenvalues for this type of analysis. This means that in order to get the buckled shape of the analysis, the displacement should be applied in the opposite direction, hence buckling is not taken into account in the "Static, Riks" analysis.

5.1.9 Visualization

After the job is completed, it is possible to visualize the deformed shape of the structure, as well as the distribution of stresses, displacements, rotations, etc. The following figures show the output of the analysis.

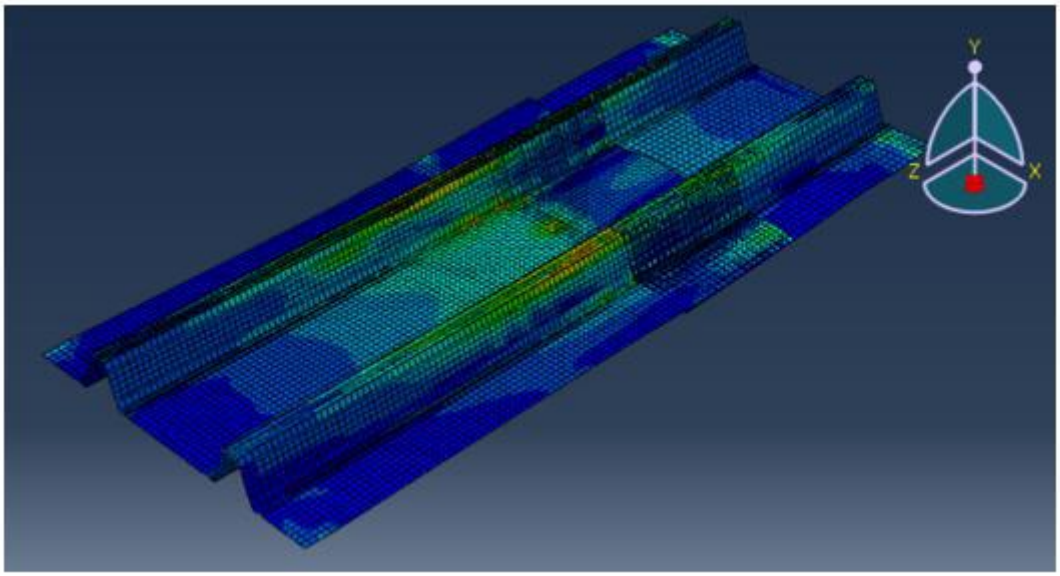

Figure 5.12 Deformed Shape FE Modelling

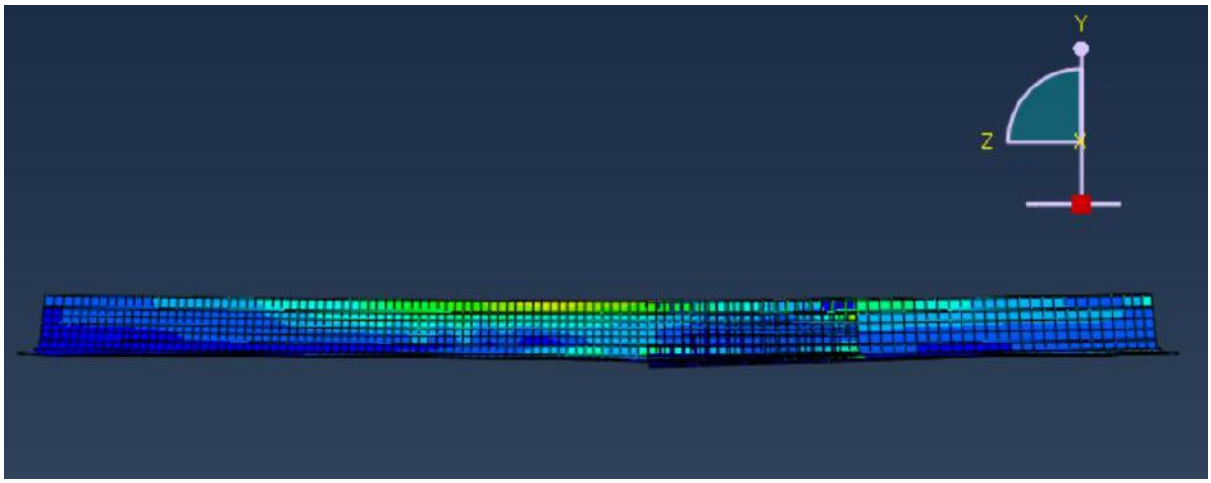

Figure 5.13 Deformed Shape Side View FEM

5.1.10 Results

The Force-Displacement graphs of the FEM are shown next and they are compared with the experimental test to see differences and similarities.

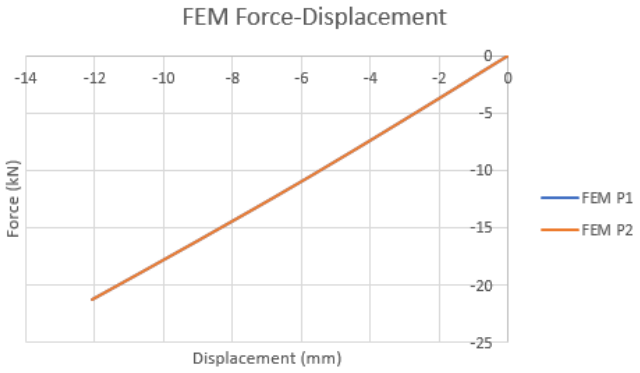

Graph 5.2 Force-Displacement FEM P1 vs P2

Graph 5.3 Experimental Test P1 vs P2

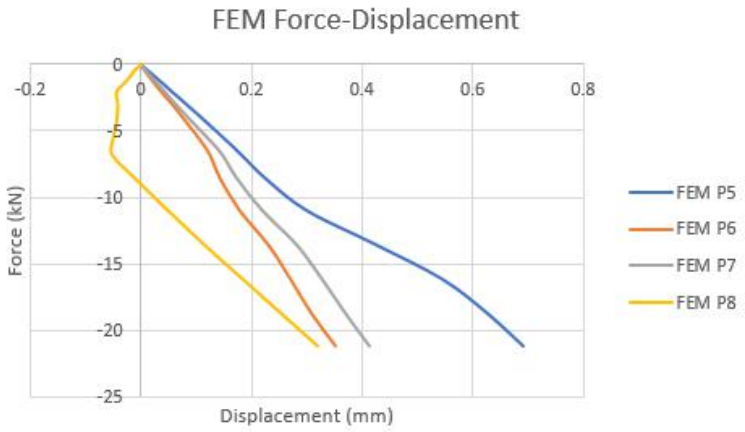

Graph 5.4 Force-Displacement FEM P5 to P8

Graph 5.5 Experimental Test P5 to P8

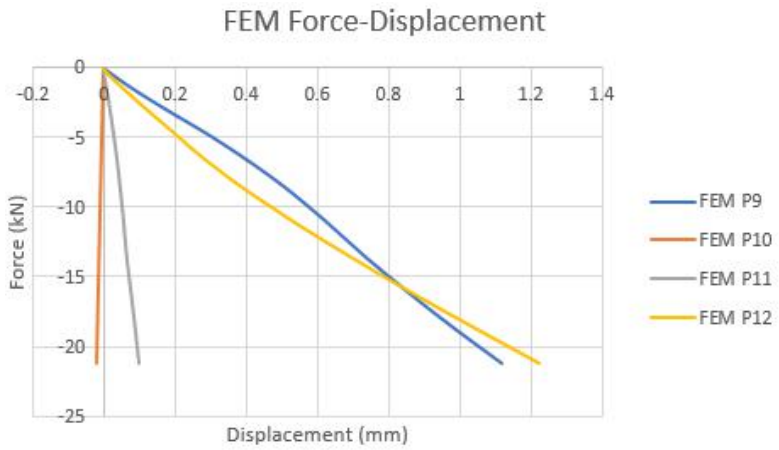

Graph 5.6 Force-Displacement FEM P9 to P12

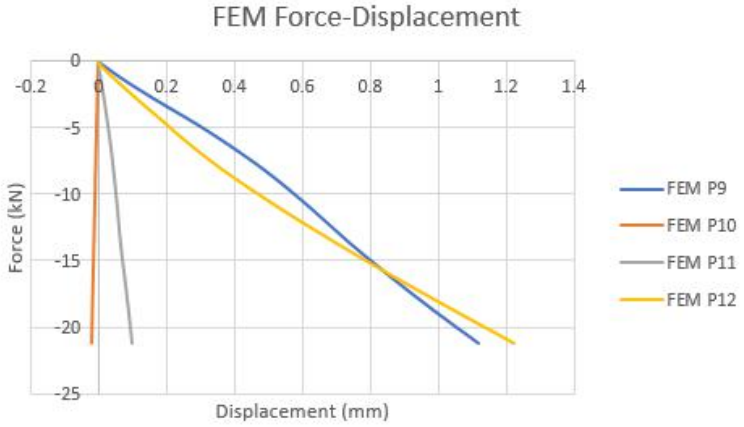

Graph 5.7 Force-Displacement P9 to P12

As we can see in the figures, the FEM results are different from the experimental test values. We can easily see that to properly simulate the experimental test, there is a lot of surface interaction occurring in the overlap between the profiles. This interaction is most certain to be the reason of the difficulties with the simulation.

6 Conclusions

Even though we found the stiffness in the overlap connection, it will be good to measure the bottom gap in another point, preferably in the web, and compare the results, to search for any significant differences.

As it were showed in the pictures, the LVDT's start to rotate at a certain deflection, resulting in possibly inaccurate results of the gap measurement, this could explain why the factor "f" does not match with the example made in the chapter 4.

Also, both profiles have the same buckling in the web where the overlap connections is located. In the thinner profile, the buckling starts in the bottom profile and then it propagates to the top profile causing deformations there leading to the failure of the system.

In the case of the 1.50mm profile the buckling that starts in the bottom profile, does not propagate to the top, instead, the system fails due to the tensile failure of the side overlap connection screws.

Certainly the behavior is similar between the two thicknesses, but it is because of the screws capacity in the thicker profile that this don't reach that point.

Regarding the stiffness calculated, it seems its relation with thickness of the profiles is somehow linear. The thicker profile is almost two times more stiff, and almost two times thicker:

- t=0.85mm

$$k = 0.4269\frac{mm}{kN}$$

$$t_d = 0.782mm$$

$$\frac{0.782}{1.424} = 0.55$$

- t=1.50mm

$$k = 0.2419\frac{mm}{kN}$$

$$t_d = 1.424mm$$

$$\frac{0.2419}{0.4269} = 0.56$$

It would be interesting to find out maybe by testing the remaining thicknesses and see if the behavior of the relationship thickness-stiffness.

We saw that it is really complex to do a proper simulation of the experimental test, as we have seen, the tendency of the deflections seems similar, but the displacements are inaccurate. This could be mainly because of the surface interaction between the profiles.

It can be good to model the LHP200 profiles without an overlap connection and make a test like this as well. By this we could start analyzing a much simpler model, to later build a complex one with the overlap.

Finally, we can see that there is a lot of room for further research and study in this subject, and there are some things that can be improved, especially in the FEM.

Annex

Experimental test comparison of similarities graphs on all points of t=0.85mm:

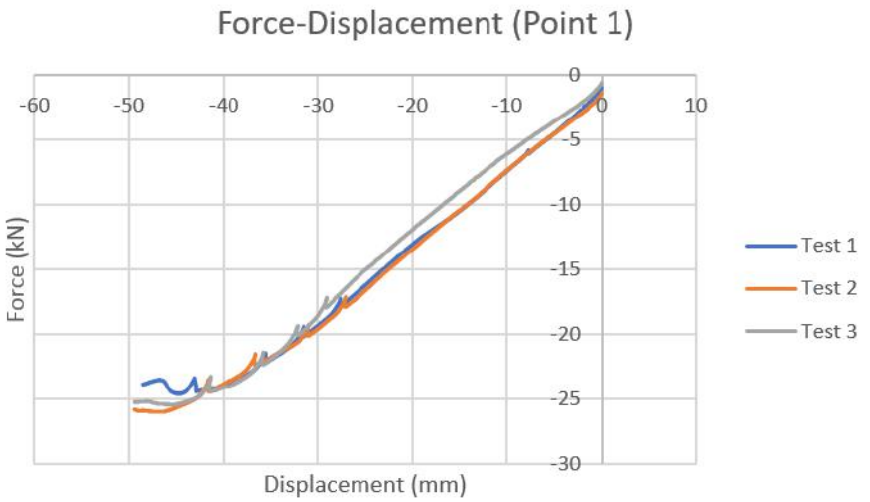

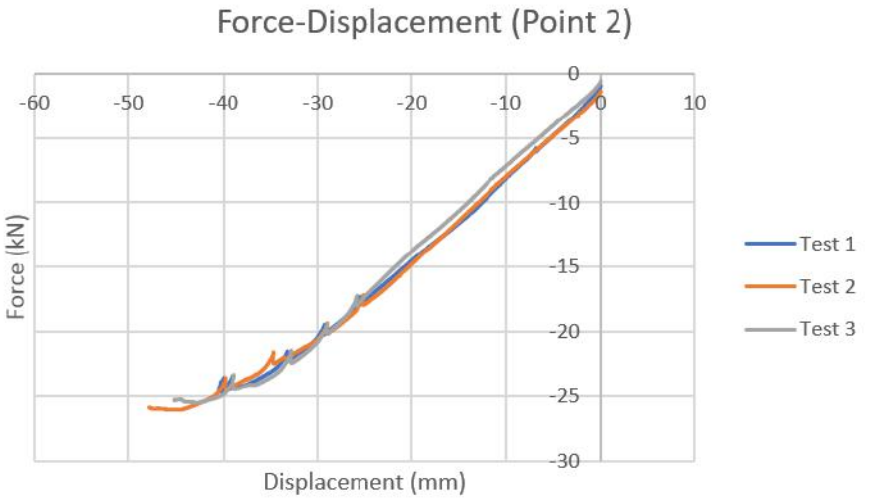

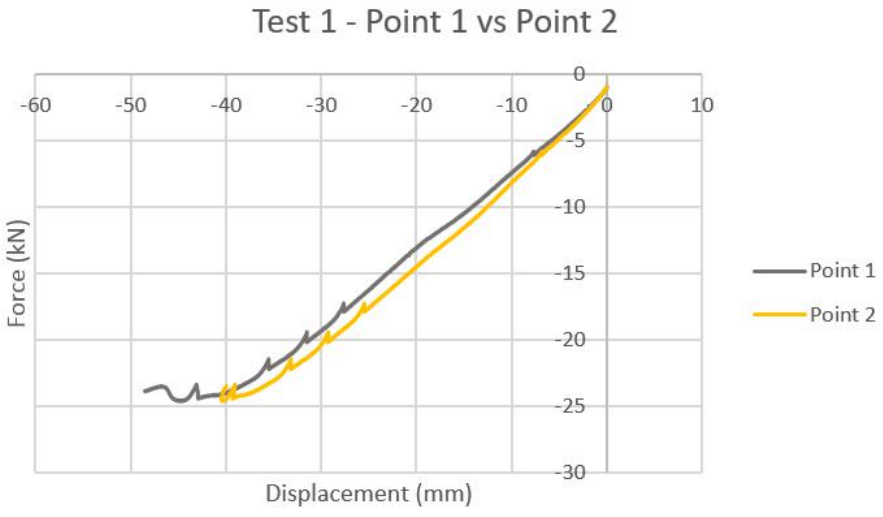

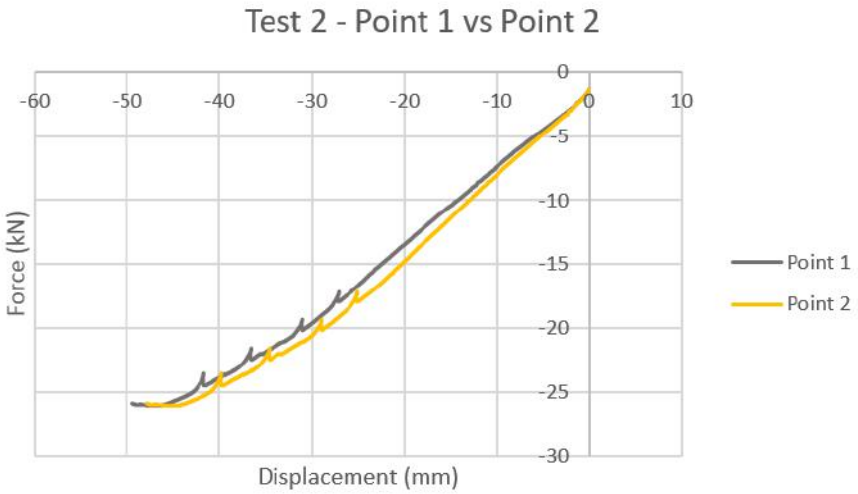
Test 2 - Point 1 vs Point 2
0
-60
-50
-40
-30
-20
-10
0
10
-5
-10
-15
-20
-25
-30
Force (kN)
Displacement (mm)
Point 1
Point 2

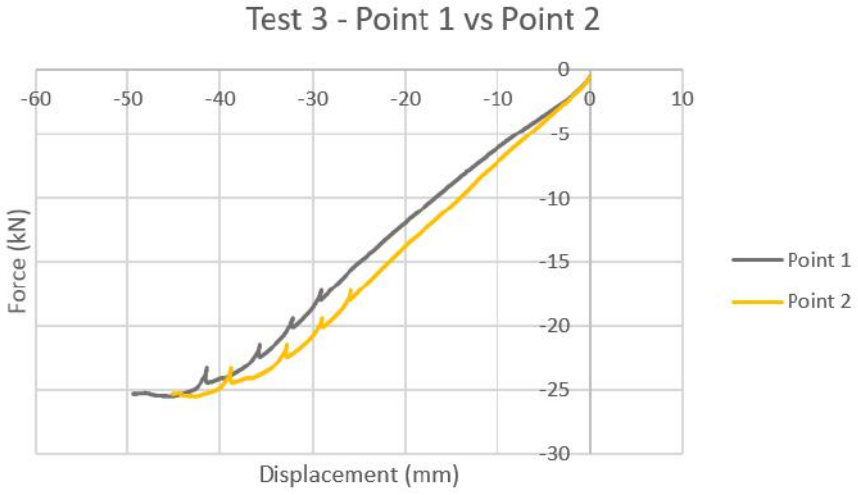
Test 3 - Point 1 vs Point 2
0
-60
-50
-40
-30
-20
-10
0
10
-5
-10
-15
-20
-25
-30
Force (kN)
Displacement (mm)
Point 1
Point 2

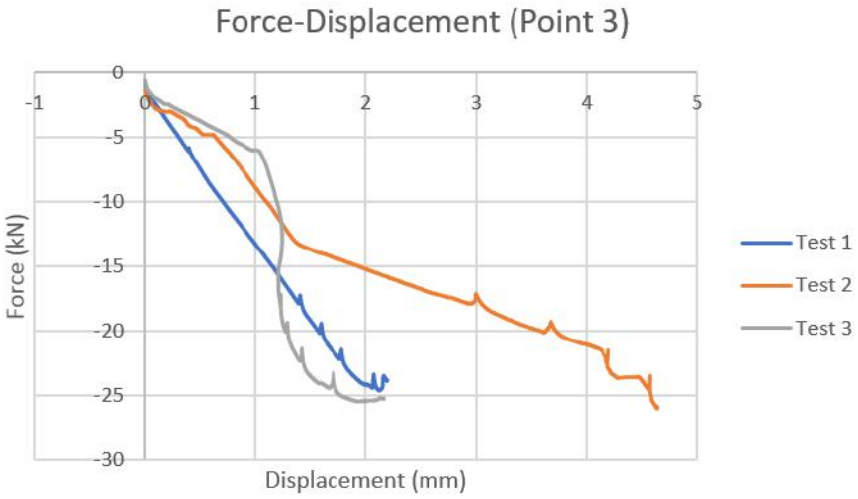
Force-Displacement (Point 3)
0
-1
0
1
2
3
4
5
-5
-10
-15
-20
-25
-30
Force (kN)
Displacement (mm)
Test 1
Test 2
Test 3

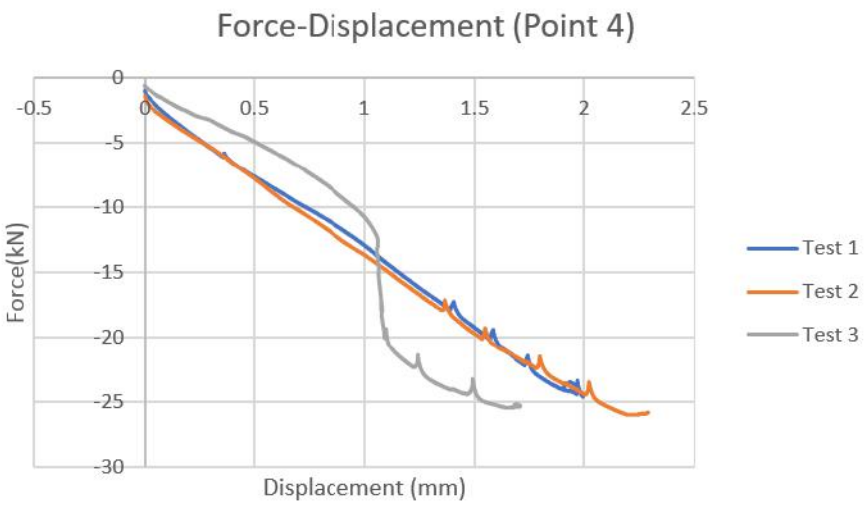
Force-Displacement (Point 4)
Force(kN)
Displacement (mm)
Test 1
Test 2
Test 3

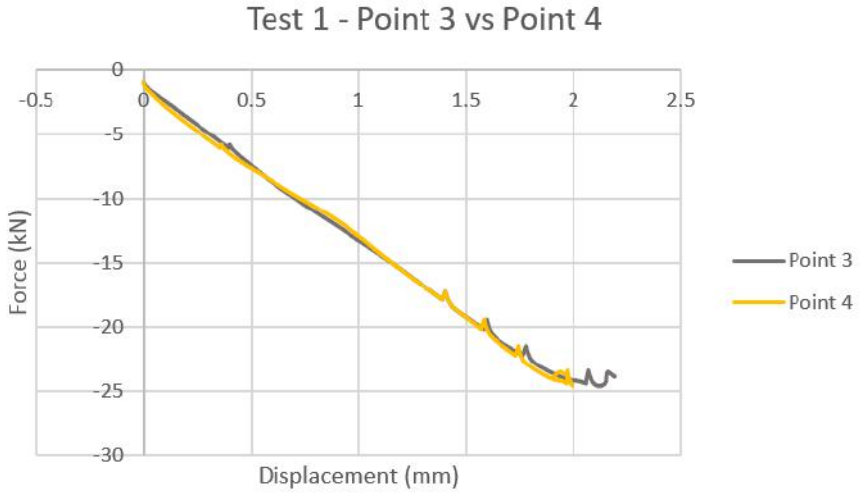
Test 1 - Point 3 vs Point 4
Force (kN)
Displacement (mm)
Point 3
Point 4

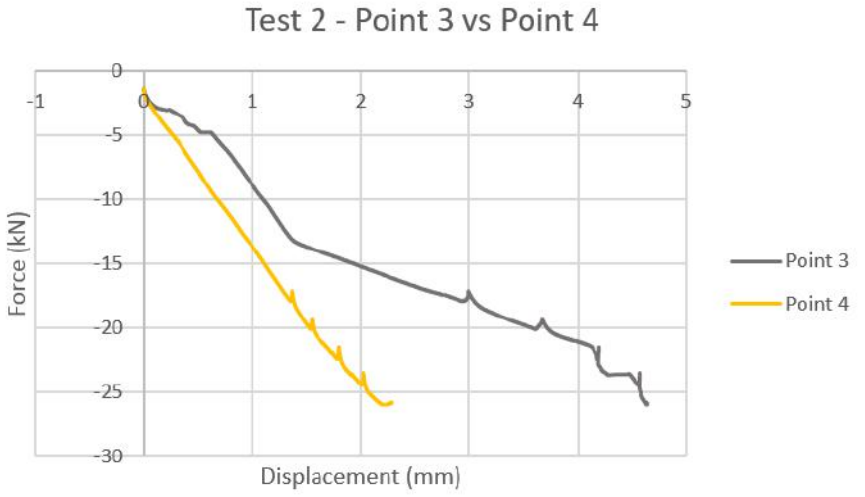
Test 2 - Point 3 vs Point 4
Force (kN)
Displacement (mm)
Point 3
Point 4

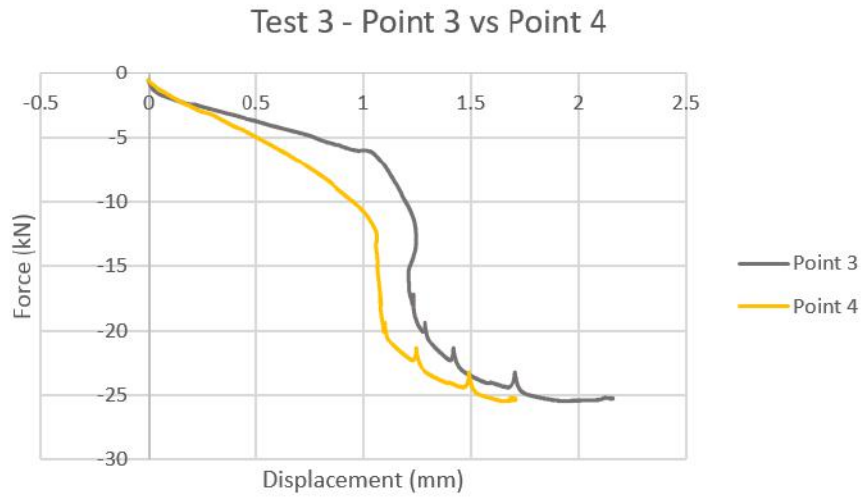
Test 3 - Point 3 vs Point 4
0
-0.5
0
0.5
1
1.5
2
2.5
-5
-10
-15
-20
-25
-30
Force (kN)
Displacement (mm)
Point 3
Point 4

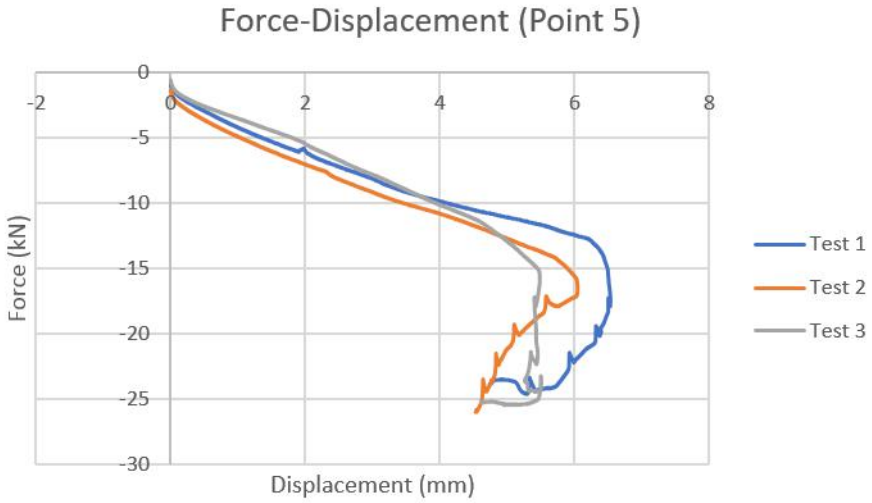
Force-Displacement (Point 5)
0
-2
0
2
4
6
8
-5
-10
-15
-20
-25
-30
Force (kN)
Displacement (mm)
Test 1
Test 2
Test 3

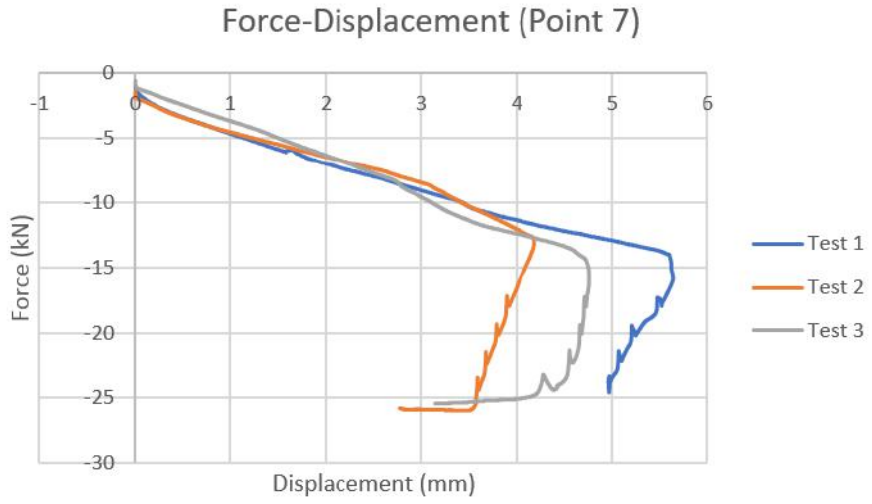
Force-Displacement (Point 7)
0
-1
0
1
2
3
4
5
6
-5
-10
-15
-20
-25
-30
Force (kN)
Displacement (mm)
Test 1
Test 2
Test 3

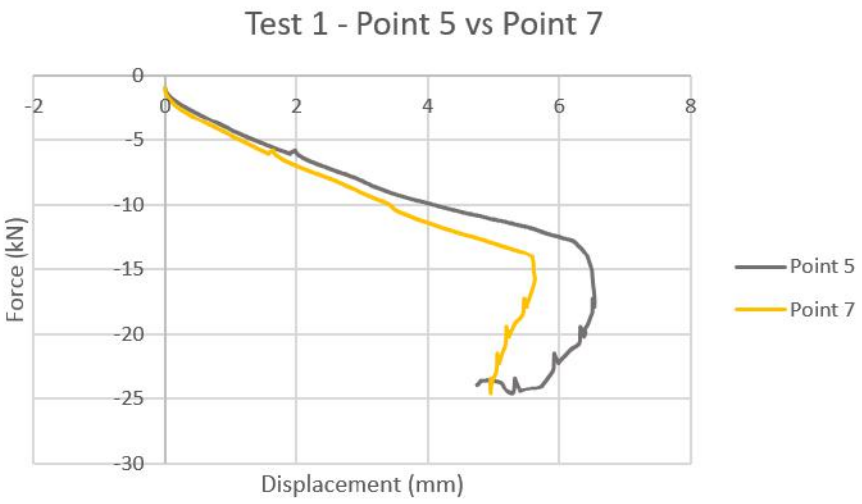
Test 1 - Point 5 vs Point 7
Force (kN)
Displacement (mm)
Point 5
Point 7

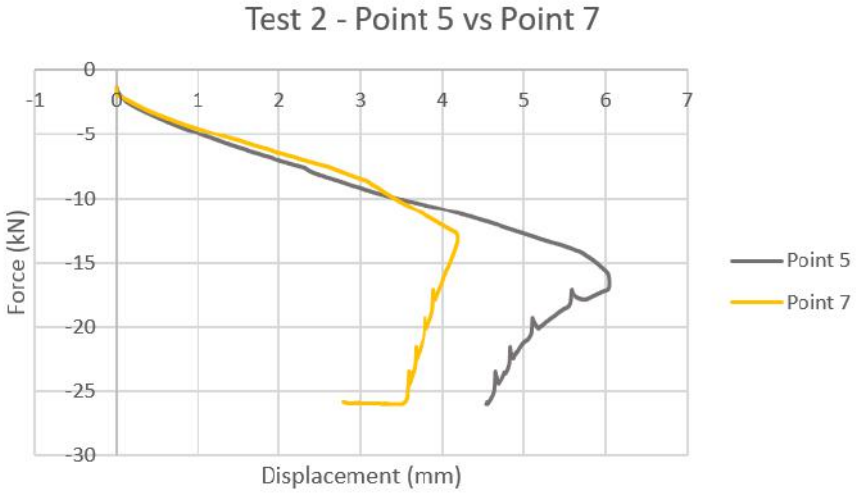
Test 2 - Point 5 vs Point 7
Force (kN)
Displacement (mm)
Point 5
Point 7

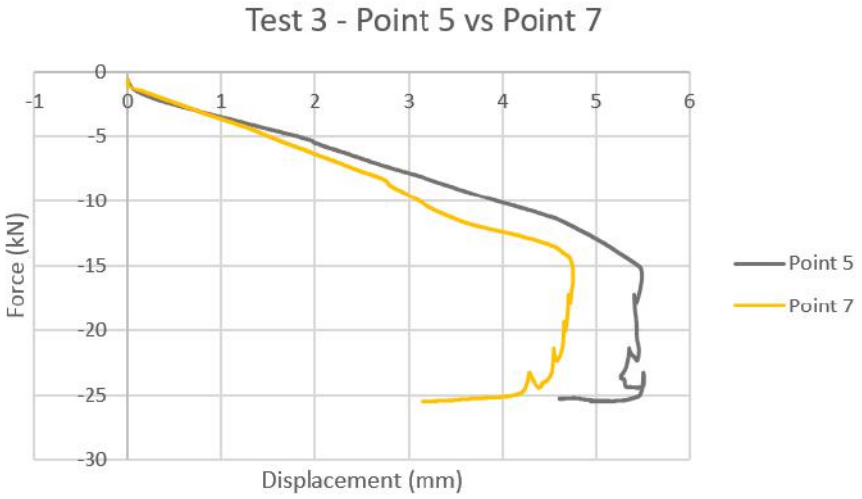
Test 3 - Point 5 vs Point 7
Force (kN)
Displacement (mm)
Point 5
Point 7

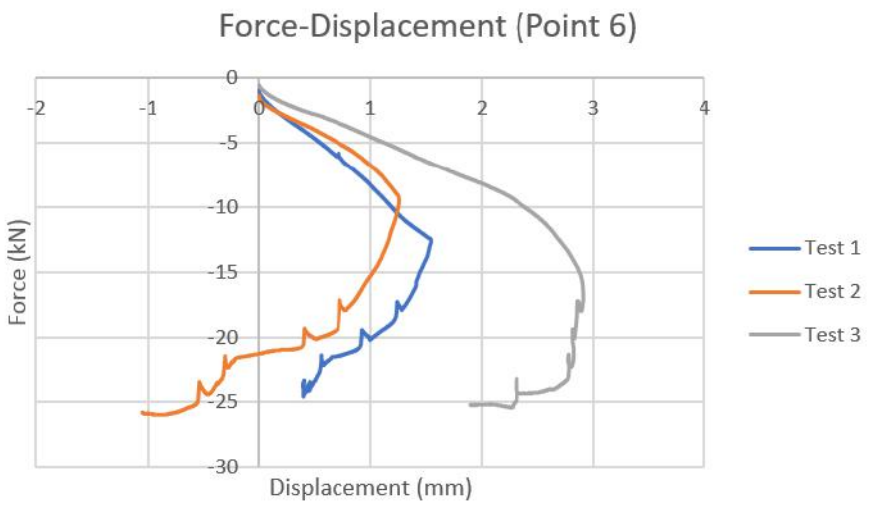
Force-Displacement (Point 6)
Force (kN)
Displacement (mm)
Test 1
Test 2
Test 3

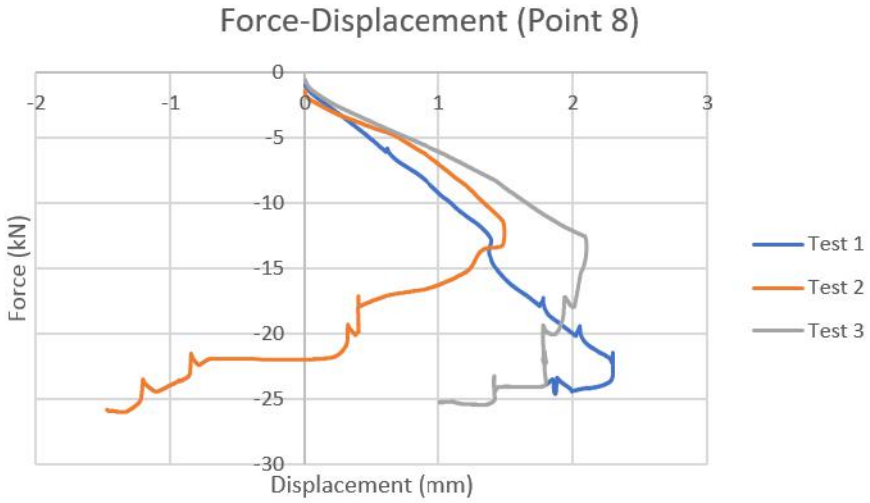
Force-Displacement (Point 8)
Force (kN)
Displacement (mm)
Test 1
Test 2
Test 3

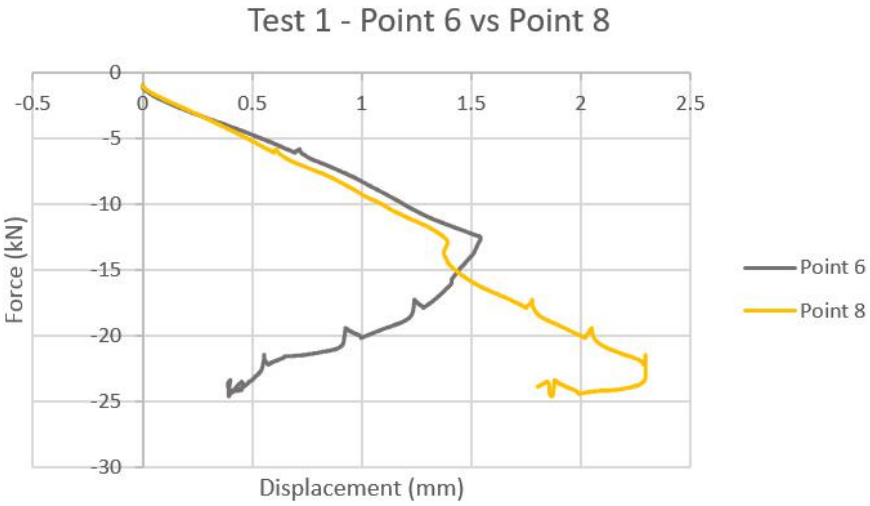
Test 1 - Point 6 vs Point 8
Force (kN)
Displacement (mm)
Point 6
Point 8

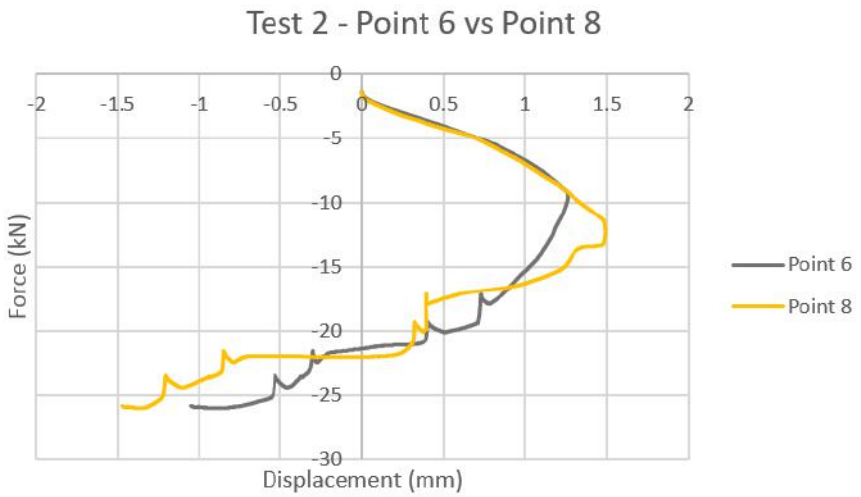
Test 2 - Point 6 vs Point 8
0
-5
-10
-15
-20
-25
-30
-2
-1.5
-1
-0.5
0
0.5
1
1.5
2
Force (kN)
Displacement (mm)
Point 6
Point 8

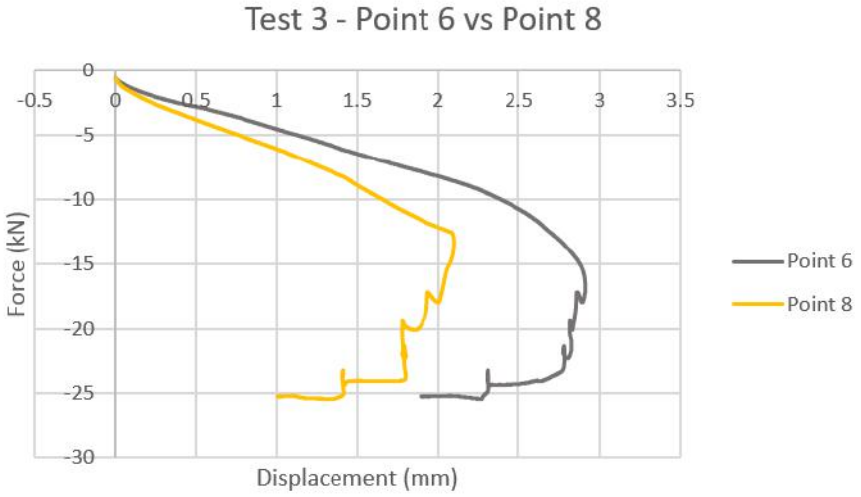
Test 3 - Point 6 vs Point 8
0
-5
-10
-15
-20
-25
-30
-0.5
0
0.5
1
1.5
2
2.5
3
3.5
Force (kN)
Displacement (mm)
Point 6
Point 8

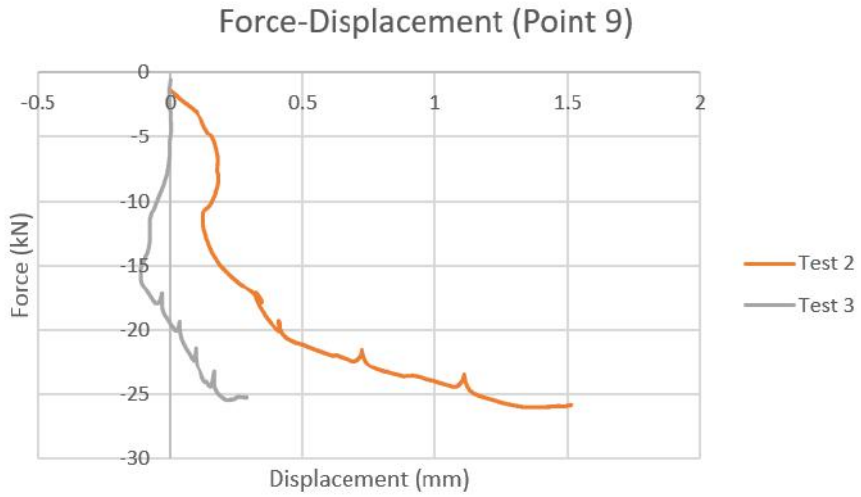
Force-Displacement (Point 9)
0
-5
-10
-15
-20
-25
-30
-0.5
0
0.5
1
1.5
2
Force (kN)
Displacement (mm)
Test 2
Test 3

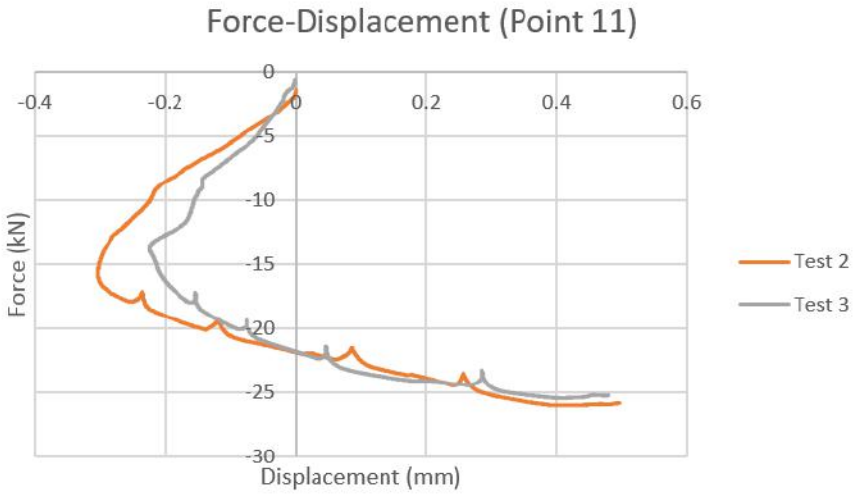

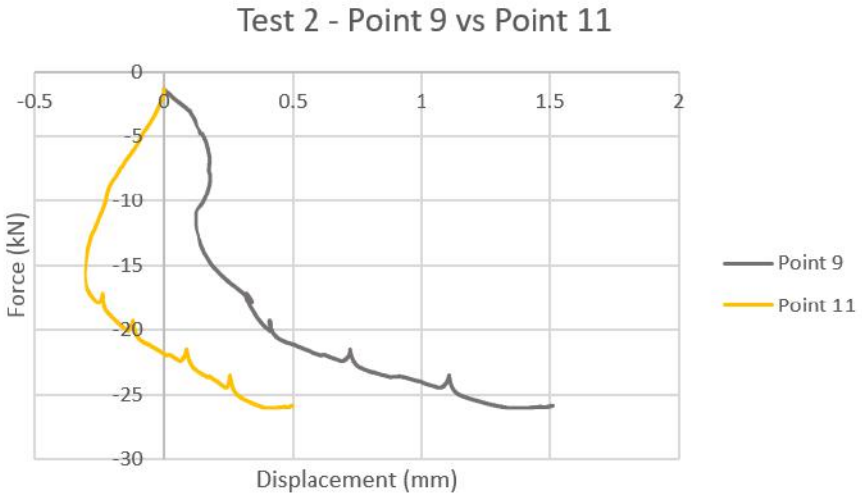

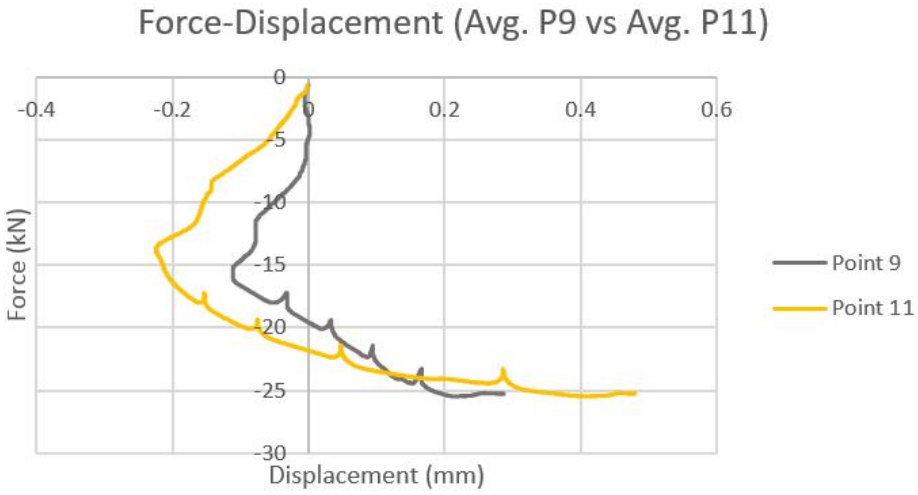

Note: values of test 1 were neglected because LVDT's fell off in at point 9 and 11

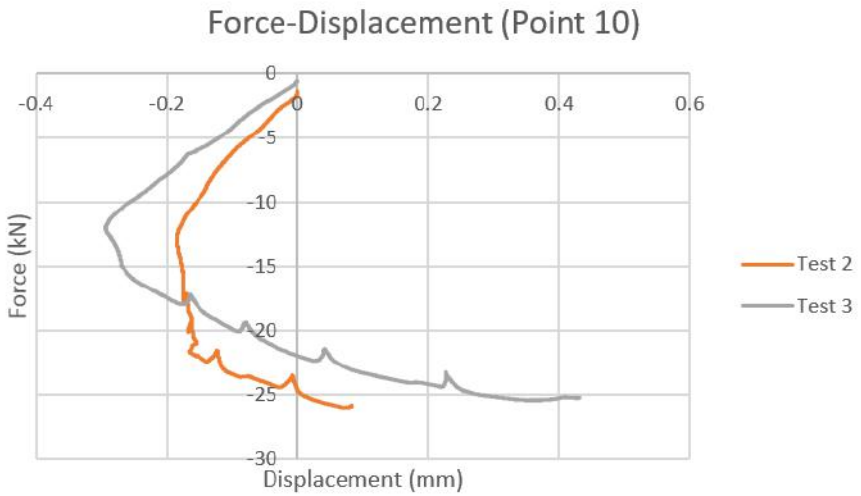
Force-Displacement (Point 10)
0
-0.4
-0.2
0
0.2
0.4
0.6
-5
-10
-15
-20
-25
-30
Force (kN)
Displacement (mm)
Test 2
Test 3

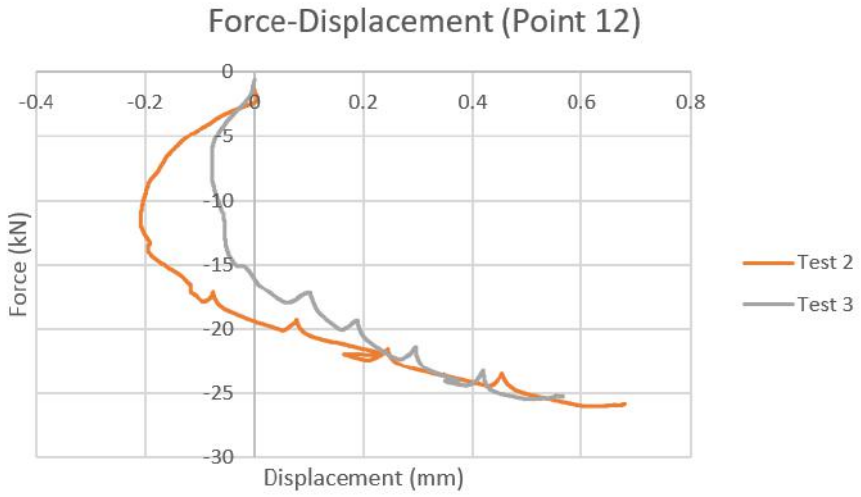
Force-Displacement (Point 12)
0
-0.4
-0.2
0
0.2
0.4
0.6
0.8
-5
-10
-15
-20
-25
-30
Force (kN)
Displacement (mm)
Test 2
Test 3

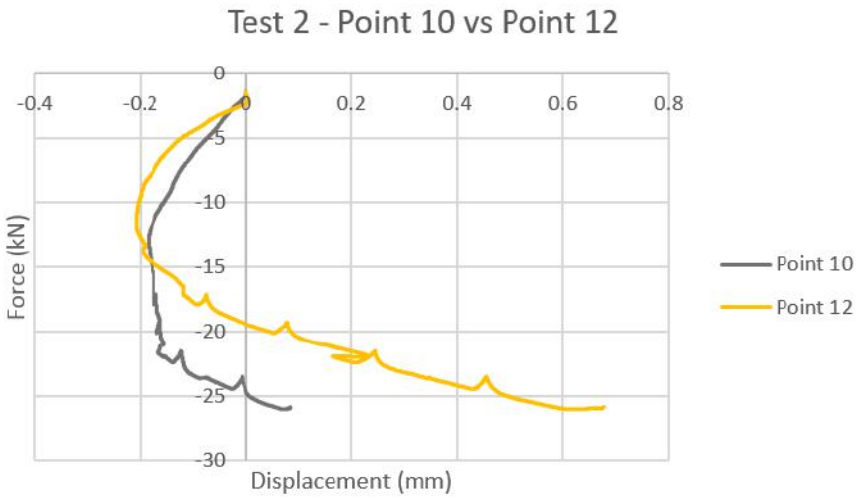
Test 2 - Point 10 vs Point 12
0
-0.4
-0.2
0
0.2
0.4
0.6
0.8
-5
-10
-15
-20
-25
-30
Force (kN)
Displacement (mm)
Point 10
Point 12

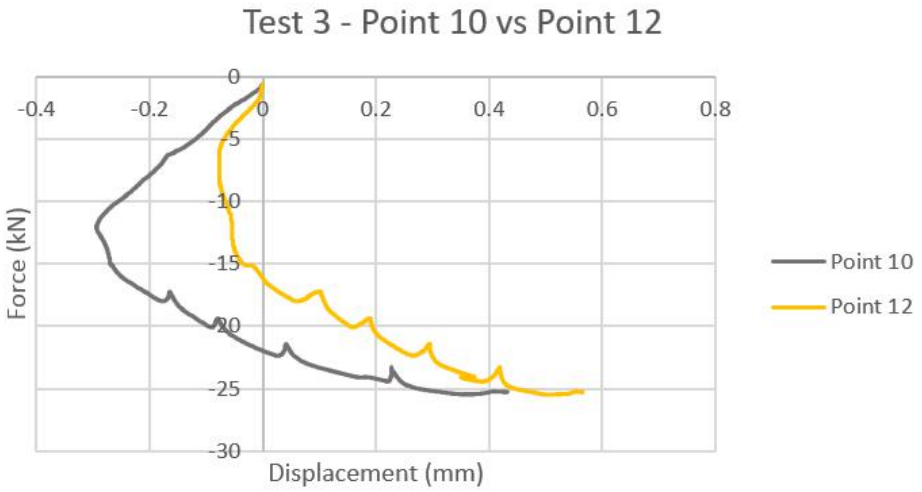

Note: values of test 1 were neglected because LVDT's fell off at point 12

Experimental test comparison of similarities graphs on all points of t=1.50mm:

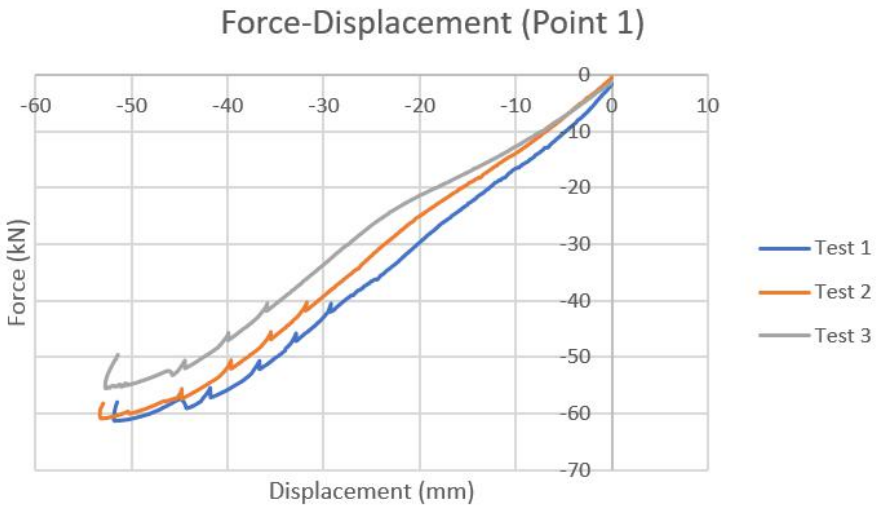

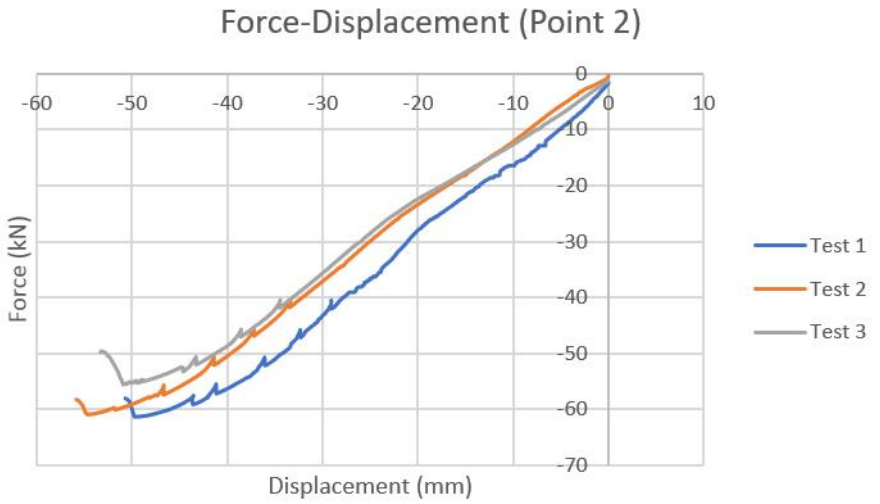

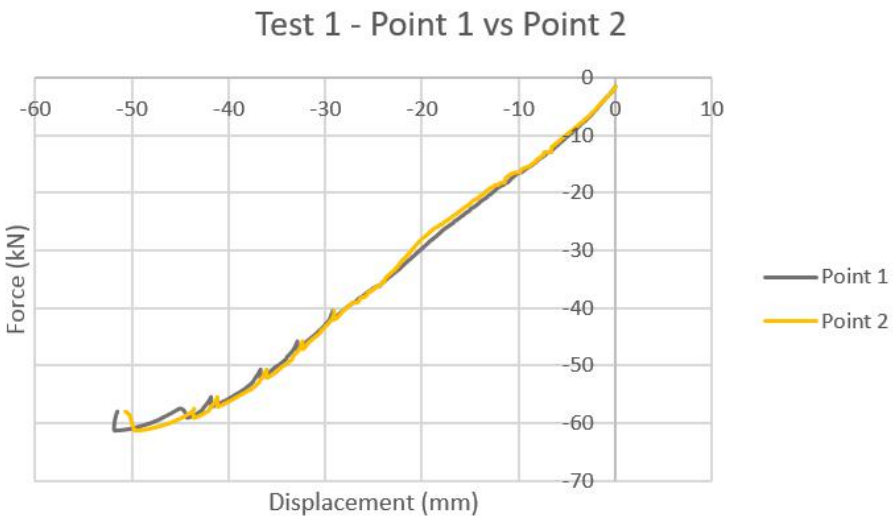
Test 1 - Point 1 vs Point 2
-60
-50
-40
-30
-20
-10
0
10
0
-10
-20
-30
-40
-50
-60
-70
Force (kN)
Displacement (mm)
Point 1
Point 2

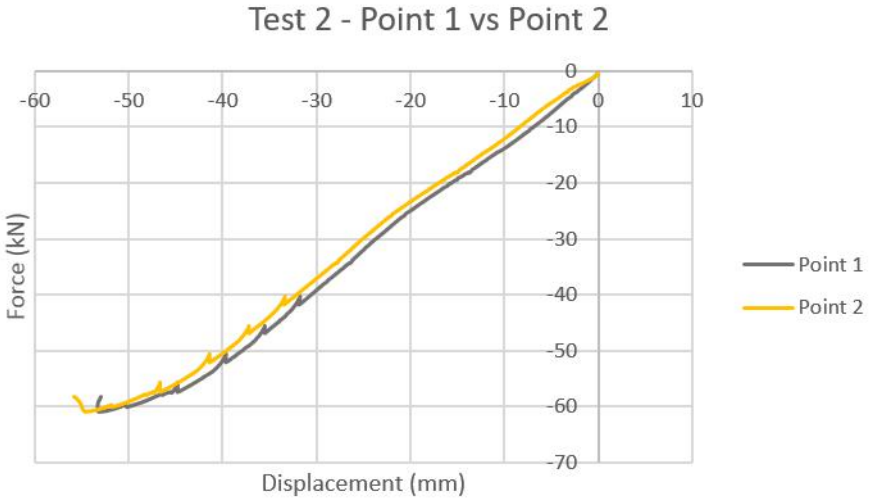
Test 2 - Point 1 vs Point 2
-60
-50
-40
-30
-20
-10
0
10
0
-10
-20
-30
-40
-50
-60
-70
Force (kN)
Displacement (mm)
Point 1
Point 2

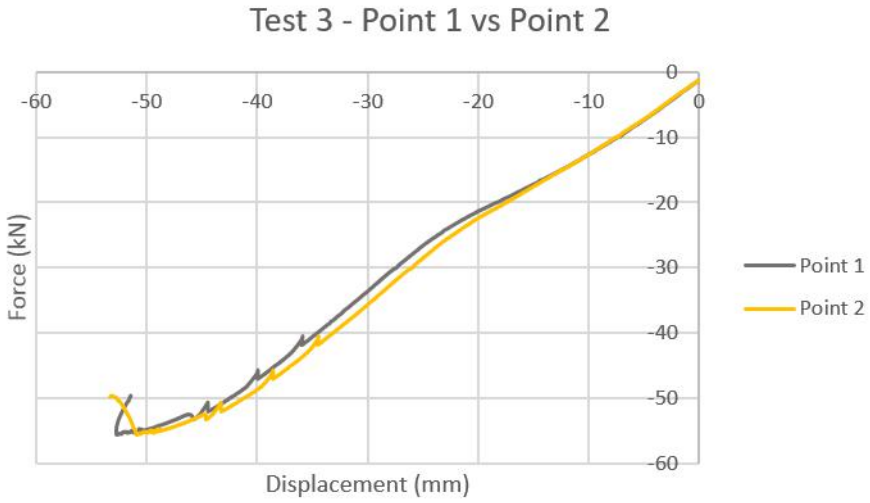
Test 3 - Point 1 vs Point 2
-60
-50
-40
-30
-20
-10
0
0
-10
-20
-30
-40
-50
-60
Force (kN)
Displacement (mm)
Point 1
Point 2

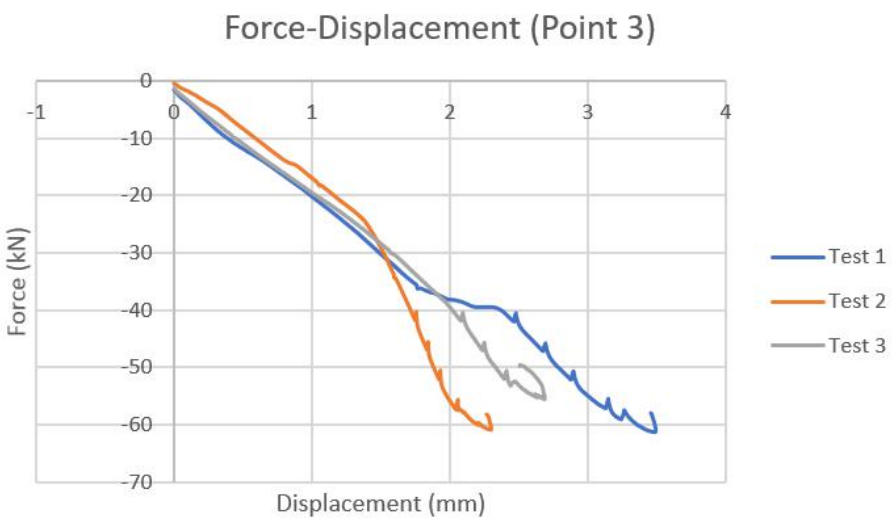
Force-Displacement (Point 3)
0
-10
-20
-30
-40
-50
-60
-70
-1
0
1
2
3
4
Force (kN)
Displacement (mm)
Test 1
Test 2
Test 3

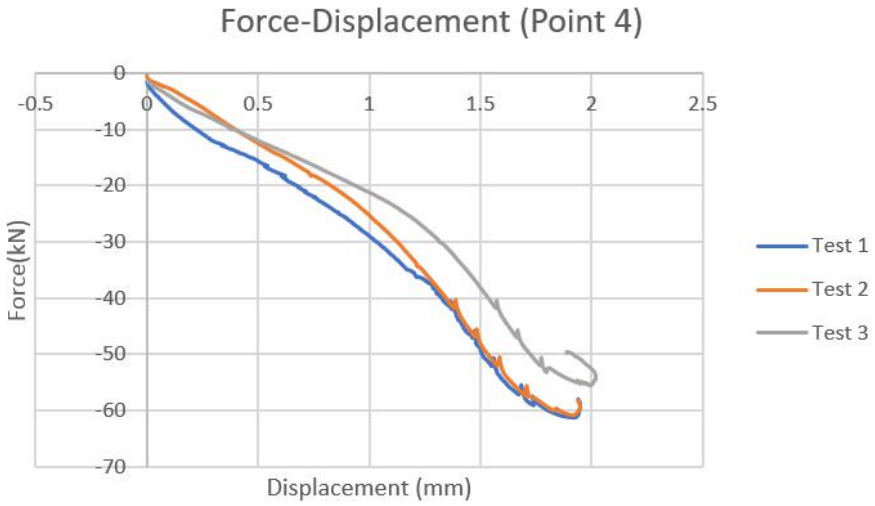
Force-Displacement (Point 4)
0
-10
-20
-30
-40
-50
-60
-70
-0.5
0
0.5
1
1.5
2
2.5
Force(kN)
Displacement (mm)
Test 1
Test 2
Test 3

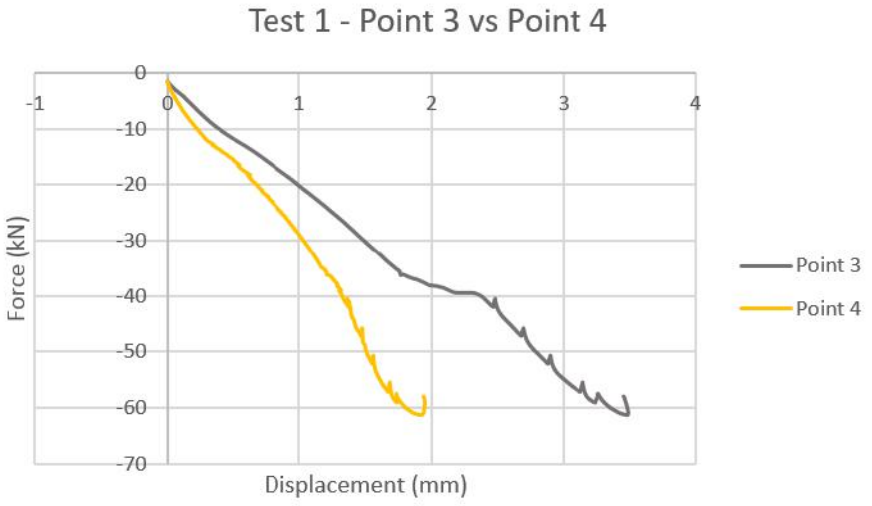
Test 1 - Point 3 vs Point 4
0
-10
-20
-30
-40
-50
-60
-70
-1
0
1
2
3
4
Force (kN)
Displacement (mm)
Point 3
Point 4

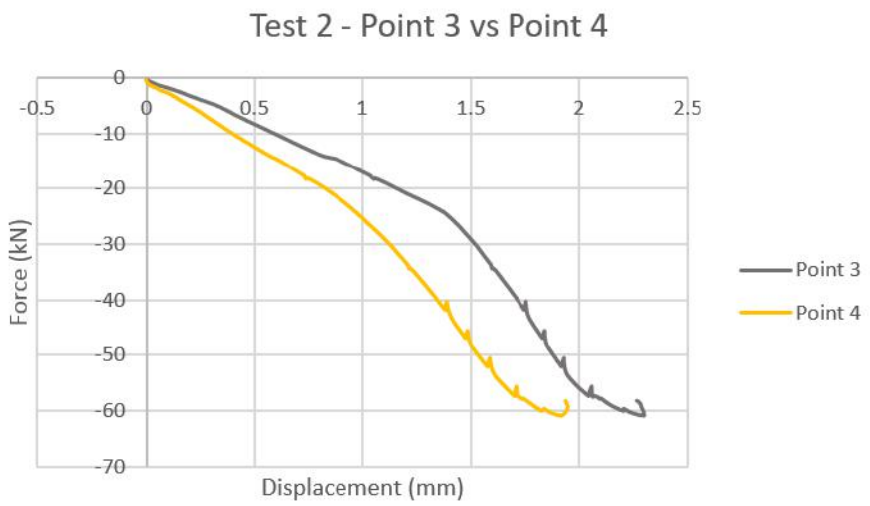
Test 2 - Point 3 vs Point 4
0
-10
-20
-30
-40
-50
-60
-70
-0.5
0
0.5
1
1.5
2
2.5
Force (kN)
Displacement (mm)
Point 3
Point 4

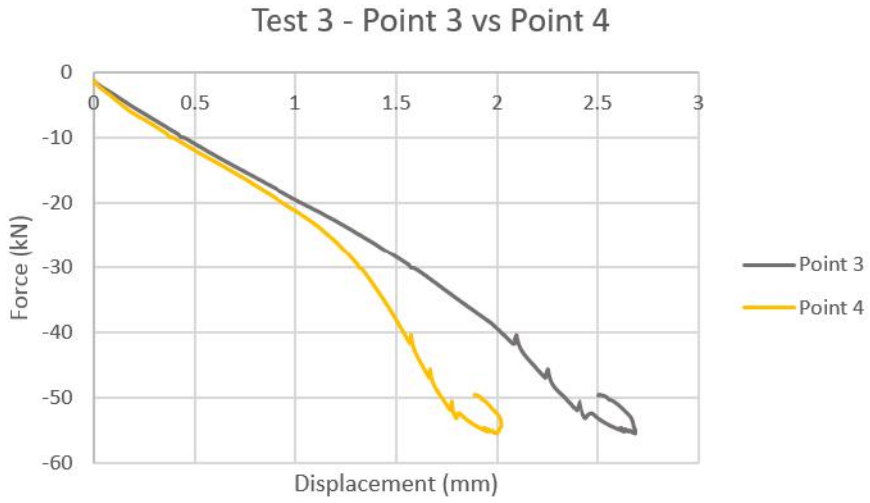
Test 3 - Point 3 vs Point 4
0
-10
-20
-30
-40
-50
-60
0
0.5
1
1.5
2
2.5
3
Force (kN)
Displacement (mm)
Point 3
Point 4

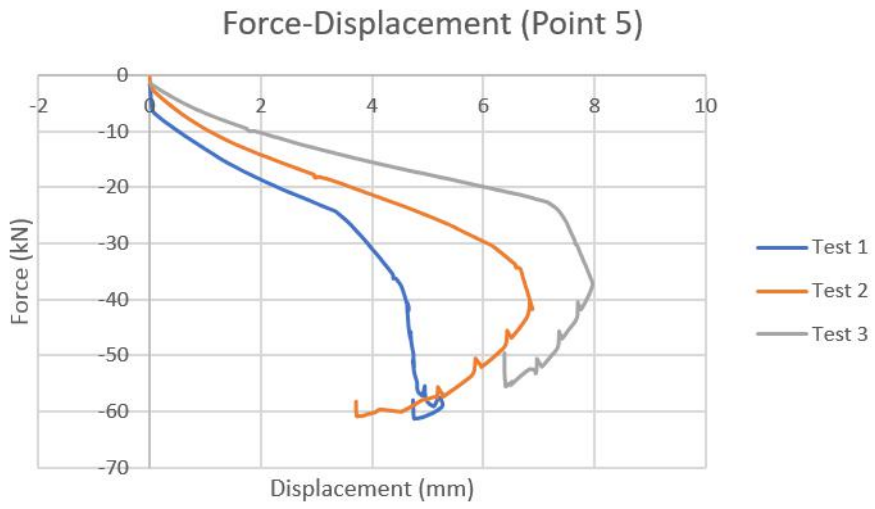
Force-Displacement (Point 5)
0
-10
-20
-30
-40
-50
-60
-70
-2
0
2
4
6
8
10
Force (kN)
Displacement (mm)
Test 1
Test 2
Test 3

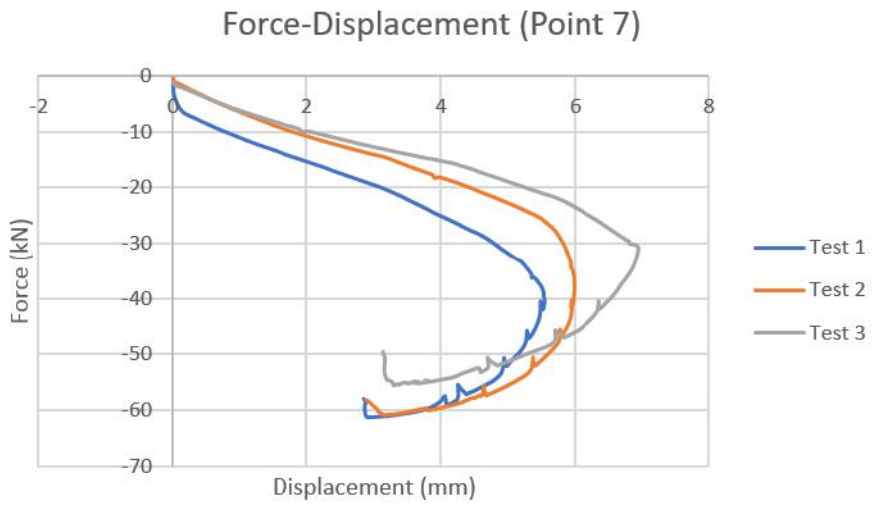
Force-Displacement (Point 7)
Force (kN)
Displacement (mm)
Test 1
Test 2
Test 3

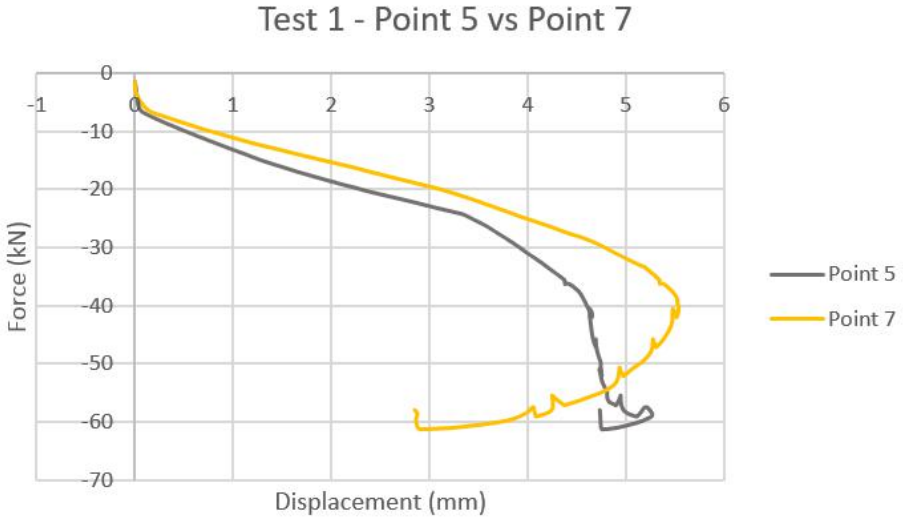
Test 1 - Point 5 vs Point 7
Force (kN)
Displacement (mm)
Point 5
Point 7

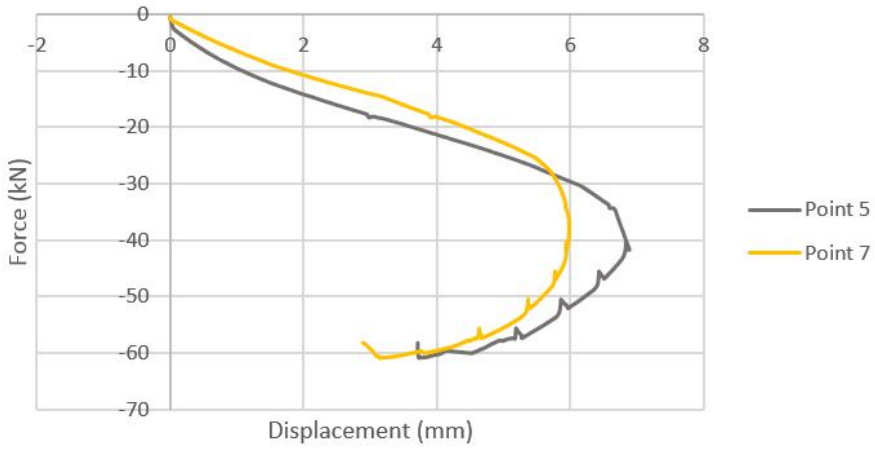
Test 2 - Point 5 vs Point 7
Force (kN)
Displacement (mm)
Point 5
Point 7

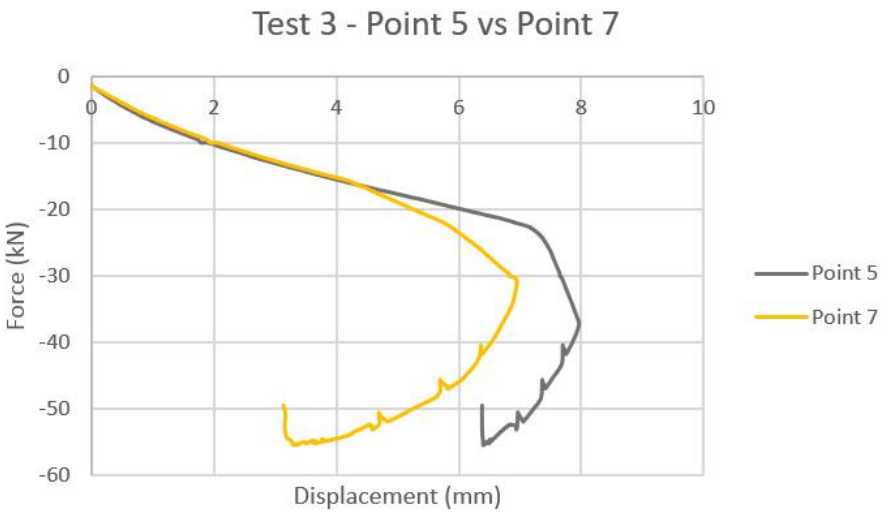
Test 3 - Point 5 vs Point 7
0
-10
-20
-30
-40
-50
-60
0
2
4
6
8
10
Force (kN)
Displacement (mm)
Point 5
Point 7

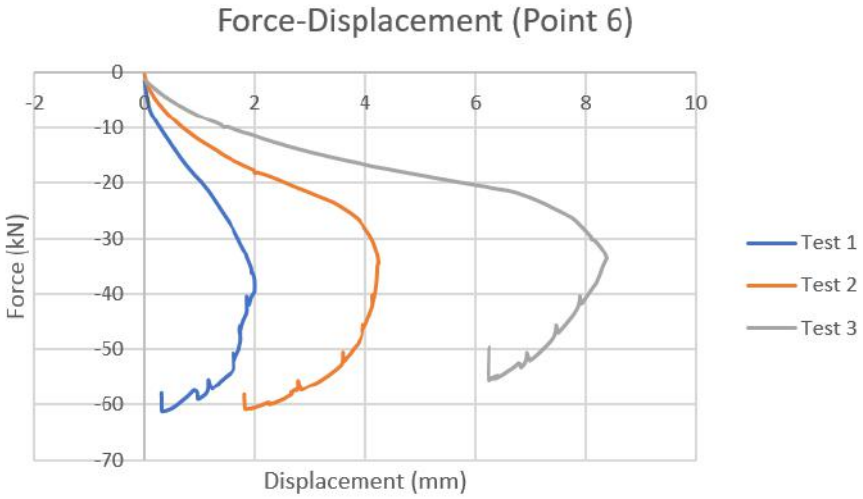
Force-Displacement (Point 6)
0
-10
-20
-30
-40
-50
-60
-70
-2
0
2
4
6
8
10
Force (kN)
Displacement (mm)
Test 1
Test 2
Test 3

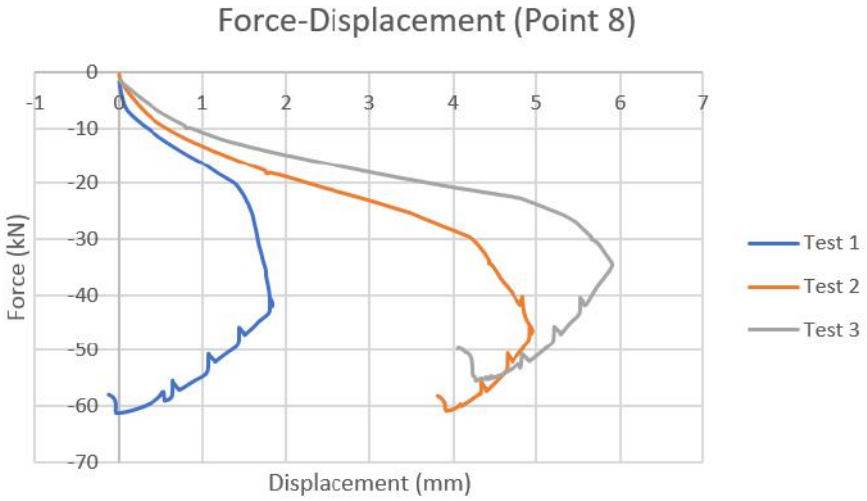
Force-Displacement (Point 8)
0
-10
-20
-30
-40
-50
-60
-70
-1
0
1
2
3
4
5
6
7
Force (kN)
Displacement (mm)
Test 1
Test 2
Test 3

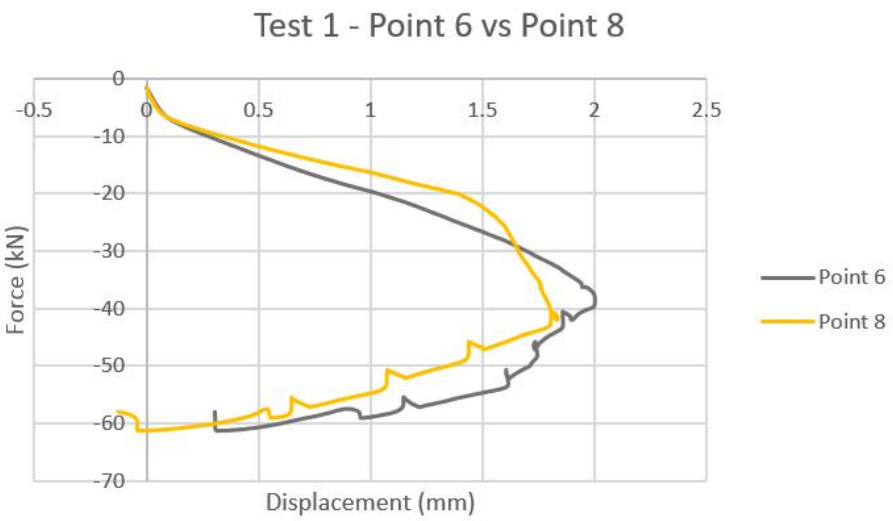
Test 1 - Point 6 vs Point 8
0
-10
-20
-30
-40
-50
-60
-70
-0.5
0
0.5
1
1.5
2
2.5
Force (kN)
Displacement (mm)
Point 6
Point 8

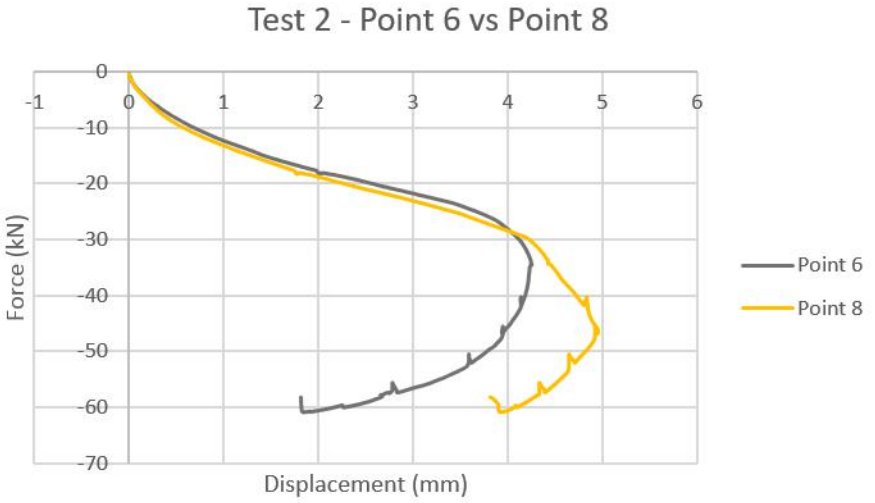
Test 2 - Point 6 vs Point 8
0
-10
-20
-30
-40
-50
-60
-70
-1
0
1
2
3
4
5
6
Force (kN)
Displacement (mm)
Point 6
Point 8

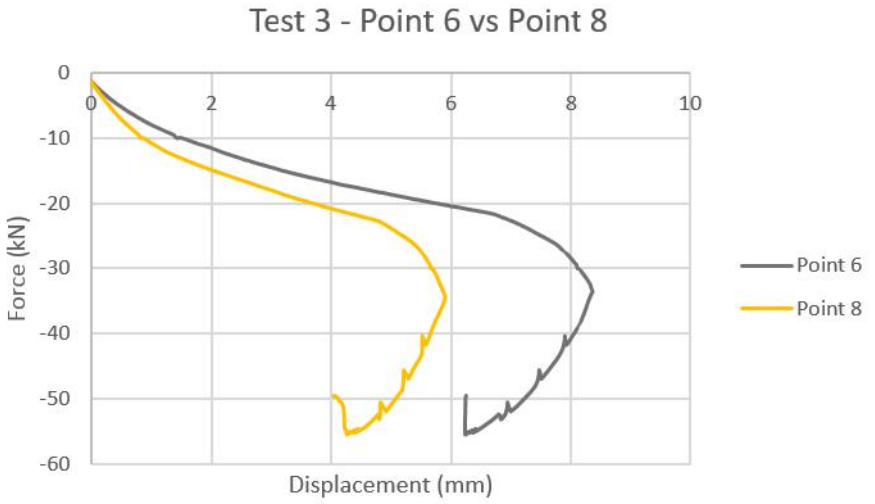
Test 3 - Point 6 vs Point 8
0
-10
-20
-30
-40
-50
-60
0
2
4
6
8
10
Force (kN)
Displacement (mm)
Point 6
Point 8

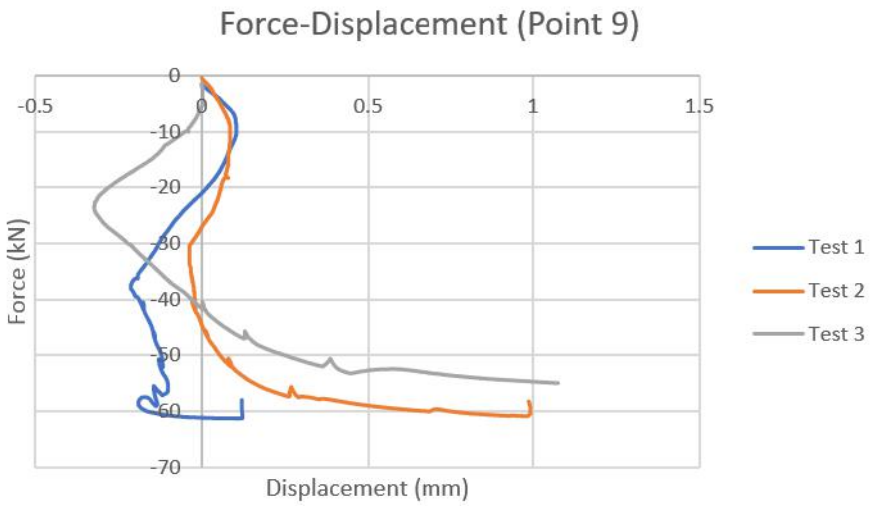
Force-Displacement (Point 9)
0
-10
-20
-30
-40
-50
-60
-70
-0.5
0
0.5
1
1.5
Force (kN)
Displacement (mm)
Test 1
Test 2
Test 3

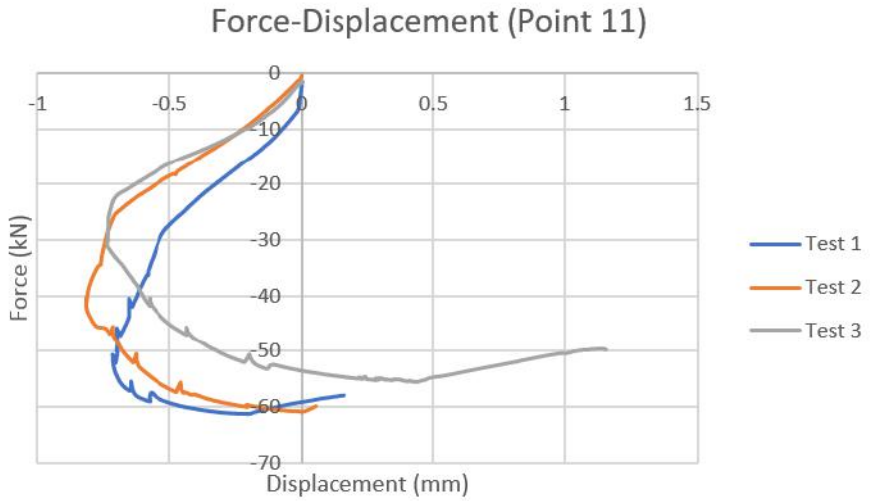
Force-Displacement (Point 11)
0
-10
-20
-30
-40
-50
-60
-70
-1
-0.5
0
0.5
1
1.5
Force (kN)
Displacement (mm)
Test 1
Test 2
Test 3

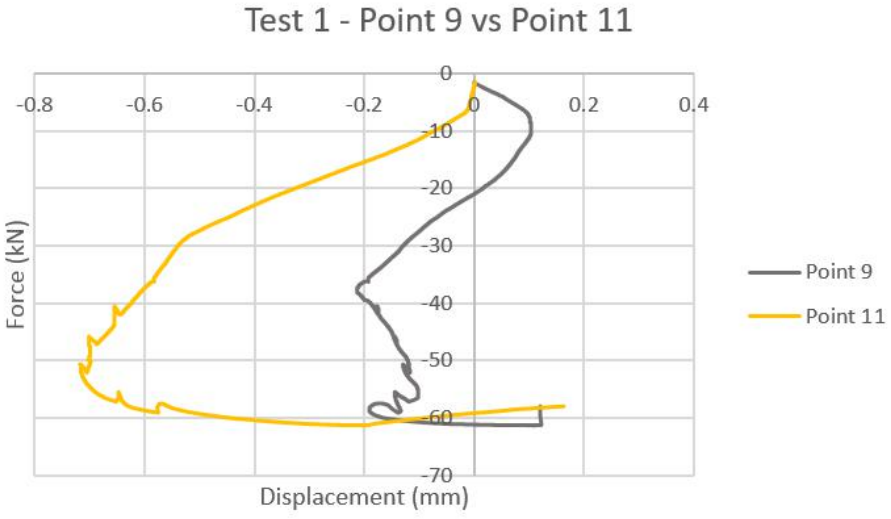
Test 1 - Point 9 vs Point 11
0
-10
-20
-30
-40
-50
-60
-70
-0.8
-0.6
-0.4
-0.2
0
0.2
0.4
Force (kN)
Displacement (mm)
Point 9
Point 11

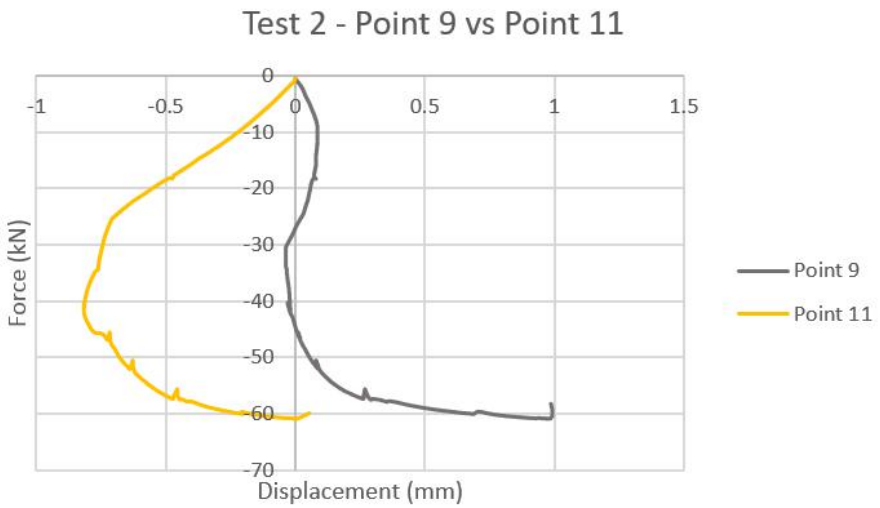
Test 2 - Point 9 vs Point 11
0
-10
-20
-30
-40
-50
-60
-70
-1
-0.5
0
0.5
1
1.5
Force (kN)
Displacement (mm)
Point 9
Point 11

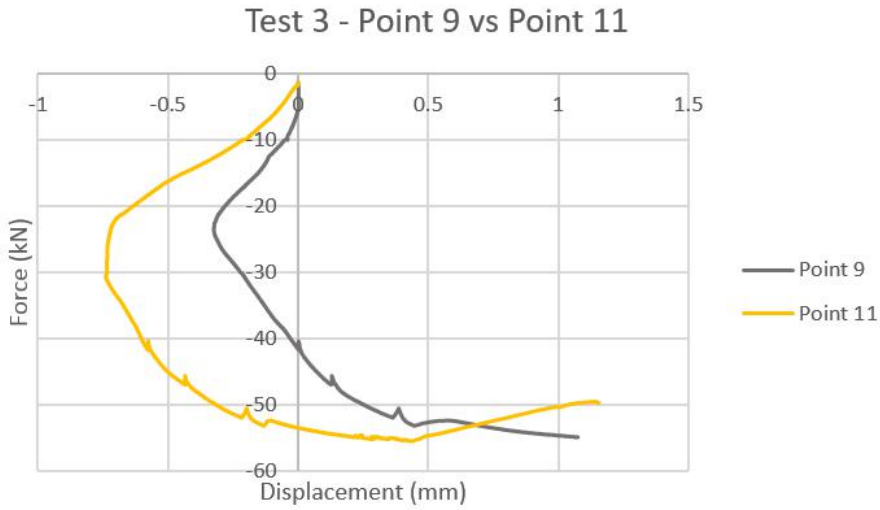
Test 3 - Point 9 vs Point 11
0
-10
-20
-30
-40
-50
-60
-1
-0.5
0
0.5
1
1.5
Force (kN)
Displacement (mm)
Point 9
Point 11

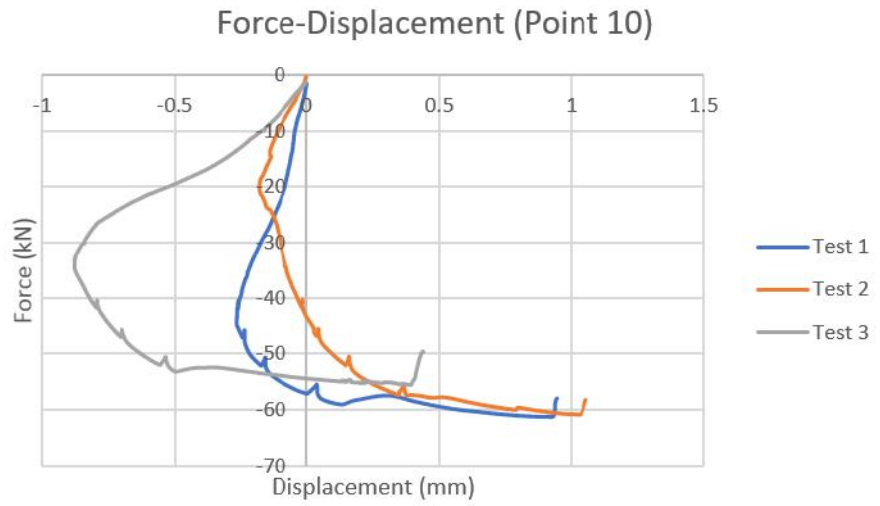
Force-Displacement (Point 10)
0
-10
-20
-30
-40
-50
-60
-70
-1
-0.5
0
0.5
1
1.5
Force (kN)
Displacement (mm)
Test 1
Test 2
Test 3

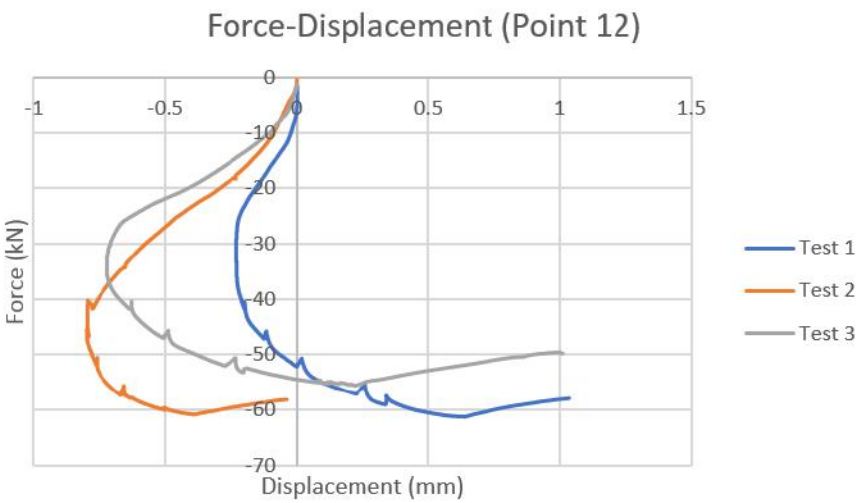
Force-Displacement (Point 12)
0
-10
-20
-30
-40
-50
-60
-70
-1
-0.5
0
0.5
1
1.5
Force (kN)
Displacement (mm)
Test 1
Test 2
Test 3

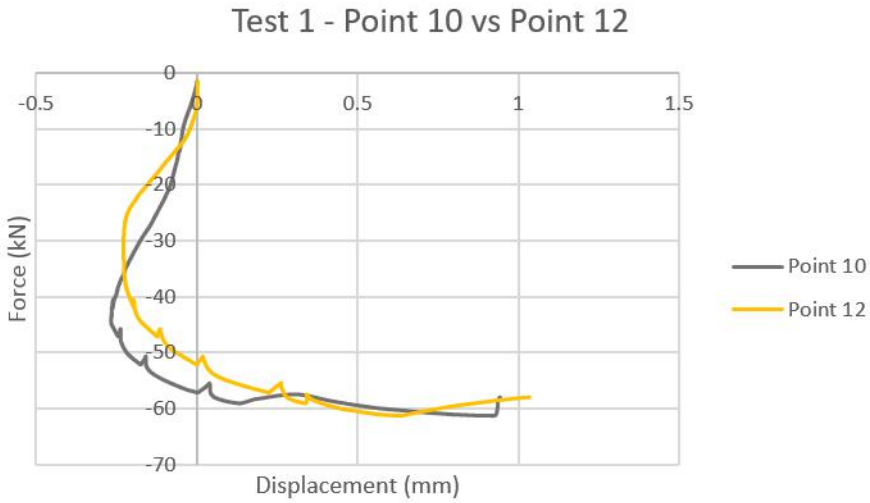
Test 1 - Point 10 vs Point 12
0
-10
-20
-30
-40
-50
-60
-70
-0.5
0
0.5
1
1.5
Force (kN)
Displacement (mm)
Point 10
Point 12

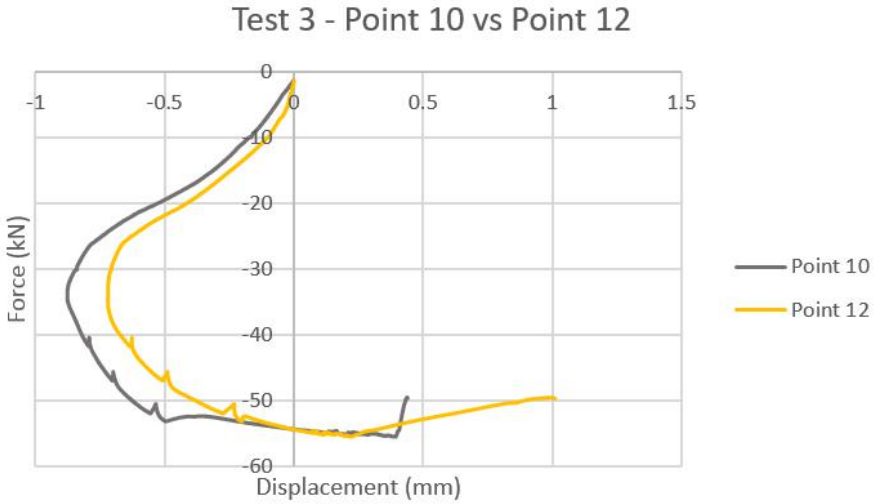
Test 3 - Point 10 vs Point 12
0
-10
-20
-30
-40
-50
-60
-1
-0.5
0
0.5
1
1.5
Force (kN)
Displacement (mm)
Point 10
Point 12

Experimental test average force-displacement graphs on all points and tests of LHP200, t=0.85mm:

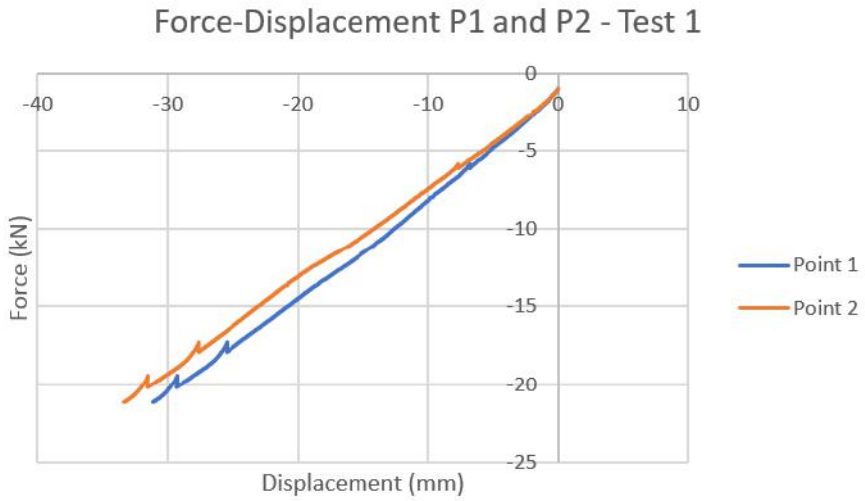

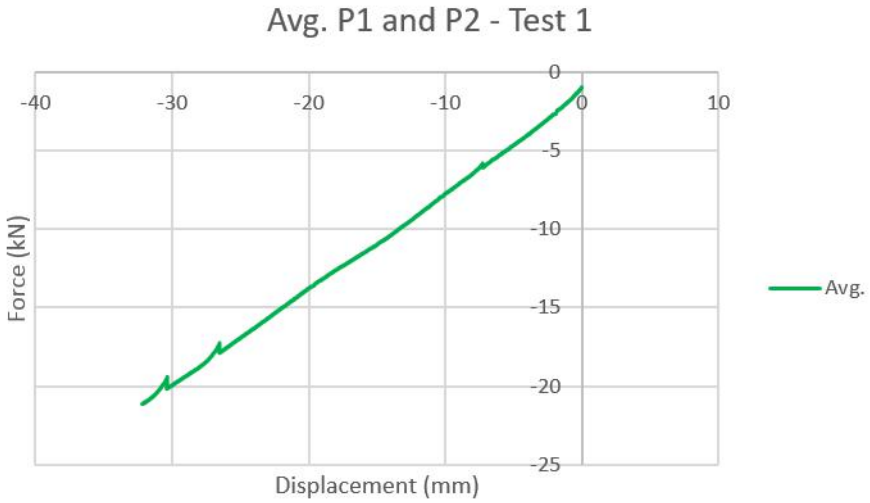

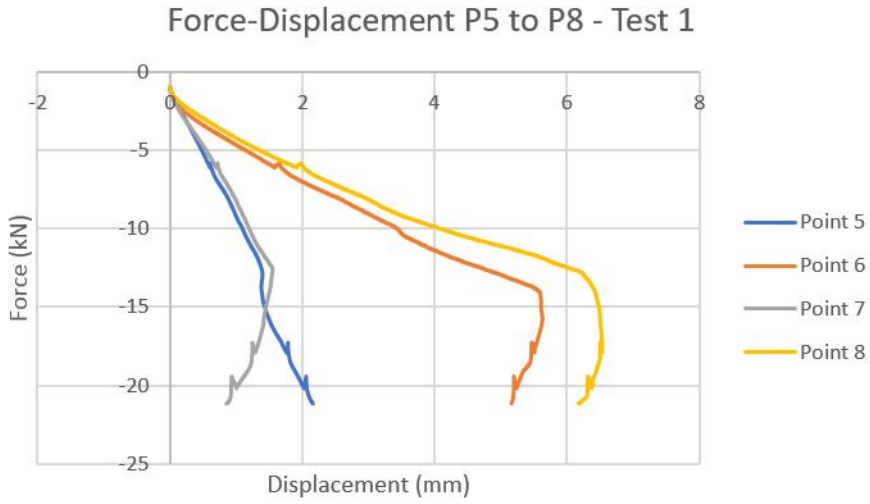

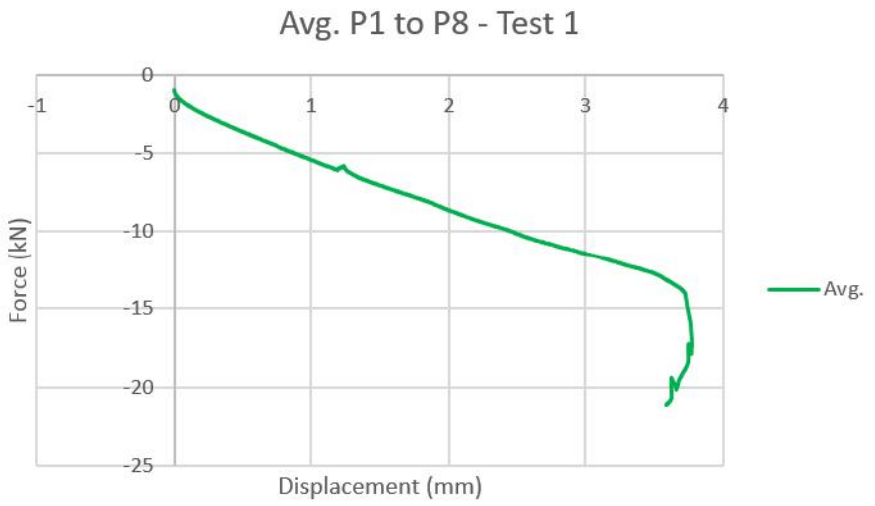

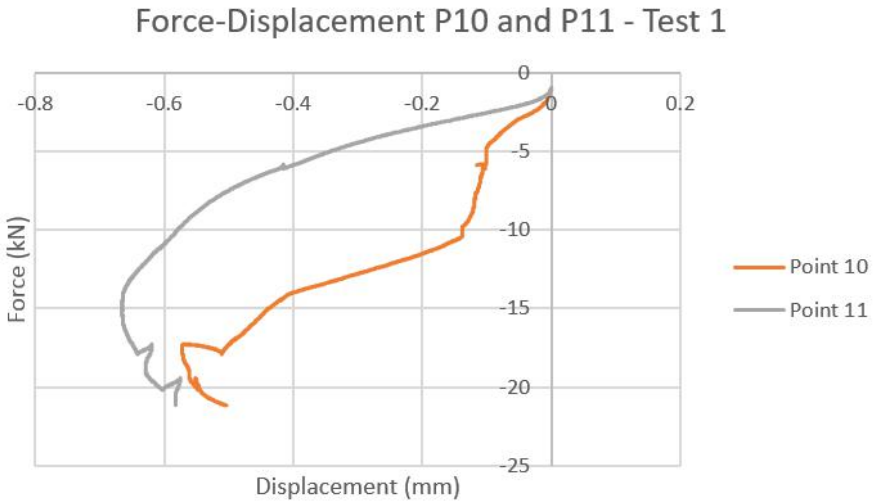

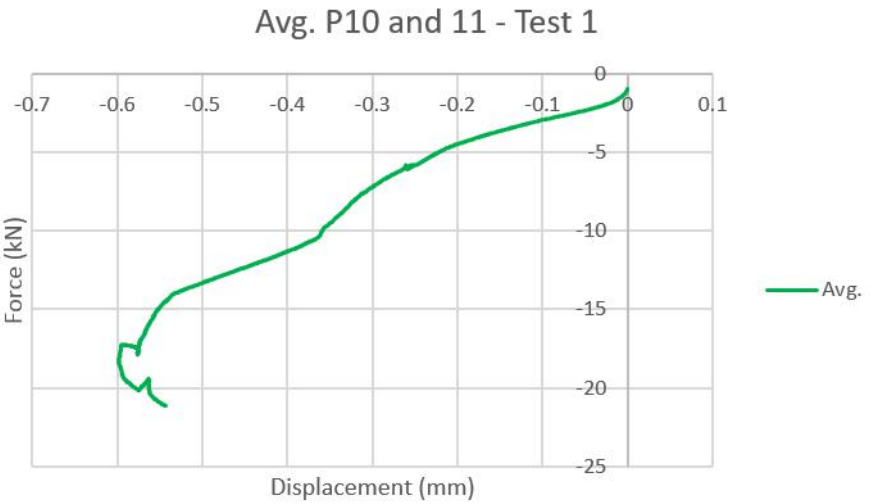

Note: values of test 1 were neglected because LVDT's fell off at point 9 and 12


Force-Displacement - Test 1
0
-40
-30
-20
-10
0
10
-5
-10
-15
-20
-25
Force (kN)
Displacement (mm)
Experimental
Theoretical No OL
Theoretical W/OL

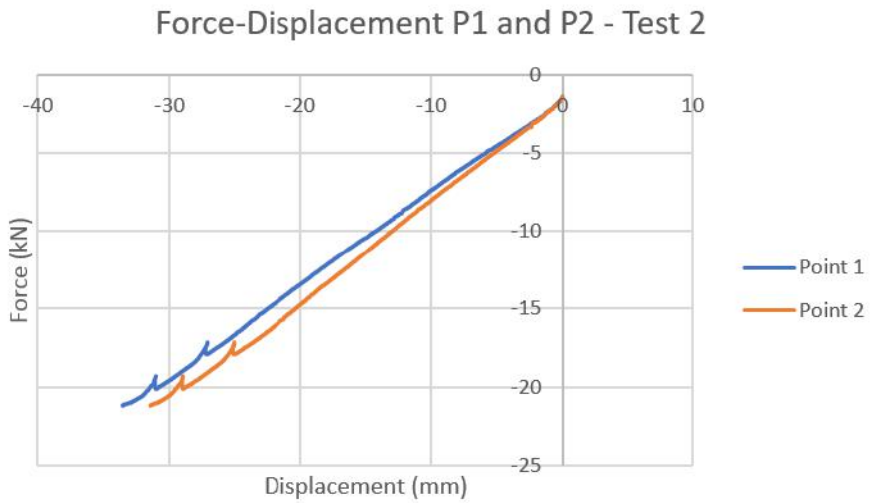
Force-Displacement P1 and P2 - Test 2
0
-40
-30
-20
-10
0
10
-5
-10
-15
-20
-25
Force (kN)
Displacement (mm)
Point 1
Point 2

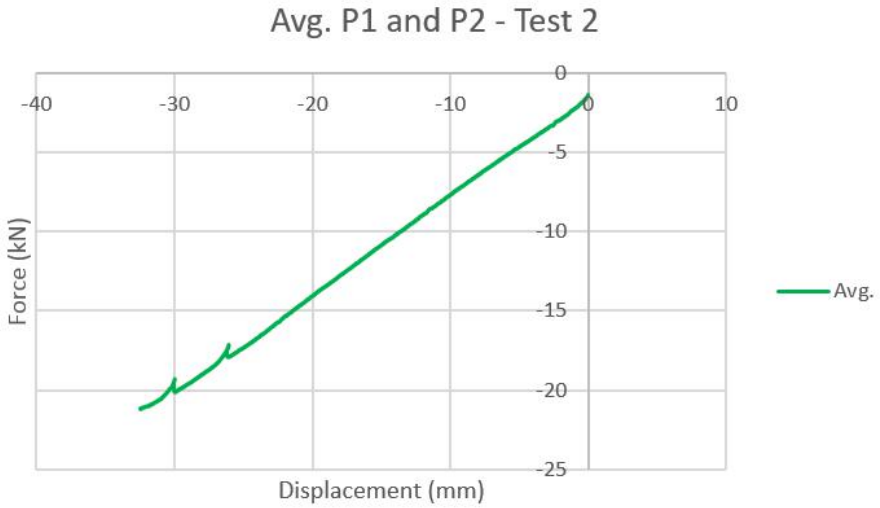
Avg. P1 and P2 - Test 2
0
-40
-30
-20
-10
0
10
-5
-10
-15
-20
-25
Force (kN)
Displacement (mm)
Avg.

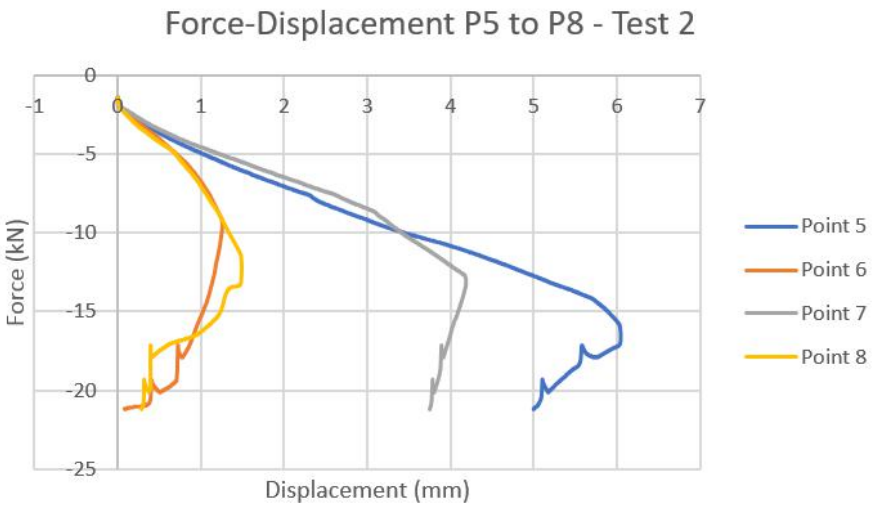
Force-Displacement P5 to P8 - Test 2
0
-1
0
1
2
3
4
5
6
7
-5
-10
-15
-20
-25
Force (kN)
Displacement (mm)
Point 5
Point 6
Point 7
Point 8

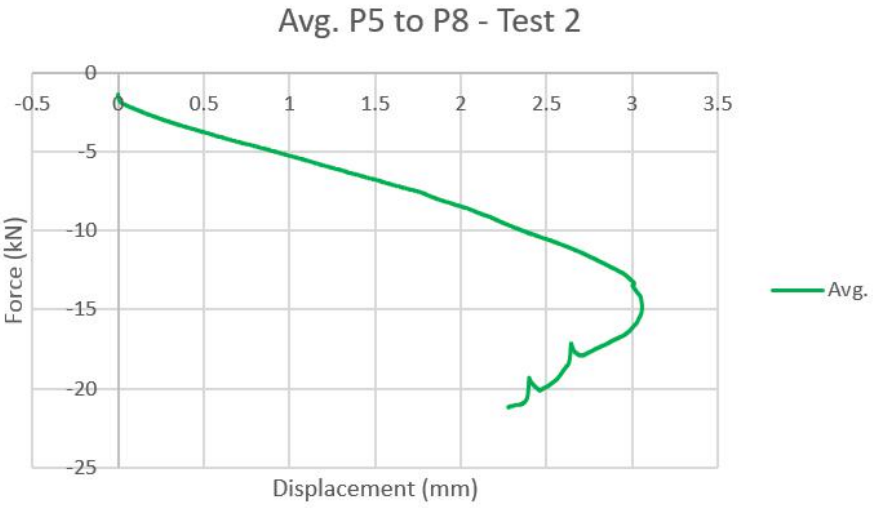
Avg. P5 to P8 - Test 2
0
-0.5
0
0.5
1
1.5
2
2.5
3
3.5
-5
-10
-15
-20
-25
Force (kN)
Displacement (mm)
Avg.

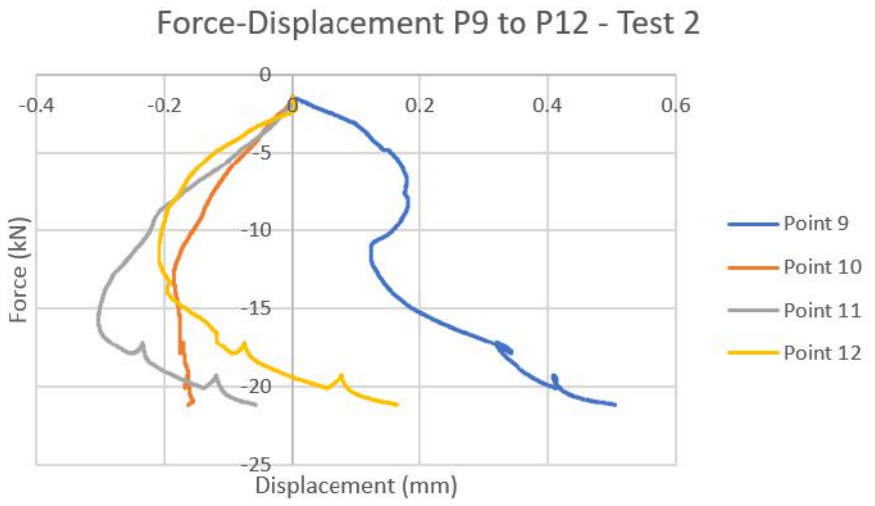
Force-Displacement P9 to P12 - Test 2
0
-0.4
-0.2
0
0.2
0.4
0.6
-5
-10
-15
-20
-25
Force (kN)
Displacement (mm)
Point 9
Point 10
Point 11
Point 12

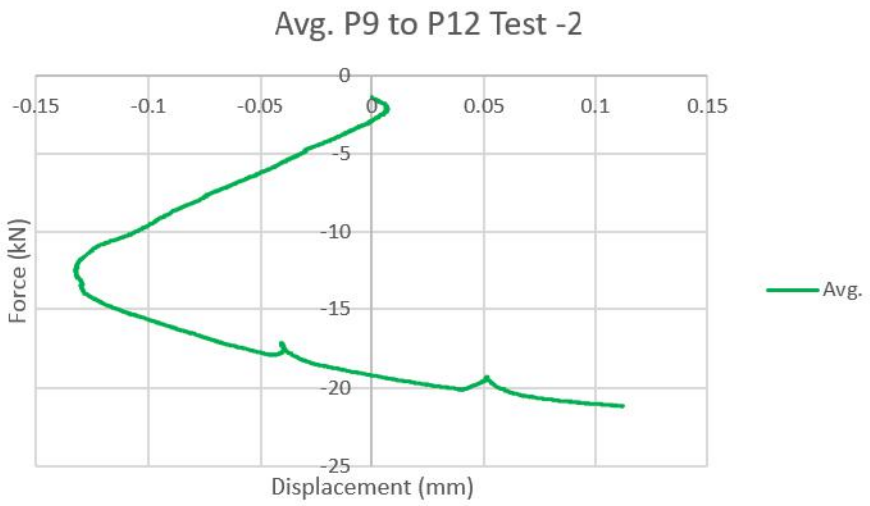
Avg. P9 to P12 Test -2
0
-0.15
-0.1
-0.05
0
0.05
0.1
0.15
-5
-10
-15
-20
-25
Force (kN)
Displacement (mm)
Avg.


Force-Displacement - Test 2
0
-50
-40
-30
-20
-10
0
10
-5
-10
-15
-20
-25
Force (kN)
Displacement (mm)
Experimental
Theoretica No OLI
Theoretical W/OL

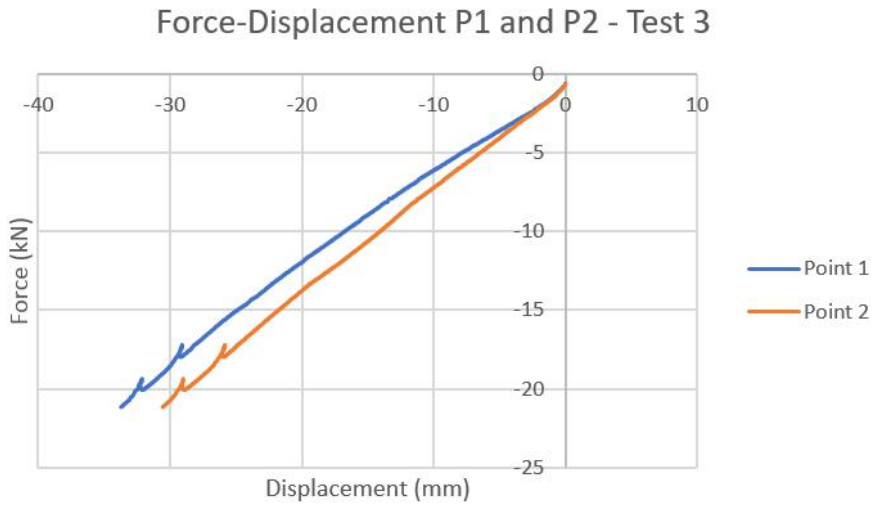
Force-Displacement P1 and P2 - Test 3
0
-40
-30
-20
-10
0
10
-5
-10
-15
-20
-25
Force (kN)
Displacement (mm)
Point 1
Point 2

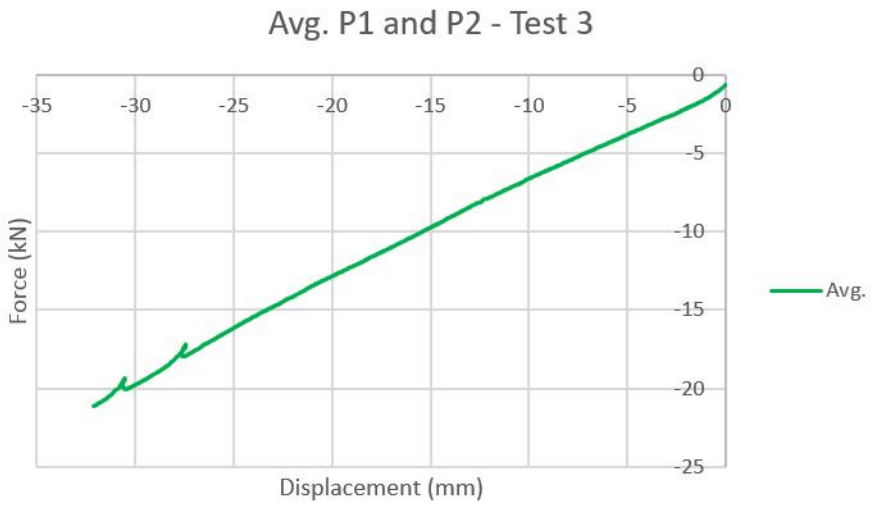
Avg. P1 and P2 - Test 3
-35
-30
-25
-20
-15
-10
-5
0
0
-5
-10
-15
-20
-25
Force (kN)
Displacement (mm)
Avg.

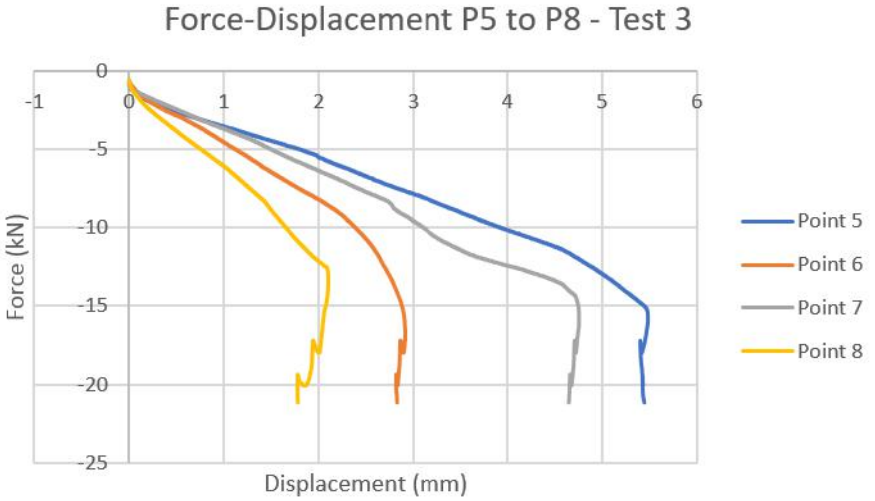
Force-Displacement P5 to P8 - Test 3
-1
0
1
2
3
4
5
6
0
-5
-10
-15
-20
-25
Force (kN)
Displacement (mm)
Point 5
Point 6
Point 7
Point 8

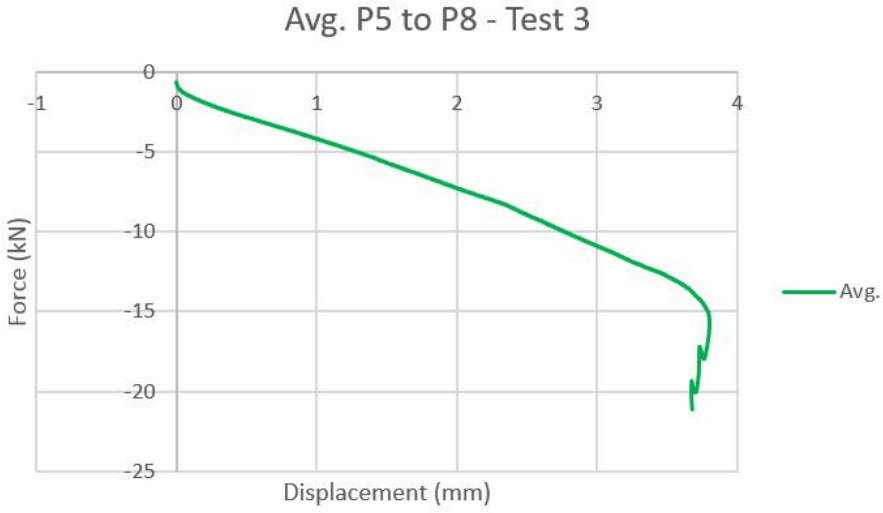
Avg. P5 to P8 - Test 3
-1
0
1
2
3
4
0
-5
-10
-15
-20
-25
Force (kN)
Displacement (mm)
Avg.

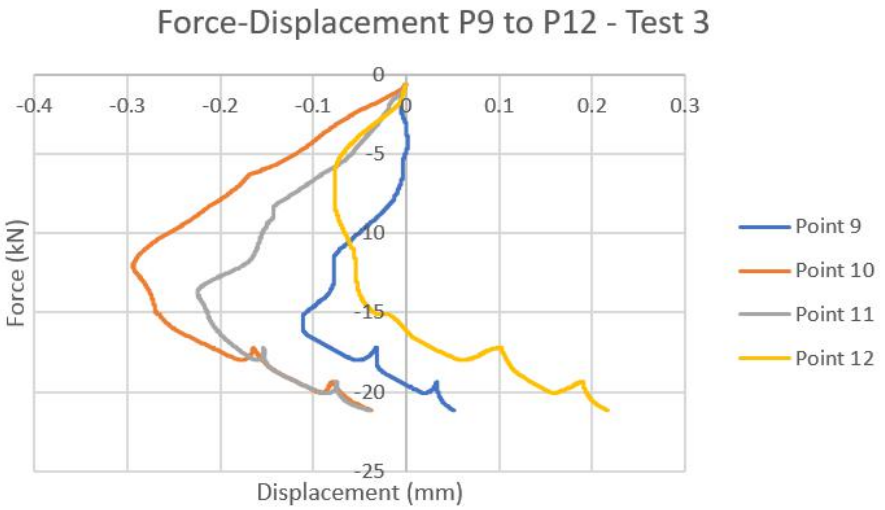
Force-Displacement P9 to P12 - Test 3
0
-0.4
-0.3
-0.2
-0.1
0
0.1
0.2
0.3
-5
-10
-15
-20
-25
Force (kN)
Displacement (mm)
Point 9
Point 10
Point 11
Point 12

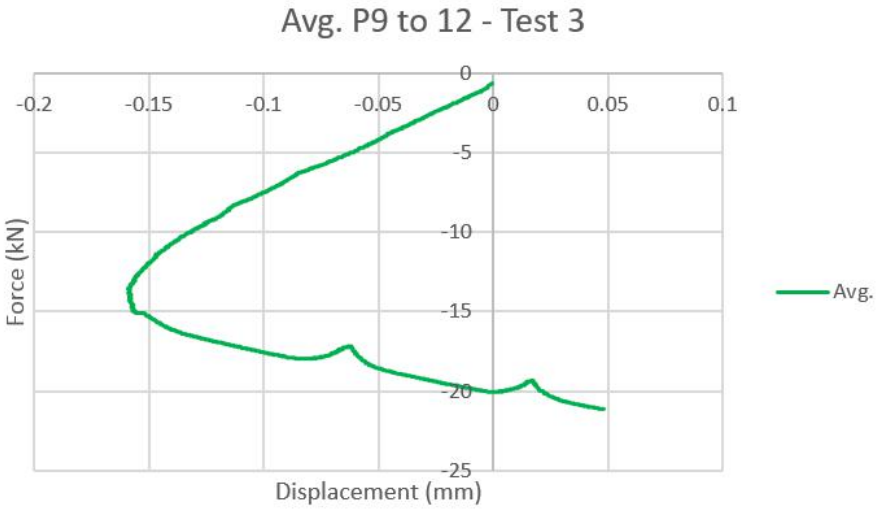
Avg. P9 to 12 - Test 3
0
-0.2
-0.15
-0.1
-0.05
0
0.05
0.1
-5
-10
-15
-20
-25
Force (kN)
Displacement (mm)
Avg.


Force-Displacement - Test 3
0
-40
-30
-20
-10
0
-5
-10
-15
-20
-25
Force (kN)
Displacement (mm)
Experimental
Theoretical No OL
Theoretical W/OL

Experimental test average force-displacement graphs on all points and tests of LHP200, t=1.50mm:

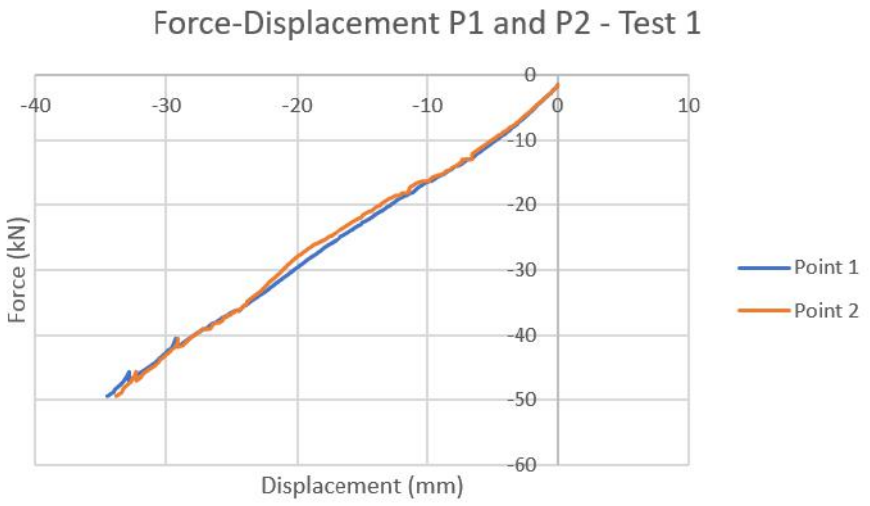

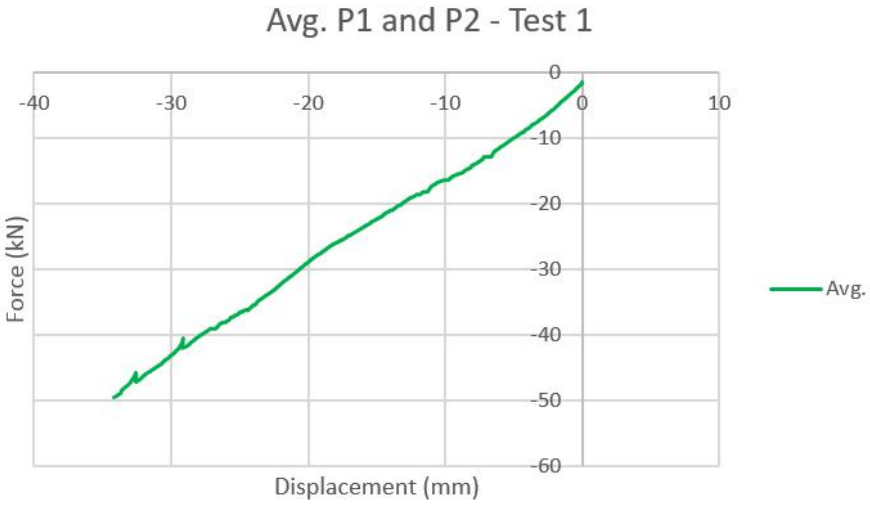

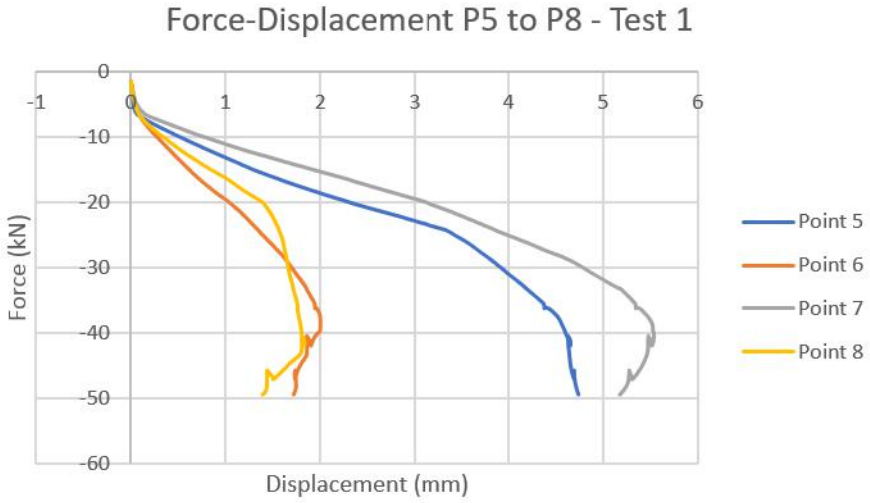

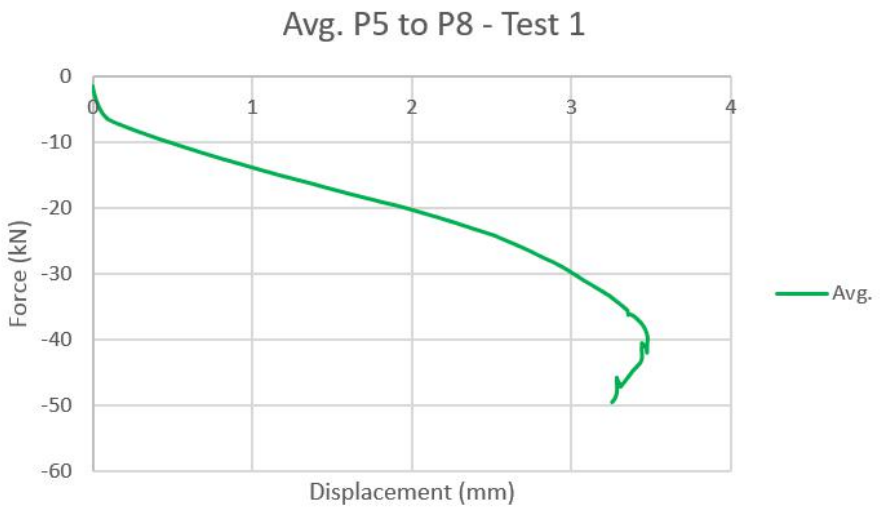
Avg. P5 to P8 - Test 1
0
-10
-20
-30
-40
-50
-60
0
1
2
3
4
Force (kN)
Displacement (mm)
Avg.

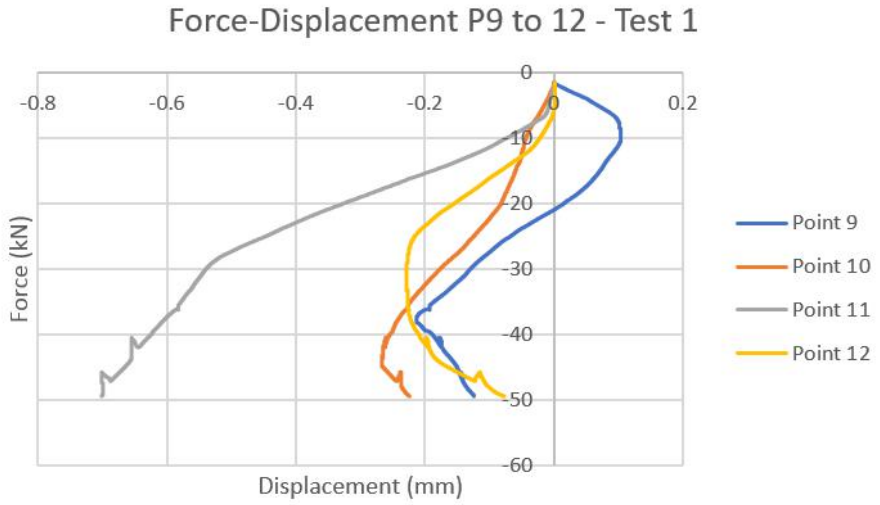
Force-Displacement P9 to 12 - Test 1
0
-10
-20
-30
-40
-50
-60
-0.8
-0.6
-0.4
-0.2
0
0.2
Force (kN)
Displacement (mm)
Point 9
Point 10
Point 11
Point 12

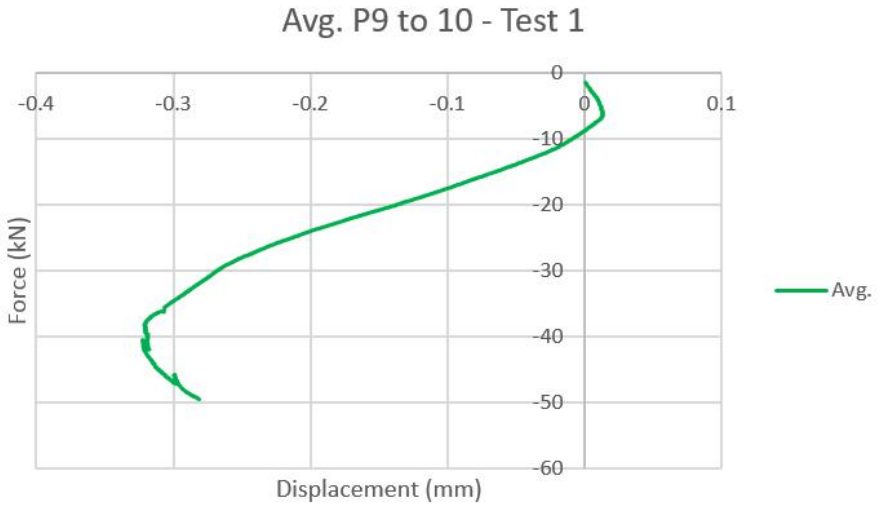
Avg. P9 to 10 - Test 1
0
-10
-20
-30
-40
-50
-60
-0.4
-0.3
-0.2
-0.1
0
0.1
Force (kN)
Displacement (mm)
Avg.

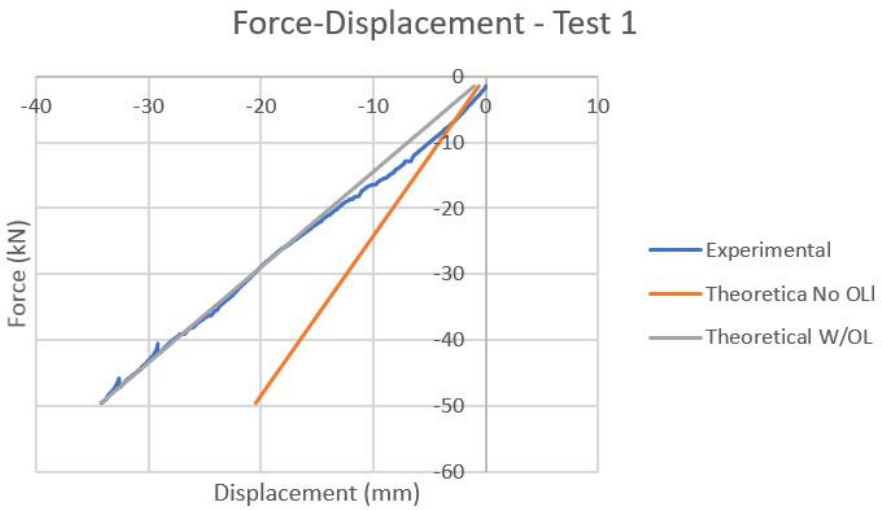
Force-Displacement - Test 1
0
-40
-30
-20
-10
0
10
-10
-20
-30
-40
-50
-60
Force (kN)
Displacement (mm)
Experimental
Theoretica No OLl
Theoretical W/OL

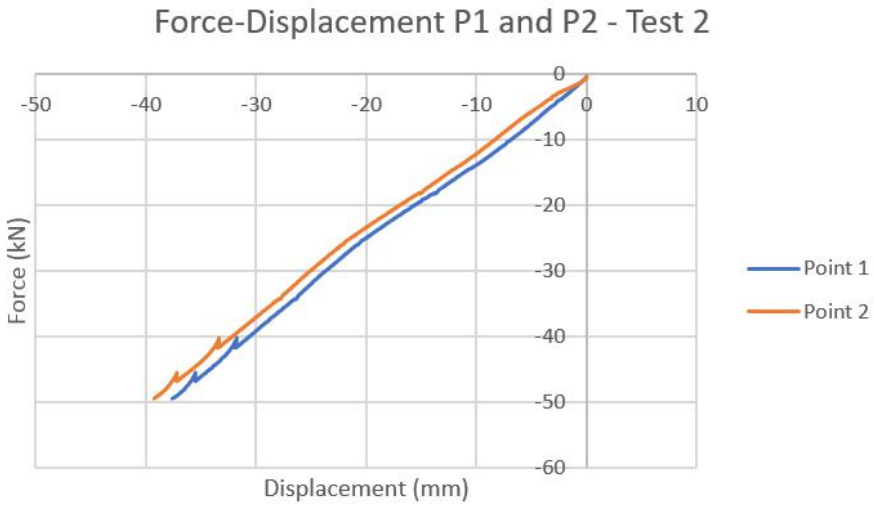
Force-Displacement P1 and P2 - Test 2
0
-50
-40
-30
-20
-10
0
10
-10
-20
-30
-40
-50
-60
Force (kN)
Displacement (mm)
Point 1
Point 2

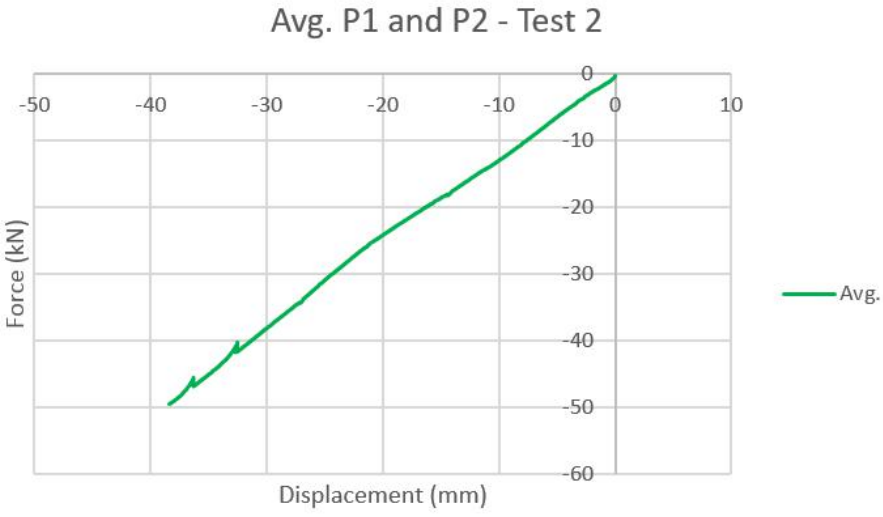
Avg. P1 and P2 - Test 2
0
-50
-40
-30
-20
-10
0
10
-10
-20
-30
-40
-50
-60
Force (kN)
Displacement (mm)
Avg.

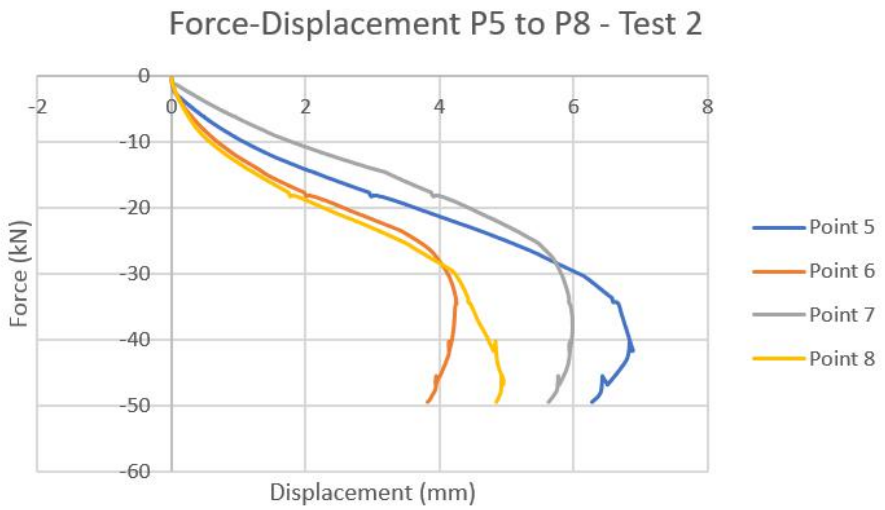
Force-Displacement P5 to P8 - Test 2
Force (kN)
Displacement (mm)
Point 5
Point 6
Point 7
Point 8

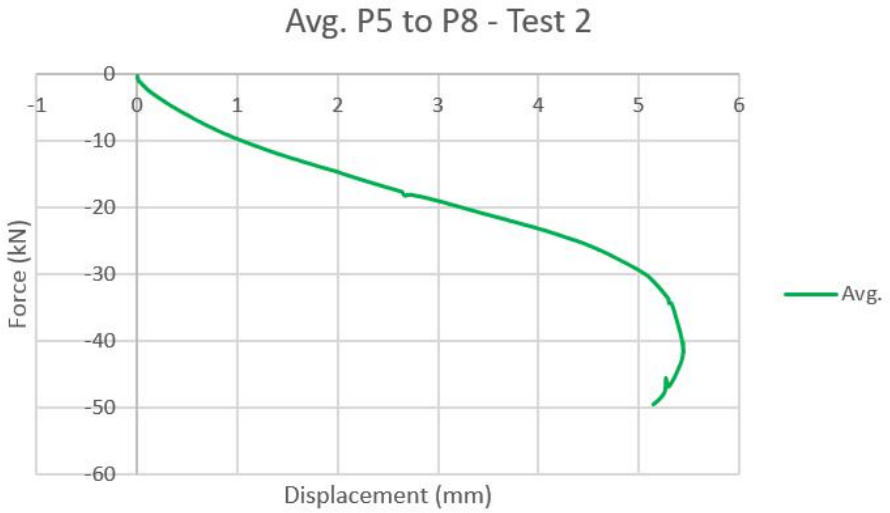
Avg. P5 to P8 - Test 2
Force (kN)
Displacement (mm)
Avg.

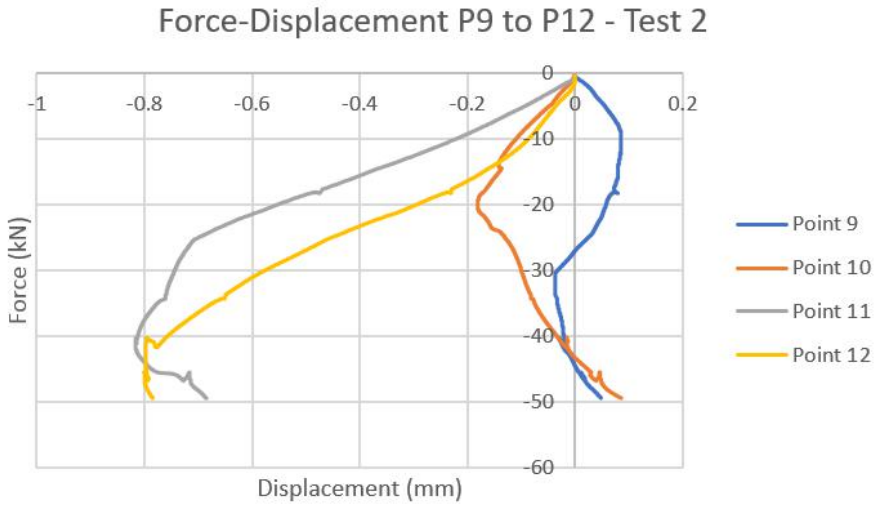
Force-Displacement P9 to P12 - Test 2
Force (kN)
Displacement (mm)
Point 9
Point 10
Point 11
Point 12

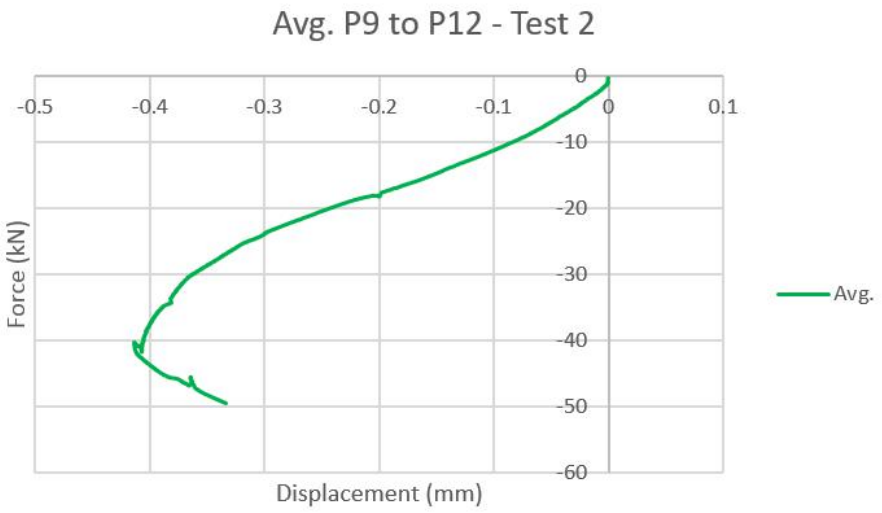
Avg. P9 to P12 - Test 2
0
-0.5
-0.4
-0.3
-0.2
-0.1
0
0.1
-10
-20
-30
-40
-50
-60
Force (kN)
Displacement (mm)
Avg.

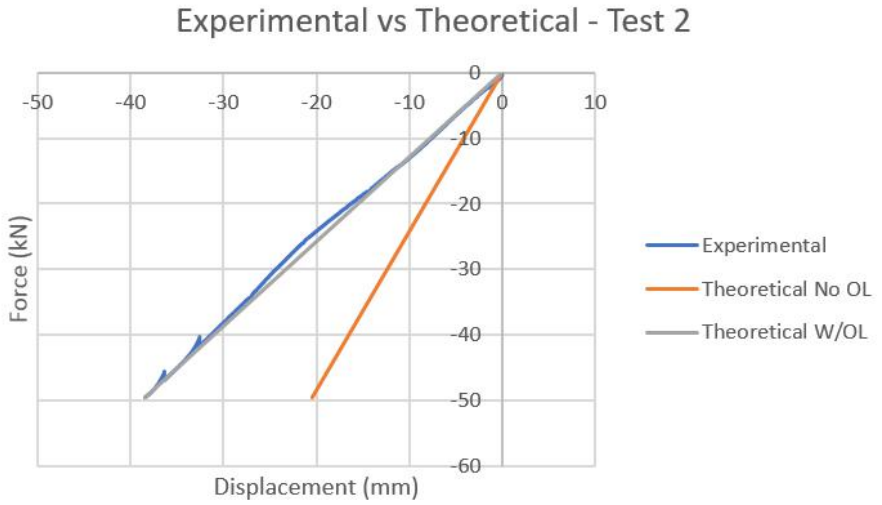
Experimental vs Theoretical - Test 2
0
-50
-40
-30
-20
-10
0
10
-10
-20
-30
-40
-50
-60
Force (kN)
Displacement (mm)
Experimental
Theoretical No OL
Theoretical W/OL

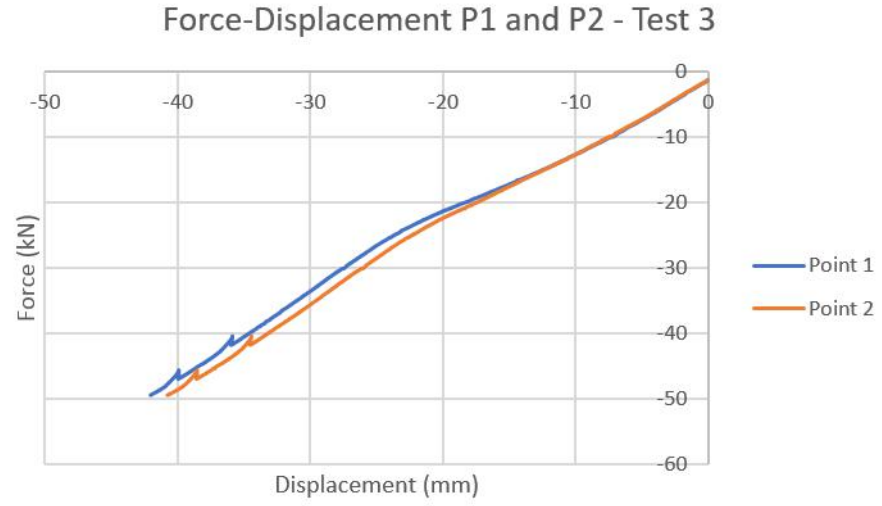
Force-Displacement P1 and P2 - Test 3
0
-50
-40
-30
-20
-10
0
-10
-20
-30
-40
-50
-60
Force (kN)
Displacement (mm)
Point 1
Point 2

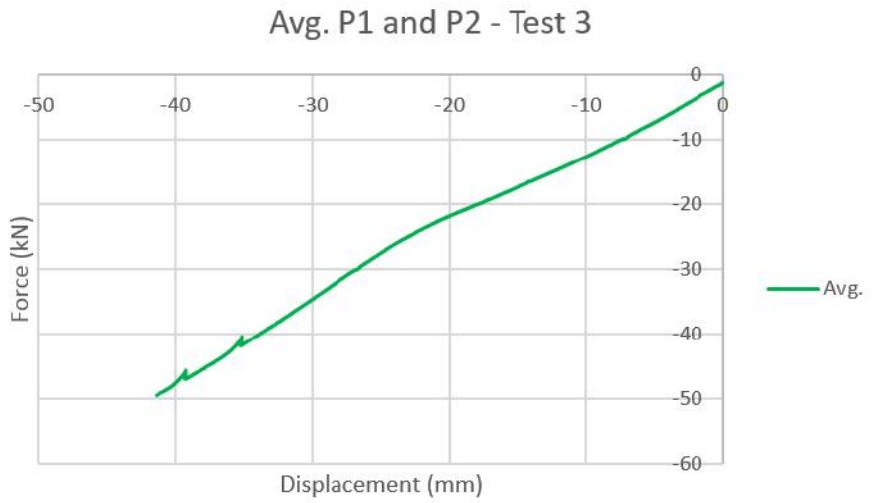
Avg. P1 and P2 - Test 3
-50
-40
-30
-20
-10
0
0
-10
-20
-30
-40
-50
-60
Force (kN)
Displacement (mm)
Avg.

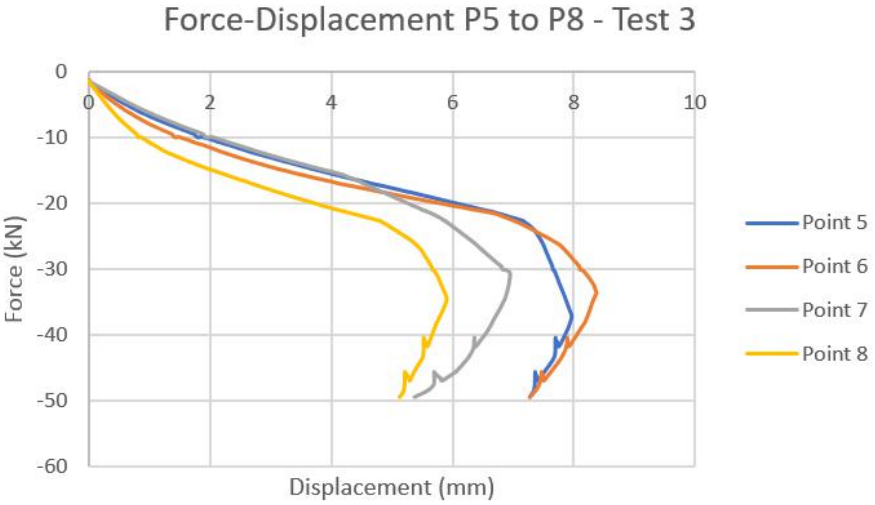
Force-Displacement P5 to P8 - Test 3
0
2
4
6
8
10
0
-10
-20
-30
-40
-50
-60
Force (kN)
Displacement (mm)
Point 5
Point 6
Point 7
Point 8

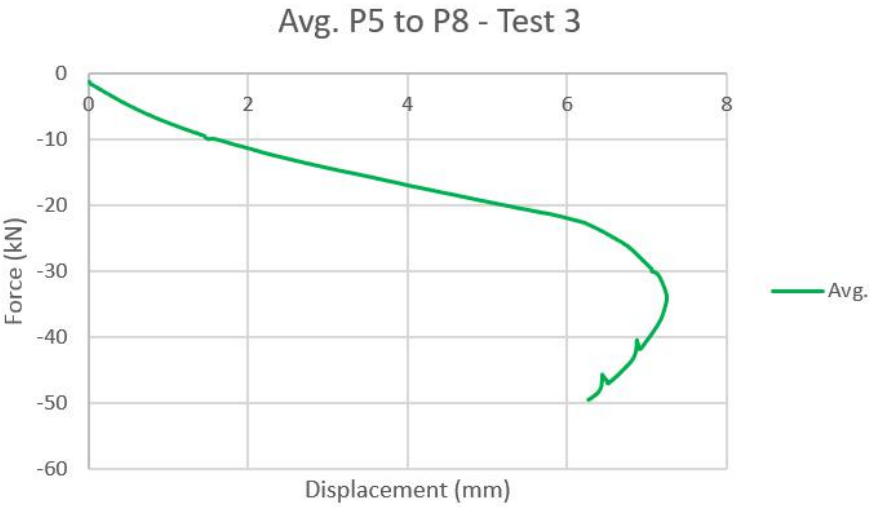
Avg. P5 to P8 - Test 3
0
2
4
6
8
0
-10
-20
-30
-40
-50
-60
Force (kN)
Displacement (mm)
Avg.

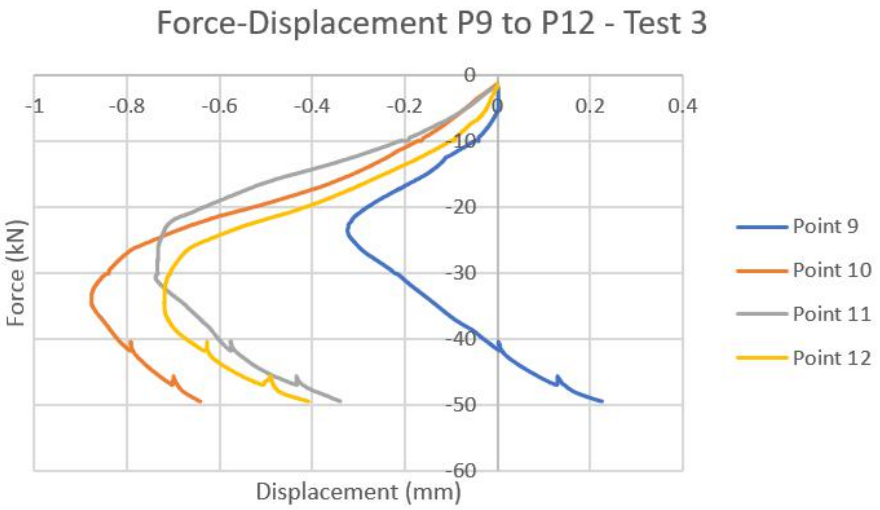
Force-Displacement P9 to P12 - Test 3
0
-1
-0.8
-0.6
-0.4
-0.2
0
0.2
0.4
-10
-20
-30
-40
-50
-60
Force (kN)
Displacement (mm)
Point 9
Point 10
Point 11
Point 12

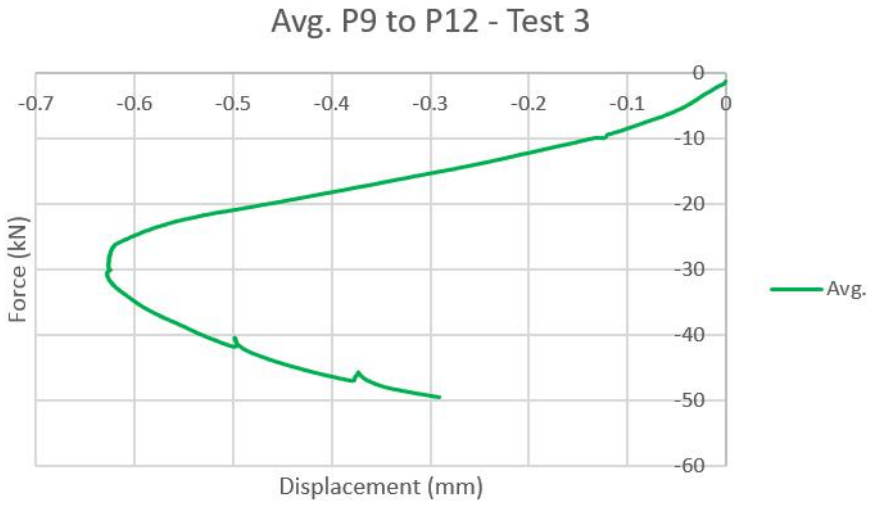
Avg. P9 to P12 - Test 3
0
-0.7
-0.6
-0.5
-0.4
-0.3
-0.2
-0.1
0
-10
-20
-30
-40
-50
-60
Force (kN)
Displacement (mm)
Avg.

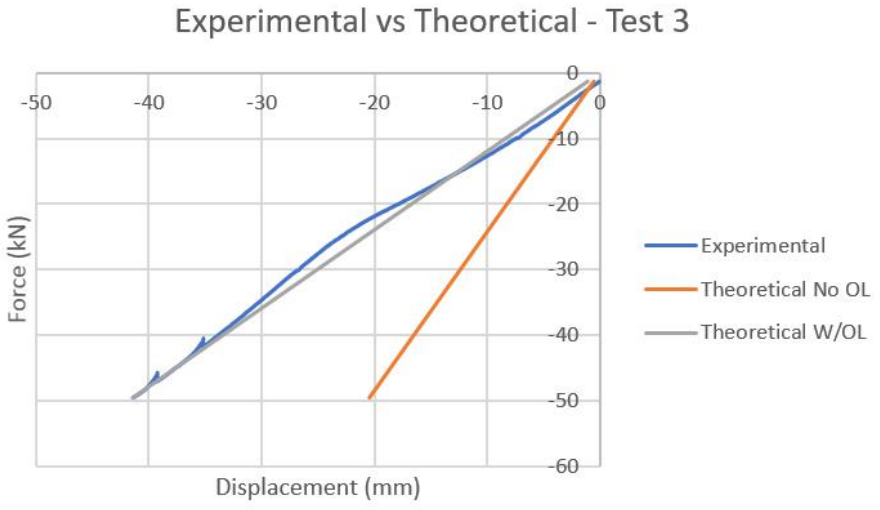
Experimental vs Theoretical - Test 3
0
-50
-40
-30
-20
-10
0
-10
-20
-30
-40
-50
-60
Force (kN)
Displacement (mm)
Experimental
Theoretical No OL
Theoretical W/OL

References

[1]: Design of cold-formed steel structures, Dan Dubina, Viorel Ungureanu, Raffaele Landolfo

[2]: http://www.steelconstruction.info/Building_envelopes

[3] Roof framing with cantilever (Gerber) girders and open web steel joists

[4] http://www.lindab.com/se/pro/products/pages/lhp-200.aspx

[5] Structural analysis, Aslam kassimali

[6] Schaum's Outline of Theory and Problems of Strength of Materials, William A. Nash, PhD

[7] Abaqus 6.12, Abaqus/CAE user’s manual